Article type: Review

Blue Single-Layer Organic Light-Emitting Diodes using Fluorescent Materials. A Molecular Design View Point.

Dr. Cyril Poriel* and Dr. Joëlle Rault-Berthelot*

Univ Rennes, CNRS, ISCR-UMR CNRS 6226, F-35000 Rennes, France

E-mail: Cyril.poriel@univ-rennes1.fr, Joelle.rault-berthelot@univ-rennes1.fr

Keywords

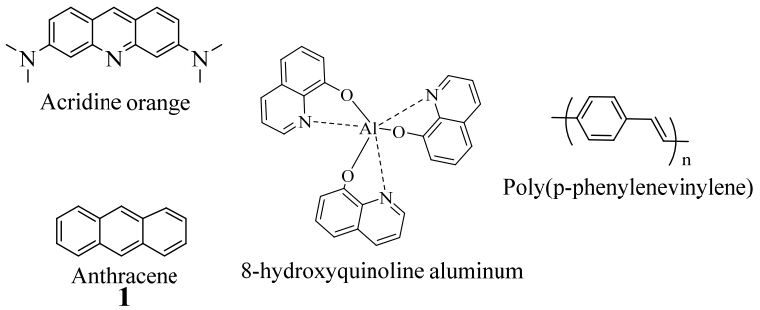
Organic Electronics, Single-Layer Organic Light-Emitting Diodes, Blue fluorescence

Abstract

Since the beginning of Organic Light-Emitting Diodes (OLEDs), blue emission has attracted the most attention and many research groups worldwide have worked on the design of materials for stable and highly efficient blue OLEDs. However, almost all the high-efficiency blue OLEDs using fluorescent materials are multi-layer devices, which are constituted of a stack of organic layers to improve the injection, transport and recombination of charges within the emissive layer. Despite the technology is mastered, it suffers from a real complexity, a high cost, and is time-consuming. Simplifying the multi-layer structure with single-layer one, simplest devices only made of the electrodes and the emissive layer has appeared as an appealing strategy for this technology. However, removing the functional organic layers of an OLED stack leads to a dramatic decrease of the performance and reaching high efficiency blue single-layer OLEDs has required intense researches and especially in term of materials design. We report herein an exhaustive review on blue emitting fluorophores, which have been incorporated in single-layer OLEDs and discuss the links between their electronic properties and the devices performance. We thus draw a structure/properties/device performance relationship map of interest for the future design of organic materials.

1. Introduction

Electroluminescence (EL) of organic material dates from 1950s after the observation of light emission from "acridine orange" thin films submitted to alternative current by Bernanose and co-workers (**Scheme 1**).[1] EL is then observed by Pope and co-workers in 1963[2] from anthracene crystals submitted to a high electric field of 400 V (Scheme 1). In 1982, Vincett and co-workers[3] prepared new devices by vacuum deposition of thin films of anthracene and observed a blue light at lower voltage: since 30 V with a 0.6 µm emitting layer thickness and since 12 V with films of 0.18 µm thickness. In 1987, Tang and Van Slyke from Eastman Kodak[4] showed that green light emission can be obtained in an OLED constituted by two thin organic layers (0.075 µm of an aromatic diamine and 0.06 µm of 8-hydroxyquinoline aluminium (Alq_3)) sandwiched between an anode of Indium Tin Oxide (ITO) and a Mg:Ag cathode (Scheme 1). Light emission was measurable since 2.5 V with an external quantum efficiency (EQE) close to 1%. From the EL spectrum, the green emission centred at 550 nm was attributed by the authors to the Alq_3 layer. The diamine layer, known to transport holes only, blocks the electrons injected from the cathode in the Alq_3 layer and favors the electron-hole recombination is this layer. This first work also showed the importance of the different organic layers in the device stack. It was the beginning of multi-layer OLEDs.



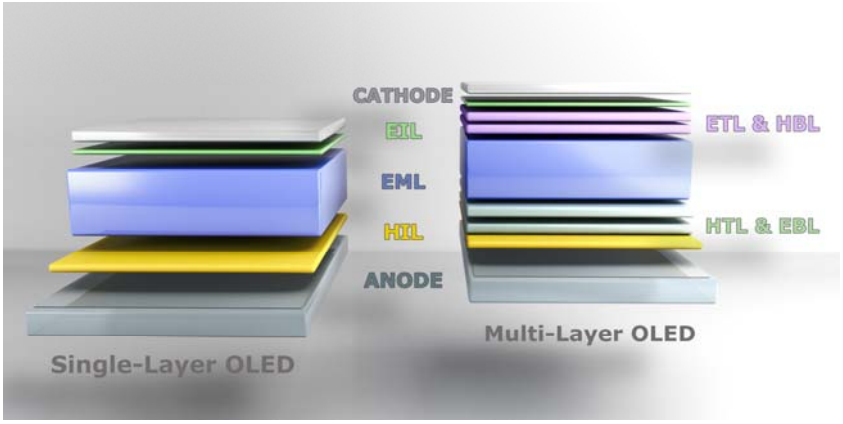
1

Scheme 1. First examples of electroluminescence in organic materials

In 1990, the group led by Friend in the Cavendish Laboratories (Cambridge, UK),[5] reported *the first OLED based on a conjugated polymer*, namely the poly(*p*-phenylene vinylene),

deposited between indium oxide anode and thin Al cathode. The threshold voltage (V_{on}) for charge injection was 14 V, the device emits green-yellow light with a modest EQE of 0.05 %. However, this reports open the way to *the wet-processes OLED technologies*.

Since the report of Tang and Van Slyke,[4] OLEDs have been an intense research field worldwide from academics and industrials and the OLED technology is nowadays released on the market.[6] Up to the end of the nineties, the OLED devices were all based on fluorescent materials.[7] As in an OLED, 25% of singlet and 75 % of triplet spin states are formed, internal quantum efficiency of fluorescent OLEDs was limited to 25 % meaning roughly an EQE lower than 5-6 %.[8] Among all the emission colour developed, blue OLEDs have been undoubtedly those, which have attracted the most attention. Indeed, blue light emission has been the most challenging notably due to the difficulty to inject charges in wide energy gap materials. For the last 25 years, reaching stable and highly efficient blue OLEDs has been an intense research field worldwide.[9] However, almost all the high-efficiency blue OLEDs using fluorescent emitters are multi-layer devices,[10] which are constituted of a stack of organic layers in order to improve the injection, transport and recombination of charges within the emissive layer (EML) (**Scheme 2**, Right). There are usually in an OLED stack, a hole injection layer (HIL), a hole transporting layer (HTL), an electron injection layer (EIL), an electron transporting layer (ETL), a hole blocking layer (HBL) and an electron blocking layer (EBL) and these layers can even be doubled. Despite the technology is mastered, it suffers from a real complexity, a high cost, and is time-consuming. Simplifying the multi-layer structure with the so-called Single-Layer OLEDs (SL-OLEDs), the simplest device only made of the electrodes and the EML has hence rapidly appeared as a promising and appealing solution in this technology (Scheme 2, Left).



Scheme 2. Schematic representation of the architecture of a Single-Layer OLED (Left) and a Multi-Layer OLED (Right)

However, removing the functional organic layers of an OLED stack often leads to a dramatic decrease of the performance and reaching high efficiency blue SL-OLEDs has required intense researches and especially in term of materials design. Indeed, if one removes all the organic layers surrounding the EML, the efficient injection, transport and recombination of charges within the device, should be insured by the EML itself and therefore the fluorophore. However, this appears to be a real obstacle to cross for blue emitting materials. Indeed, blue fluorophores usually possess a high HOMO and a low LUMO energy rendering the injection of charges in such materials very difficult. This has been one of the main issue to address in this field. Common properties required for high-performance blue emitting materials can be summarized as follows: (1) blue light emission between 380 and 500 nm with maximum wavelength around 450 nm; (2) a narrow full width at half maximum less than 60 nm; which produces low Commission Internationale de l'Eclairage (CIE) y-coordinate of less than 0.10 for TVs and cell phones; (3) thermal and morphological stability for stable device operation and a long device lifetime; (4) balance charge transport between electrons and holes flow and (5) adequate HOMO/LUMO energy levels for charge recombination and injection.

Gathering all these properties in a single molecule is far from being an easy task and requires very precise designs. Indeed, as soon as one tries to adjust the HOMO/LUMO energy levels

of an organic semi-conductor (OSC) with the Fermi levels of OLED electrodes, its gap is contracted and the emission wavelength is bathochromically shifted. This design strategy can hence lead to a material in which the charges can be more easily injected (the gap is contracted) but with an emission wavelength no more in the blue region. Trying to find the best compromise between adequate HOMO/LUMO energy and a blue emission has been the main challenge to address in the molecular design of efficient fluorophores for blue SL-OLEDs. This particularity has strongly restrain the development of such materials. However, for the last thirty years, research groups have developed many different molecular design strategies, which have led in some cases to high performance blue SL-OLEDs. Reaching high performance SL-OLEDs by molecular engineering of the fluorophore and understanding why this fluorophore can provide such high performance are the two pillars of this field and the purpose of the present review.

In the present exhaustive review, we summarize the state of art at the end of 2019 of organic semi-conductors ('small molecule' and oligomeric structures) used as *blue emitting EML in SL-OLED* devices. In order to help researchers for the future design of blue fluorophores for SL-OLEDs, we have developed in this review a molecular approach and have tried to connect the electronic properties (HOMO/LUMO energy levels, emission wavelength, quantum yield, mobilities of the charge carriers…) to the devices performances (EQE, V_{on}, EL spectra…). This allows to reach an accurate structure/properties/device performance relationship map of interest for the future of this technology.

Unless otherwise indicated, the simplest and more often used SL-OLED architecture found in literature is ITO/PEDOT:PSS/EML/Ca/Al, labelled as "device 1" in the following. It consists (i) in a transparent glass anode covered by ITO, itself covered by a thin poly(3,4-ethylenedioxythiophene):poly(4-styrenesulfonate) (PEDOT:PSS) film in order to facilitate the

hole injection at the anode and the EML and (ii) an Al cathode film separated from the EML by a thin layer of Ca. The EMLs are deposited either by thermal evaporation (TE-EML) or by solution processes (SP-EML).

This review reports 116 OSCs, their main physicochemical properties and their efficiencies as active layer in blue SL-OLEDs (137 devices). The review is divided in two main parts describing first polycyclic aromatic OSCs including or not heteroatoms and a second part presenting bipolar OSCs.

2. Blue Single-Layer OLEDs using pure hydrocarbon OSCs

2.1. Anthracene

Historically, this is in 1963, that Pope & al.[2] described the first SL-OLED using anthracene single crystals (**1**, Scheme 1) as EML. The light-blue emission occurs at very high V_{on} > 100V. In 1982, Vincett and co-workers described an emission perceptible since a V_{on} of 30 V from a SL-OLED using a 0.6 μm layer of **1** sandwiched between a 15 nm layer of gold as anode and a glass covered by 50 nm of Al as cathode.[3] More intense blue emission at even lower V_{on} (12 V) was observed with TE-SL**1** having a thinner **1** EML (0.18 μm) (**Table 1**). The EL spectrum presented a maximum at 420 nm in accordance with the photoluminescence (PL) spectrum.[11] These first examples (EQE of 0.06 %) have shown that it was possible to control the OLED wavelength with the OSC (accordance of the EL and PL spectra).

Over the years, several other famous π-conjugated fragments have been used to construct efficient fluorophores for blue emitting OLEDs. One can cite fluorene, dihydroindenofluorene, pyrene, truxene… In the following section, we introduce the use of these fragments as pure hydrocarbon (PHC) fluorophores in SL-OLEDs.

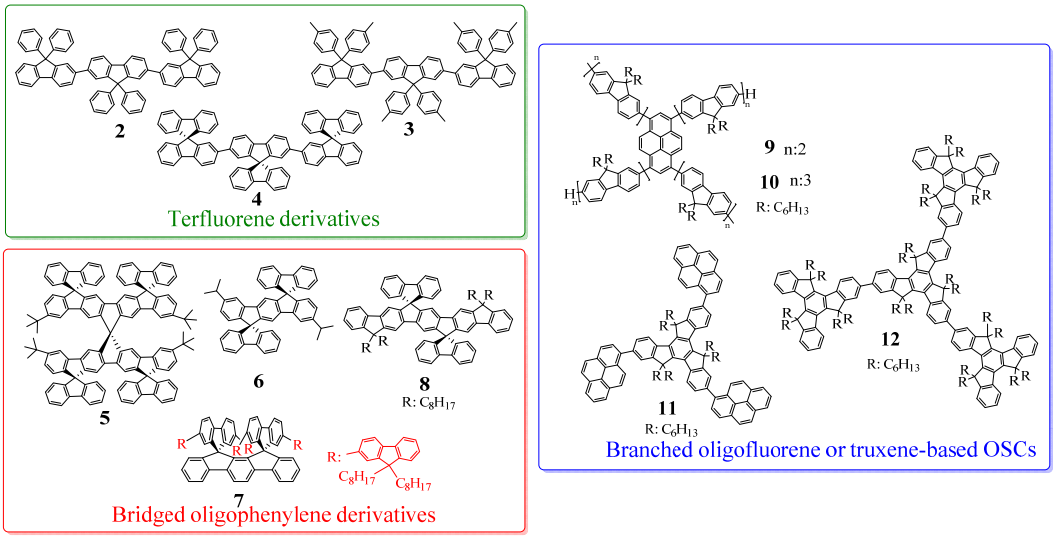


Figure 1. Pure hydrocarbon OSCs **2-12**

Device numbering and structure		V_{on} [V]	λ_{EL} [nm]	EQE_{max} [%]	CE_{max} [cd A^{-1}]	PE_{max} [lm W^{-1}]	CIE 1931 [x, y]	Ref
TE-SL**1**	Gold(15nm)/**1**(0.18µm)/Al(50nm)/Glass	12	420,447,479	0.06	-	-	-	[3]
SP-SL**2**	Device 1: **2**	5.6	-	0.08	0.07	0.03	0.17, 0.08	[12]
TE-SL**3**	ITO/PEDOT:PSS/**3**(100nm)/LiF/Al	8	-	0.15	-	-	-	[13]
TE-SL**4**	ITO/PEDOT:PSS/**4** (100nm)/LiF/Al	8	-	0.15	-	-	-	[13]
TE-SL**5**	ITO/**5** (100nm)/LiF/Al	4.7	440		1.31			[14]
TE-SL**6**	ITO/PEDOT:PSS/**6**/Ca	7	399, 416, 483, 587	-	0.90	0.19	0.21, 0.16	[15]
SP-SL**7**	ITO/PEDOT:PSS/**7**/Ca	7	464	-	0.05	-	0.19, 0.23	[16]
TE-SL**8**	ITO/PEDOT:PSS/**8**/Ca	10	-	-	0.015	-	-	[17]
SP-SL**9**	ITO/PEDOT:PSS/**9**(100nm)/CsF-Al	3.6	-	-	1.28	-	0.19, 0.32	[18]
SP-SL**10**	ITO/PEDOT:PSS/**10**(100nm)/CsF-Al	4.2	-	-	1.75	-	0.20, 0.32	[18]
SP-SL**11**	Device 1: **11**(100nm)	3.3	417(sh), 445, 471	$3.5\ 10^{-4}$	$4\ 10^{-4}$	-	0.16, 0.23	[19]
SP-SL**12**	ITO/PEDOT:PSS/**12**(100nm)/Ba/Al	3.6	430, 460	-	0.07	-	-	[20]

CE: current efficiency, PE: power efficiency, sh: shoulder, -: not available

Table 1. Performance of SL-devices with OSCs **1-12** as EML

	λ_{abs}^{sol}/ λ_{abs}^{film} [nm]	λ_{PL}^{sol}/ λ_{PL}^{film} [nm]	Φ^{sol}/ Φ^{film} [%]	HOMO [eV]	LUMO [eV]	Ref
1	357(THF)/-	402(THF)/380,400,422,450,475	-	-5.55[a]	-2.43[a], -2.31[c]	[11, 21]
2	352(Tol), 355($CHCl_3$)/-	395,417(Tol), 395,413,441($CHCl_3$)/413,426	88(Tol), 99(AcEt)/39	-5.71[a]	-2.52[c]	[12, 22]
3	354($CHCl_3$)/350	393, 414, 441 ($CHCl_3$)/405, 430	99(AcEt)/90	-5.50[d]	-2.40[c]	[13, 22]
4	353($CHCl_3$)/350	393, 412, 441($CHCl_3$)/405,430	99(AcEt)/90	-5.60[d]	-2.54[c]	[13, 22]
5	312,334,360,379(*p*-xylene)/-	386,406(*p*-xylene or DCM)/419	76(CyHx)/-	-5.62[a]	-2.43[c]	[14]
6	231,254,300,311,333,340,348(DCM)/-	351,359, 370(DCM)/-	66(CyHx)/-	-5.66[a]	-2.07[a], -2.22[c]	[15]
7	326(sh),343,354(THF)/-	402,422,450(sh)(THF)/-	80(THF)/-	-5.38[a], -5.07[b]	-2.05[a], -2.25[c], -1.36[b]	[16]
8	339,355,373,394(DCM)/375,396	397,420(CyHx)/405,425,447	90(CyHx)/-	-5.36[a]	-2.10[a], -2.29[c]	[17]
9	405,351(THF)/406,352	466(THF)/474	-	-5.65[a]	-	[18]
10	364(THF)/366	467(THF)/474	-	-5.71[a]	-	[18]
11	352(THF)/372	423(THF)/474	97(THF)/26	-5.36[a]	-2.67[c]	[19]
12	310, 349 (Tol)/349	386,405,430(sh)(Tol)/385, 405	99/60	-5.77[a]	-2.52[a]	[23]

THF: tetrahydrofuran, DCM: CH_2Cl_2, CyHx: cyclohexane, Tol: toluene, AcEt: ethylacetate, sh: shoulder, underline the most intense band, -: not available, λ_{abs}^{sol}/ λ_{abs}^{film}: absorbance wavelength in solution/ absorbance wavelength in film, λ_{PL}^{sol}/ λ_{PL}^{film}: photoluminescence wavelength in solution/ photoluminescence wavelength in film, Φ^{sol}/ Φ^{film}: fluorescent quantum yield in solution/ fluorescent quantum yield in film, HOMO: highest occupied molecular orbital, LUMO: lowest unoccupied molecular orbital

[a]: from cyclic voltammetry, [b]: from theoretical calculation, [c]: from optical energy gap (ΔE^{opt}) (LUMO=ΔE^{opt} -HOMO^{el}),[d]: from solid state EPS

Table 2. Selected electronic properties of OSCs **1-12**

2.2. Terfluorene derivatives

Fluorene based materials (oligomers[24] and polymers[25]) are surely those which have been the most studied to date in the field of blue OLEDs.[25-26] The fluorene molecule itself possesses a PL spectrum with λ_{PL} at 302 nm[27] and the emission can be then easily red shifted by linking several fluorene molecules (λ_{PL}(difluorene): 385 nm,[24b, 28] λ_{PL}(terfluorene): 394 nm[29]). In this context, terfluorenes have been particularly investigated. Thus, a solution-processed SP-SL**2** using hexaphenyl-terfluorene (**2**, **Figure 1**)[12] as EML in a device 1 configuration emits light since 5.6 V, reaches an EQE of 0.08 % with bluish purple CIE coordinates of (0.17, 0.08). However, the EL spectra of SP-SL**2** significantly depends on the driving voltage and become broader in the 480-700 nm range at a high driving voltage of 14 V inducing a shift of the emission towards light blue (CIE: 0.22, 0.22). This unwanted green emission band (GEB) has been the subject of intense researches worldwide and assigned either to molecular aggregation[30] and/or so-called keto defects.[17, 31] The origin of this GEB remains nevertheless not perfectly understood and recent works on cyclofluorenes provide new elements on this feature.[32]

TE-SL**3** and TE-SL**4** (**3** and **4**, Figure 1),[13] exhibit blue EL from the terfluorenyl fragments with an EQE of 0.15 % for both devices. Despite the very high fluorescent quantum yield of **3** and **4** (Φ^{film}: 90%) (**Table 1 2**),[22] and the relatively good and even well balanced mobilities of hole (μ_h) and electron (μ_e) for both **3** (μ_h: 2 10^{-4} cm^2/V.s & μ_e > 4 10^{-4} cm^2/V.s) and **4** (μ_h: 2 10^{-3} cm^2/V.s & μ_e > 6 10^{-4} cm^2/V.s),[33] the low EL efficiencies suggest poor confinement of excitons in the EML. These first results already show the difficulty to design efficient PHC emitters for blue SL-OLEDs. One can already note that terfluorenyl-based devices using **2-4** as EML present different performances depending on the nature of the cathode (Ca/Al or LiF/Al) and on the EML deposition process (SP or TE).

2.3. Bridged oligophenylene derivatives

Recently, Müllen and co-workers synthesized a new extended spirobifluorene-based OSC **5**. In **5**, four fluorene units and two ladder tetraphenylene units are linked thanks to five spiro-bridges (Figure 1).[14] Due to the orthogonal configuration of the six π-conjugated systems, intermolecular aggregation in solid-state is prevented. The symmetric mirror images of the absorption and emission spectra, as well as the very small Stokes shift (4 nm in *p*-xylene) coincide with the super-rigid molecular structure of **5** possessing a high Φ^{sol} (76%) in cyclohexane. TE-SL**5** emits blue light (λ_{EL}: 440 nm) with a V_{on} of 4.7 V and a CE_{max} of 1.31 cd/A.

Other extended analogues of fluorenes are dihydroindenofluorenes (DHIFs)[34] which are versatile and efficient building blocks used as fluorescent EML in OLEDs,[15-16, 35] n-type materials for organic field-effect transistors[36] and as host materials for phosphorescent OLEDs.[37] DHIFs belong to bridged terphenyl family and possess different phenyl linkages (*para*/*meta*/*ortho*) and different ring bridging (*anti/syn*).[34, 37-38] Compared to fluorene, DHIFs present a red shifted absorption and emission and higher Φ^{sol} translating both the extension of conjugation and a more rigid structure.

TE-SL**6** emits blue light (CIE: 0.21; 0.16) since 7 V and reaches a CE_{max} of 0.9 cd A^{-1}, which was an interesting performance in 2007.[15] The EL spectrum displays however parasite emissions, which may come from the oxidation of the *i*-propyl groups borne by **6**.

SP-SL**7** emits light with a V_{on} of 7 V and a low CE of 0.05 cd A^{-1}.[15] The EL spectrum displays one emission peak in the blue region at 464 nm (CIE: 0.19, 0.23) similar to the solid state PL spectrum. As the emission of the terfluorenyl units generally occurs around 400/430 nm (see above emission of **2**-**4**), the main emission of **7** at 464 nm was attributed to excimers, which formation arises from stacked face-to-face terfluorenyl units. SP-SL**7** is one of the rare

examples of OLED which emission comes from excimers generated from intramolecular interactions.[16, 35b, 39]

In **8**, the central π-conjugated core is a bridged penta-*para*-phenylene spiro-linked to two fluorenyl units, the two other bridges being substituted by octyl chains for solubility purpose (Figure 1).[17] The solid state PL spectrum of **8** presents a λ_{max} at 425 nm and a large band around 500/600 nm similar to the GEB observed with polyfluorenes[40] and attributed herein to the oxidation of dialkyl bridge heads.[17] Despite a high Φ^{sol} (90%) and a HOMO level fitting that of ITO-PEDOT:PSS (-5.36 eV for **8** vs -5.15 eV for ITO-PEDOT:PSS[41]), TE-SL**8** presents a very weak efficiency (CE: 0.015 cd A^{-1}).[17]

2.4. Pyrene-centred starburst oligofluorenes or truxene-based OSCs

Star-shaped molecules have appeared as interesting fluorophores in SL-OLEDs (Figure 1, Right).[18-20] As an example, pyrene-centred starburst difluorene **9** or terfluorene **10** with solid state PL centred at 474 nm have been used as EML in SP-SL**9** and SP-SL**10** *resp.*[18] With **9**, V_{on} was low (3.6 V) and CE_{max} reached 1.28 cd A^{-1}. With **10**, the performance was even higher with CE_{max} reaching 1.75 cd A^{-1}. Each device shows blue-green emission, (CIE: 0.19, 0.32 with **9** and 0.20, 0.32 with **10**), similar to the solid state PL emission[18] without any additional emission band. This shows the interest of the pyrene-centred starburst fluorene-dimer or fluorene-trimer molecular design to avoid the formation of parasite GEB.

Truxene, a planar heptacyclic polyarene that can be considered as three annulated fluorene moieties, is the corner stone of an important class of π-conjugated star-shaped materials.[42] Substituted by three pyrenyl units, truxene **11**[19] presents in dilute THF solution a non-structured PL spectrum centred at 423 nm corresponding to the emission of the pyrenyl units (Table 2). In the solid state, the PL spectrum is red-shifted to 474 nm due to excimer emission induced by the stacking of pyrenyl units.[39b, 43] In accordance with intermolecular interactions,

a decrease of Φ^{sol} (97 %) to Φ^{film} (26 %) is measured. As **11** possesses good solubility due to the six *n*-hexyl chains of the truxene core, spin-coated devices were investigated (Table 1). SP-SL**11** performances are nevertheless very low (V_{on}: 3.3 V, EQE: 3.5 10^{-4} %), but interestingly, the broad EL spectrum is similar to the solid state PL spectrum showing that the emission arises from the pyrene excimers which are hence stable in a device. This is in accordance with other works on the subject.[35b]

Another π-conjugated dendrimer **12** constructed solely with one central truxene decorated by three truxenyl units has also been used as EML in SL-OLEDs.[23] The solid state PL spectrum of **12**[23b] is similar to that recorded in toluene solution[23a] indicating that formation of aggregates in the solid state is prevented because of the rigid and bulky structure of **12**. However and despite a blue emission is reached (430/460 nm), SP-SL**12**[20] displays low performance (CE_{max} of 0.07 cd A^{-1}).

In conclusion of this first part, the use of PHC fluorophores as EML in SL-OLEDs, always leads to low device performances. The three best devices (SP-SL**10**: 1.75 cd A^{-1}, TE-SL**5**: 1.31 cd A^{-1} and SP-SL**9**: 1.28 cd A^{-1}) use very large molecular structures which avoid π/π intermolecular interaction. The low performances of the other devices may be due to (i) a misfit between the HOMO/LUMO levels of the OSCs and the electrode work-functions (WF) rendering the charge injection difficult both at the anode and at the cathode and (ii) the mobilities of electrons and/or holes in these OSCs, probably low and unbalanced, rendering difficult the recombination of electron and hole in the EML. It should be stressed that, in all these articles, charge carriers mobilities are very rarely reported.

Thus, at this stage, more sophisticated molecular designs were needed in order to reach higher performances. One way to improve the charge injection and mobilities in OSCs consists in the introduction of hole-transporting (electron-rich fragment) and/or electron-transporting (elec-

tron-poor fragment) units on the main polycyclic backbone. As it will be detailed below, literature reports many examples of incorporation of donor and acceptor fragments through different molecular design strategies. They have been here classified in three main categories: "*π-donor*", "*π-acceptor*" and "*donor-acceptor*". These designs are at the origin of the improvement of SL-OLED performances and are described below. It should nevertheless be mentioned that PHC materials have not been forsaken in 2019 and are nowadays a very much sought family of OSCs notably for phosphorescent OLEDs (PhOLEDs). Indeed, many host materials for PhOLEDs are PHC based,[37a, 44] this is due to the high stability of such materials in working device conditions.

3. OSCs constructed on the association of a π-conjugated core and an electron-donating fragment: π-donor design

As presented above, most of the OLEDs use as anode a transparent glass electrode in order to allow the emitted light observation from this side of the device. This glass is consequently coated by a thin film of conducting material rendering the glass conducting enough to allow the holes injection from the anode to the EML. Most of the time, the thin conducting layer is made of ITO which exhibits excellent light transmission characteristics in visible while maintaining high electrical conductivity. The published values of ITO WF ranges from -5.53 eV to -4.10 eV, although most of the publications seem to converge into the range -4.60 / -4.70 eV.[45] However, for devices in which the EML is directly deposited on the ITO anode, the oxidation of the OSC by oxygen diffusing out of the ITO limits the device lifetime.[46] A solution to this problem has been found with the introduction of a thin organic hole-injecting film, PEDOT:PSS, between the ITO and the EML. This has led to an improvement of the device lifetime and also of the performance. Additional reasons of this device efficiency improvement are linked to a better organization of the interface PEDOT:PSS/EML compared

to the ITO/EML one (notably the roughness) and to a decrease of the ITO/PEDOT:PSS WF compared to that of ITO.[47] Reported values for the WF of ITO/PEDOT:PSS exhibit a significant spread from -4.80 to -5.20 eV.[48] Although ITO/PEDOT:PSS appears to be the most common anode used in OLEDs, some works also report the coating of ITO by MoO_3 (-5.2 eV)[48], Dipyrazino[2,3-f:2',3'-h]quinoxaline 2,3,6,7,10,11-hexacarbonitrile (HATCN) (from -4.45 eV to -5.95 eV increasing HATCN thickness),[49] CuI (-5.3 eV)[48] or copper-phtalocyanin (CuPc).[50] Therefore, the so-called single-layer devices are not strictly "single-layer".

A different way to improve the hole injection from the anode to the EML is to raise the HOMO energy of the OSC by molecular engineering. This can be done by linking electron-rich fragments to the main π-conjugated core of the OSC. Some examples are reported below. For clarity purpose, in the figures of the following sections, the π-systems are highlighted in yellow and the donor groups in green.

3.1. Donor-π-Donor design (D-π-D)

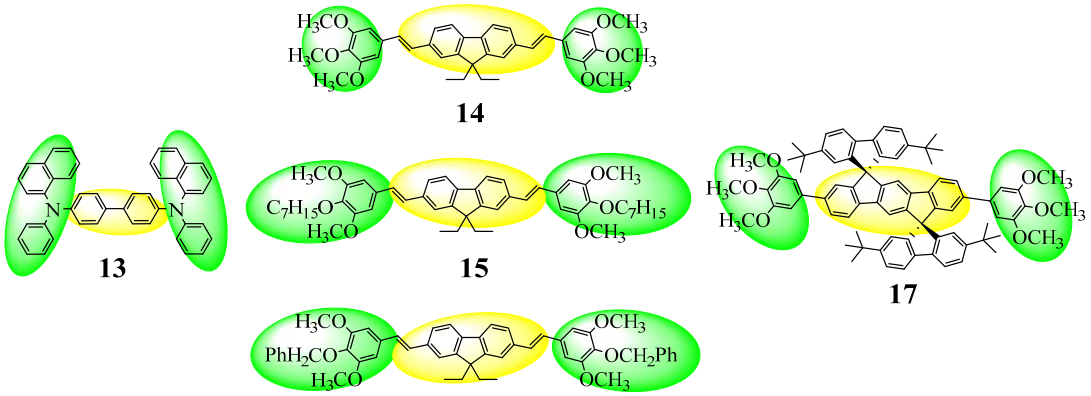


Figure 2. D-π-D design (OSCs **13-17**)

Device numbering and structure		V_{on} [V]	λ_{EL} [nm]	EQE_{max} [%]	CE_{max} [cd A^{-1}]	PE_{max} [lm W^{-1}]	CIE 1931 [x, y]	Ref
TE-SL**13**	ITO/ PEDOT:PSS/**13**(120nm)/Ca/Ag	4	426	-	0.1	-	-	[41]
SP-SL**14**	Device 1 **14**	3	470-480	-	0.51	-	0.19, 0.40	[51]
SP-SL**15**	Device 1 **15**	4	488	-	1.02	-	-	[51b]
SP-SL**16**	Device 1 **16**	5	485	-	0.05	-	-	[51b]
TE-SL**17**	ITO/PEDOT/**17**(40nm)/Ca	10.8	452	-	0.016	0.004	0.23, 0.24	[35b]

Table 3. Performance of SL-devices with OSCs **13-17** as EML

	λ_{abs}^{sol}/ λ_{abs}^{film} [nm]	λ_{PL}^{sol}/ λ_{PL}^{film} [nm]	Φ^{sol}/ Φ^{film} [%]	HOMO [eV]	LUMO [eV]	Ref
13	340($CHCl_3$), 339(THF)/-	450(THF, $CHCl_3$)/445	-/-	-5.5 [a]	-2.4 [b]	[41, 52]
14	380($CHCl_3$)/-	416,440($CHCl_3$)/460	93/-	-	-	[51a]
15	382($CHCl_3$)/-	419,444($CHCl_3$)/454,478	85/-	-	-	[51b]
16	382($CHCl_3$)/-	419,445($CHCl_3$)/460,480	69/-	-	-	[51b]
17	315,329,362(THF)/316,337,364	391,412(THF)/402,422	90/-	-5.43 [a]	-2.26 [c]	[35b]

[a]: from cyclic voltammetry, [b]: from theoretical calculation, [c]: from ΔE^{opt}-$HOMO^{el}$

Table 4. Selected electronic properties of OSCs **13**-**17**

Figure 2 presents several OSCs constructed on the D-π-D design possessing either a central biphenyl core in **13**, a 9,9-diethyl-2,7-divinyl-fluorenyl core in **14-16** or a DHIF core in **17**.

TE-SL**13**[41] emits blue light since 4 V with λ_{EL} at 426 nm blue shifted compared to the solid state PL spectrum (λ_{PL} : 445 nm[52b]) (**Table 3** and **Table 4**). The performance of TE-SL**13** is low with CE_{max} of only 0.1 cd A^{-1}.

Despite using similar fluorophores as EML, SP-SL**14**-SL**16** present different efficiencies.[51] SP-SL**16** is the less efficient with a CE_{max} of only 0.05 cd A^{-1}. The performance increases then from SP-SL**16** to SP-SL**14** with a CE_{max} of 0.51 cd A^{-1}. Finally, the performance of SP-SL**15** is twice that of SP-SL**14** with CE_{max} > 1 cd A^{-1}. The three devices emit light at low V_{on} (3 to 5 V) and their EL spectra are centred at 470/488 nm.

Despite similar physicochemical properties in solution (Table 4) showing the weak influence of the donor group, fluorophores **14-16** show different efficiencies when incorporated in SL-OLEDs. Changing the 4-methoxy group of the terminal phenyl-ethenyl group in **14** to an heptyloxy group in **15** significantly improved the CE_{max} while a change to a 4-benzyloxy group in **16** greatly degraded the performances. The poor performance of SP-SL**16** is assigned by the authors to a morphological instability on heating accompanied by a chemical instability. Increasing the length of the central core with a [1,2-*b*]-DHIF[35b] instead of a fluorene does not lead to an increase of the OLED performances (CE: 0.016 cd A^{-1} and CIE: (0.23, 0.24)).

3.2. π-conjugated cores with Donor units at the periphery

Figure 3 gathers OSCs possessing a central π-conjugated core decorated by increasing number of donor units at the periphery: three (**18-19**), four (**20-24**), six (**29**), eight (**25-28**) and twelve (**30**).

1,3,5-tristyrylbenzene **18**, endowed with electron-donating and solubilizing hexyloxy chains has been used in SP-SL**18**.[53] V_{on} is very high (~15 V) and the CE very low (0.07 cd A^{-1}). The maximum of the EL spectrum is at 438 nm and a weak GEB is also observed (**Table 5**).

Truxene decorated with three N-phenyl-N-pyrenyl substituents (**19**) is a blue emitter with a solid-state PL spectrum centred at 480 nm (**Table 6**).[19] For SP-SL**19**, a blue emission is observed (CIE: 0.17, 0.36). The performances of the device, though still very low (EQE 1.5 10^{-3} %) are of four times higher than that reported for SP-SL**11**[19] showing that the incorporation of amines in such structures could become an interesting strategy.

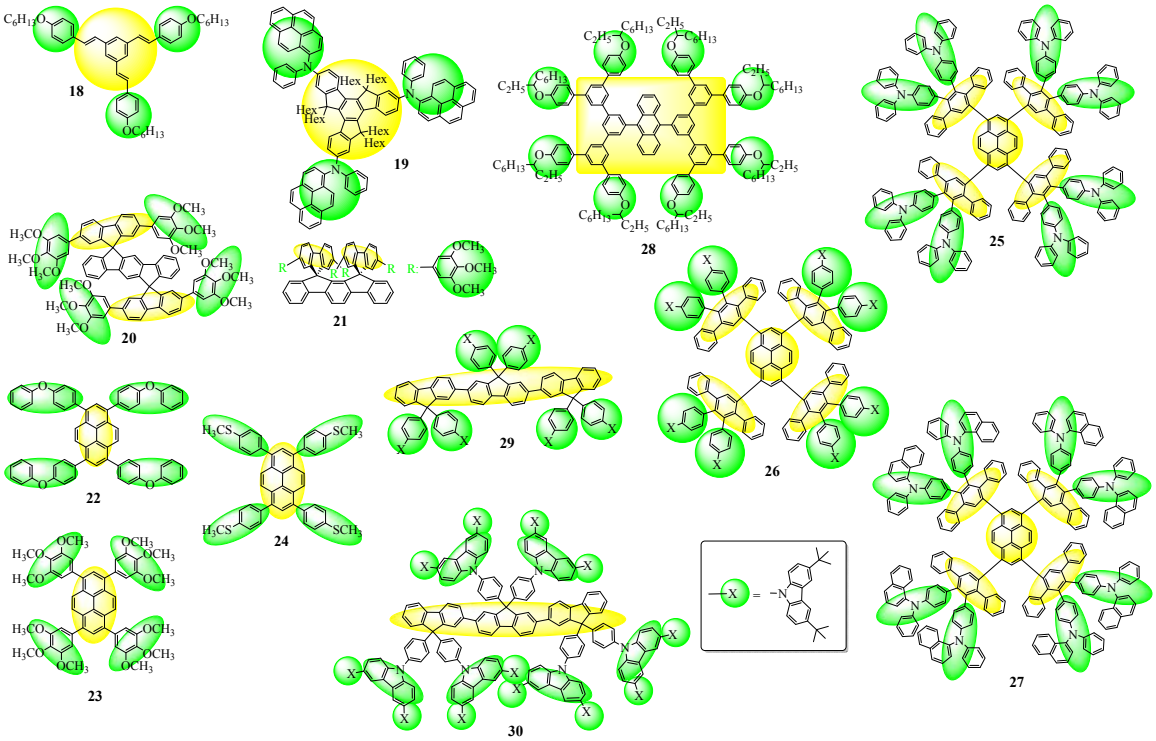


Figure 3. Dendrimers with donor groups at the periphery (OSCs **18-30**)

20 and **21** are positional isomers and only differ by their DHIF core, [1,2-*b*]-IF in **20** and [2,1-*a*]-IF in **21**, on which are linked the 2,7-disubstituted fluorenyl cores.[34, 35b] In both OSCs, the central core is built on a bridged *para*-terphenyl unit, however, in **20**, the two spiro bridges are in an *anti*-geometry (the two fluorenyl units do not interact) whereas in **21** the two spiro bridges are in a *syn*-geometry (the two fluorenyl cores do interact). In this last configuration, the emission arises from the intramolecular interactions of the cofacial fluorenes. TE-SL**20** emits light at a high V_{on} of 7.2 V with a low CE_{max} of 0.031 cd A^{-1}. Changing the EML (**21** instead of **20**), leads to a decrease of V_{on} (5 V *vs* 7.2 V for TE-SL**21** and TE-SL**20** *resp.*) and similar CE_{max} (0.037 cd A^{-1} *vs* 0.031 cd A^{-1} for TE-SL**21** and TE-SL**20** *resp.*). In addition, TE-SL**20** and TE-SL**21** display different EL spectra and hence different CIE coordinates. EL spectrum of TE-SL**20** presents, in addition to the band centred at 432 nm, an additional GEB at ca. 540 nm. The chromatic coordinates of the devices TE-SL**20** are (0.24, 0.24) corresponding to a light blue colour. Interestingly, TE-SL**21** exhibits a nice structureless band with a maximum at 447 nm without any undesired GEB, clearly signifying that the molecules of **21** in the thin-film are isolated enough to avoid any π-π intermolecular interaction. This site isolation is a key feature to ensure an efficient fluorescence and highlights the potential of the molecular design of **21** for blue OLED applications. This specific architecture allowing intramolecular interactions between the cofacial "2,7-bis(3,4,5-trimethoxyphenyl)-9H-fluorene" units is an interesting platform to reach deep-blue emission at wavelengths impossible to reach with structurally related oligo "aryl-fluorenyl-aryl" derivatives. Despite very weak performances were obtained in these works, the molecular design strategy, using intramolecular interaction to generate blue light, was interesting and has then led later to more efficient green and blue multi-layer devices.[35b, 39b, 43]

Device numbering and structure		V_{on} [V]	λ_{EL} [nm]	EQE_{max} [%]	CE_{max} [cd A^{-1}]	PE_{max} [lm W^{-1}]	CIE 1931 [x, y]	Ref
SP-SL**18**	ITO/PEDOT:PSS/**18**/Al	15	438	-	0.07	-	-	[53]
SP-SL**19**	Device 1 **19**	< 2	480	1.5 10^{-3}	1.5 10^{-3}	-	0.17, 0.36	[19]
TE-SL**20**	ITO/PEDOT/**20**(50nm)/Ca	7.2	432	-	0.031	0.011	0.24, 0.24	[35b]
TE-SL**21**	ITO/PEDOT/**21**(45nm)/Ca	5	447	-	0.037	0.018	0.19, 0.19	[35b]
TE-SL**22**	Device 1 **22**(80nm)	2.8	471	-	2.0	-	0.16, 0.20	[54]
TE-SL**23**	Device 1 **23**(80nm)	2.9	479, 484(sh)	-	2.6	-	0.15, 0.24	[54]
TE-SL**24**	Device 1 **24**(80nm)	2.9	470	-	0.005	-	0.15, 0.24	[54]
SP-SL**25**	Device 1 **25**(80nm)	5	-	-	0.006	-	0.16, 0.15	[55]
SP-SL**26**	Device 1 **26**(80nm)	6.6	-	-	0.06	-	0.16, 0.16	[55]
SP-SL**27**	Device 1 **27**(80nm)	5.2	-	-	0.24	-	0.16, 0.20	[55]
SP-SL**28**	ITO/PEDOT:PSS/**28**/Ba/Al	5.8	442	0.82	-	-	0.16, 0.08	[56]
SP-SL**29**	Device 1 **29**	4.5	-	0.24	0.16	0.09	0.18, 0.06	[12]
SP-SL**30**	Device 1 **30**	5.3	-	0.11	0.05	0.02	0.17, 0.04	[12]

Table 5. Performance of SL-devices with OSC **18-30** as EML

Pyrene-based dendrimers with different peripheral donor chromophores have also been used in SL-OLEDs. In a first series, the central pyrenyl core is directly linked to four donor groups: 4-phenoxyphenyl in **22**, 3,4,5-trimethoxyphenyl in **23**, 4-(methyl-thio)phenyl in **24** (Figure 3).[54] TE-SL**22** and TE-SL**23** present interesting performances. These devices emit sky-blue light (CIE: 0.16, 0.2 and 0.15, 0.24, *resp.*) since 2.8/2.9 V and CE_{max} reach 2.0 and 2.6 cd A^{-1} *resp.* The presence of the sulfur atom in **24** leads to very low performance for TE-SL**24** (CE_{max} 0.005 cd A^{-1}). Note that **24** possesses a lower Φ^{film} (0.50) compare to **22** or **23** (0.75 and 0.88 *resp.*).

	$\lambda_{abs}{}^{sol}$/ $\lambda_{abs}{}^{film}$ [nm]	$\lambda_{PL}{}^{sol}$/ $\lambda_{PL}{}^{film}$ [nm]	Φ^{sol}/ Φ^{film} [%]	HOMO [eV]	LUMO [eV]	Ref
18	325/356,325,400	402, 420/438	77/-	-5.71[a]	-2.91[b]	[53]
19	412/422	490/480	45/-	-5.49[a]	-2.82[b]	[19]
20	314,331,337,345(THF)/317,334,341,351	381,393(THF)/406	75/-	-5.49[a]	-2.04[c]	[35b]
21	314(sh),328,340(THF)/330, 350	457(THF)/463	35/-	-5.33[a]	-1.94[c]	[35b]
22	From 384(CyHx) to 391(DMF)/-	From 425(CyHx) to 434(DMSO)/-	98($CHCl_3$)/74.7	-5.40[a]	-2.45[c]	[54]
23	From 384(CyHx) to 395(DMSO)/-	From 432(CyHx) to 440(DMSO)/-	85($CHCl_3$)/88.1	-5.40[a]	-2.45[c]	[54]
24	From 396(CyHx) to 403(DMSO)/-	From 437(CyHx) to 450(DMSO)/-	80($CHCl_3$)/50.6	-5.40[a]	-2.52[c]	[54]
25	308,392(THF)/311,391	432(THF)/451	65-71(THF)/-	-5.36[a]	-2.40[a], -2.42[c]	[55]
26	298,392(THF)/299,393	430(THF)/434	59-75(THF)/-	-5.59[a]	-2.44[a], -2.63[c]	[55]
27	312,370(THF)/ 314,370	432(THF)/445	59-54(THF)/-	-5.27[a]	-2.35[a], -2.33[c]	[55]
28	261, 360, 375, 400/261, 360, 375, 400	416, 434(sh)/418, 433(sh)	100/-	-5.65[a]	-2.76[c]	[56]
29	348,298/-	394,414/407,426	94/52	-5.52[a]	-2.32[c]	[12]
30	349,298/-	395,417/406,426	69/36	-5.35[a]	-2.15[c]	[12]

DMF: N,N-dimethylformamide, DMSO:dimethyl sulfoxide, [a]: from cyclic voltammetry, [b]: from theoretical calculation, [c]: from ΔE^{opt}-$HOMO^{el}$

Table 6. Selected electronic properties of OSCs **18-30**

In a second series (**25-27**), the central pyrenyl core is even more decorated with four terphenyl cores, each of them substituted by two donor groups: triphenylamine in **25**, 3,6-di-*tert*-butyl-9-phenyl-9*H*-carbazole in **26** and N,N-diphenylnaphthalen-2-amine in **27** (Figure 3).[55] In solid state, these fluorophores emit from the central pyrenyl core with PL spectra centred around 435-450 nm. SP-SL**25**-SP-SL**27** are less efficient than the above described TE-SL**22**-TE-SL**23**. SP-SL**27** emits a blue light (CIE: 0.16, 0.20) at 5.2 V and reaches 0.24 cd A^{-1}. Despite **22** and **23** possess similar energy gap of 2.95 eV, the V_{on} of TE-SL**22** and TE-SL**23** are lower (2.8/2.9 V) than that of SP-SL**27** (5.2 V). The efficiencies difference may come from the EML deposition process (TE *vs* SP). This seems to indicate that the design of **25-27** with the four terphenyl antenna around the central pyrene core is not favourable to obtain efficient blue emitters. Finally, compared to the previously described **9** and **10** pyrene-centred oligofluorenes, the emitted colour with the present D-π-D compounds appears blue shifted with CIE: 0.16, 0.15 for SP-SL**25** or 0.16, 0.20 for SP-SL**27** and 0.19, 0.32 for SP-SL**9** and 0.20, 0.32 for SP-SL**10**.

Anthracene-cored dendrimer (**28**, Figure 3) using 1,3,5-phenylene-based dendrons is highly soluble due to the presence of the six 2-ethylhexyloxy peripheral groups and has been used in SP-SL**28**.[57] The device reveals an interesting EQE of 0.82 %, a V_{on} of 5.8 V and the EL spectrum shows emission maximum at 442 nm (CIE: 0.16, 0.08).

Other deep-blue emitting terfluorenes (**29** and **30**) constructed on **2** and functionalized with donor carbazole dendrons have also been designed.[12] In **29**, the terfluorenyl core is decorated by six carbazole units. In **30**, each carbazole unit is linked to two additional carbazoles leading to a shell of eighteen carbazoles around the central terfluorenyl unit. As reported above for SP-SL**2**, the EL spectrum of SP-SL**29** is not stable and is dependent on the driving voltage. When increasing the driving voltage from 6 V to 14 V, a distinct broad emission

band in the range of 480-700 nm appears in addition to the classical blue emission at 400/430 nm. This evolution of the EL spectrum leads to the shift of the emitted colour from blue (CIE: 0.18, 0.06) to pink (CIE: 0.29, 0.15). The parasite emission for SP-SL**29** has been ascribed by the authors to "electromer" emission, which means emission from a pair of chemically identical molecules charged by electrons and holes, which are statistically independent of each other.[39b, 57] This is a regular issue in SL-OLEDs.

Such evolution of the EL spectrum was nevertheless not observed for SP-SL**30** where the blue emission remains stable whatever the driving voltage (CIE: 0.17, 0.04). However, despite the excellent EL stability, SP-SL**30** performances are modest with EQE_{max} only reaching 0.11 % compared to 0.24 % obtained with SP-SL**29**.

The presence of the N-phenyl-carbazole at C9 position of the fluorene units suppress the aggregation of the terfluorene backbone and therefore improve the colour stability of **30**. This effect is not observed for **29**. However, despite an increase of the HOMO energy level of **30** (-5.35 eV) compare to that of **29** (-5.52 eV) and that of **2** (-5.71 eV) thanks to the introduction of the carbazole dendrons around the terfluorenyl core, the performance of SP-SL**30** remains weak. The easier hole injection from PEDOT:PSS to **30** is not sufficient to increase the excitons formation probably due to unbalanced charge transport in the EML.

3.3. Branched and star-shaped OSCs with non-conjugated donor-carbazoles

With the aim of increasing the hole injection and of improving the quality of the films while retaining optical, thermal and electronic properties of the emitting cores, the group of Ma has designed a series of OSCs in which carbazole donor units are linked through non-conjugating alkyl spacers (butyl or hexyl) to different π-systems (**Figure 4**).[58]

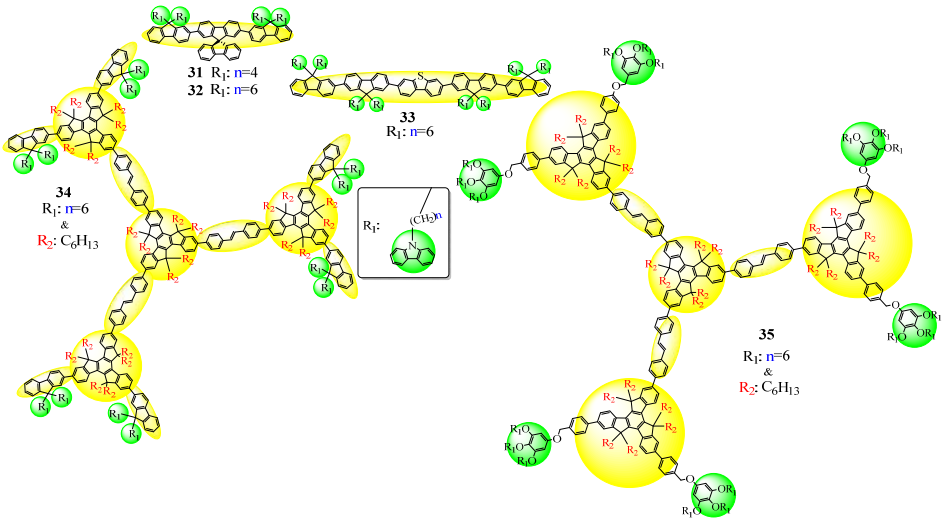


Figure 4. Branched or star-shaped OSCs with non-conjugated carbazoles (OSCs **31**-**35**)

The different OSCs possess an extended π-system that is a terfluorene in **31**[59] and **32**[58a, 58b, 59] or a dibenzothiophene linked to two difluorenyl units in **33**.[58e] Depending on the number of fluorenyl units, those devices are therefore decorated with either four carbazole units in **31**-**32** or with eight carbazole units in **33**. Except for **31**, in which the fluorene-carbazole linkage is a *n*-butyl linkage, the linkage between the C9 atom of the fluorene and the nitrogen atom of the carbazole is an hexyl chain.

Device numbering and structure		V_{on} [V]	λ_{EL} [nm]	EQE_{max} [%]	CE_{max} [cd A^{-1}]	CIE 1931 [x, y]	Ref
SP-SL**31**	ITO/PEDOT:PSS(30nm)/**31**/Ba/Al	-	-	0.36	0.13	-	[59]
SP-SL**32**a	ITO/PEDOT:PSS(30nm)/**32**(~80nm)/Ba(5nm)/Al(200nm)	4.5	416	0.31	0.11	0.16, 0.05	[58a, 58b]
SP-SL**32**b	ITO/PEDOT:PSS(30nm)/**32**/Ba/Al	-	-	1.89	0.69	-	[59]
SP-SL**33**	ITO/PEDOT:PSS(40nm)/**33**(80nm)/CsF(1.5nm)/Al(120nm)	3.4	-	1.70	0.90	0.17, 0.09	[58e]
SP-SL**34**	ITO/PEDOT:PSS/**34**(100nm)/Ba/Al	3.7	430, 460	-	0.40	0.15, 0.09	[20]
SP-SL**35**	ITO/PEDOT:PSS/**35**(100nm)/Ba/Al	3.2	430, 460	-	0.65	0.15, 0.09	[20]

Table 7. Performance of SL-devices with OSC **31**-**35** as EML

	λ_{abs}^{sol}/ λ_{abs}^{film} [nm]	λ_{PL}^{sol}/ λ_{PL}^{film} [nm]	Φ^{sol}/ Φ^{film} [%]	HOMO [eV]	LUMO [eV]	Ref
31	346(THF)/-	394(THF)/425	99/-	-5.49[a]	-	[59]
32	346(THF)/292, 349	394(THF)/425	99/-	-5.47[a]	-	[59]
33	369(THF)/372	410(THF)/443	93/36	-5.43[a]	-2.44[a,b]	[59]
34	347, 365(sh),384(sh)(THF)/-	430,460(THF)/-	95/21	-5.60[a]	-2.60[b]	[20]
35	330, 378(THF)/-		94/19	-5.70[a]	-2.70[b]	[20]

[a]: from cyclic voltammetry, [b]: from ΔE^{opt}-HOMO[el]

Table 8. Selected electronic properties of OSCs **31**-**35**

SP-SL**33** emits light since 3.4 V, reaches a high EQE_{max} of 1.7 % and presents a blue emission (CIE: 0.17, 0.09) (**Table 7**). SL-OLEDs with a different cathode (Ba/Al instead of

CsF/Al) were tested using **31** or **32** as EML. The best performances are reported for SP-SL**32**b (EQE_{max}: 1.89 %). As the only difference between **32** and **31** is the length of the alkyl chain between the fluorene and the carbazole, which has no significant impact on their HOMO/LUMO energy levels (**Table 8**), the difference of performance between the two SL-OLEDs is therefore related to the morphological film properties.

The efficiencies of SP-SL**31** and SP-SL**32**b are strongly higher than that using a model compound[59] with hexyl chains instead of carbazole units as EML (CE_{max} = 0.13 cd A^{-1} , 0.69 and 0.0048[59] cd A^{-1} respectively). This can be assigned to a better hole injection in the formers due to the presence of electron-rich carbazoles units.

34 and **35** are extended star-shaped π-conjugated dendrimers based on truxenyl cores decorated by non-conjugated carbazoles linked by fluorenyl groups (**34**) or by trialkyloxyphenyl (**35**) (Figure 4).[20] Both dendrimers show good solubility in common organic solvents, which is a good criterion for solution processed devices preparation. **34** and **35** possess similar energy gap (3 eV) indicating that the modification of the periphery of the dendrimers does not affect their effective conjugation length (Table 8). SP-SL**34** and SP-SL**35** present similar EL spectra than SP-SL**12** possessing a truxene central core decorated by three additional truxene units showing that the functionalization of the dendrimers only changes the charge transport without changing the HOMO/LUMO energy levels. This is a crucial point when designing such fluorophores. With the same device structure, SP-SL**34** and SP-SL**35** show a pronounced enhancement of CE_{max} compared to SP-SL**12**. CE_{max} increases from 0.07 cd A^{-1} for SP-SL**12** to 0.4 cd A^{-1} for SP-SL**34** and 0.65 cd A^{-1} for SP-SL**35**. These results may indicate that the introduction of carbazole units effectively improves the balance of electron and hole transport significantly enhancing the device performances.

3.4. D-$(\pi)_3$ and D-$(\pi)_6$ design

Other star-shaped molecules with central donor cores surrounded by fluorescent chromophores have also been designed. This design has been called herein **D-$(\pi)_3$** or **D-$(\pi)_6$** as a function of the number of substituting aromatic units (**Figure 5**). The central donor core is either a triphenylamine (**36-37**), a carbazole (**38**) or a triazatruxene (**39-43**) whereas the fluorescent external chromophore consists either in: (i) two pyrenyl and one fluorenyl units (**36**), (ii) three fluorenyl units (**39**), (iii) three difluorenyl units (**40**), (iv) three terfluorenyl units (**37-38** and **41**) or (v) six difluorenyl units (**42**) or six terfluorenyl units (**43**). SL-OLEDs have been prepared with nevertheless different architectures rendering the comparison of the device performances quite difficult.

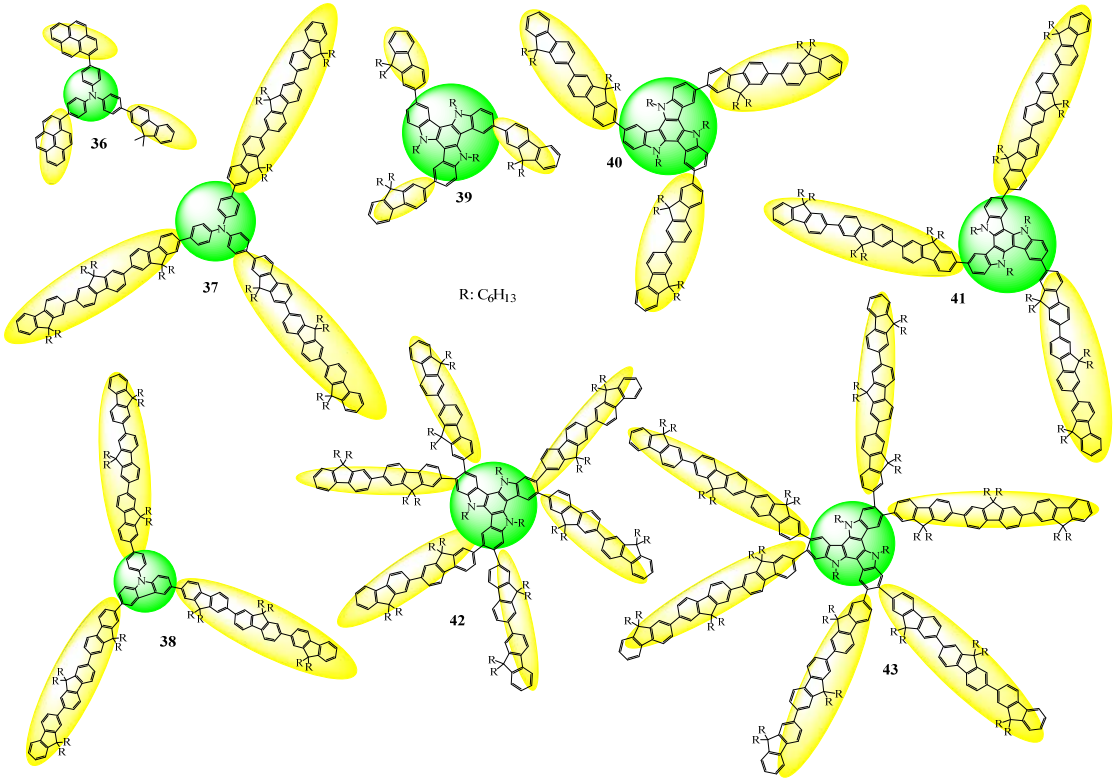


Figure 5. Donor-$(\pi)_3$ and Donor-$(\pi)_6$ design (OSCs **36-43**)

Device numbering and structure		V_{on} [V]	λ_{EL} [nm]	EQE_{max} [%]	CE_{max} [cd A^{-1}]	PE_{max} [lm W^{-1}]	CIE 1931 [x, y]	Ref
TE-SL**36**	ITO/**36**(100nm)/LiF(0.5nm)/Mg:Ag	2.7	476	-	0.07	-	0.17, 0.29	[60]
SP-SL**37**	ITO/PEDOT:PSS/**37**/LiF/Ca/Al	4	437, 457(sh)	-	-	-	0.16, 0.08	[61]
SP-SL**38**	ITO/PEDOT:PSS/**38**/LiF/Ca/Al	6	415, 437, 467(sh)	-	-	-	0.18, 0.11	[61]
SP-SL**39**	ITO/PEDOT:PSS/**39**(100nm)/Ba/Al	4	454	0.24	0.17	-	0.17, 0.14	[62]
SP-SL**40**a	ITO/PEDOT:PSS/**40**(100nm)/Ba/Al	3.5	444, 465(sh)	1.35	0.98	-	0.16, 0.14	[62]
SP-SL**40**b	Device 1 **40**	3.5	444, 460	-	0.9	0.8	0.15, 0.10	[63]
SP-SL**41**a	ITO/PEDOT:PSS/**41**(100nm)/Ba/Al	3.3	444, 465(sh)	2.16	1.56		0.16, 0.15	[62]
SP-SL**41**b	Device 1 **41**	3.5	444, 460	-	1.7	1.7	0.15, 0.11	[63]
SP-SL**41**c	ITO/PEDOT:PSS/**41**/LiF(3nm)/Ca(20nm) /Al(100nm)	4.0	-	-	1.0	0.7	0.15, 0.10	[63]
SP-SL**42**	Device 1 **42**	3.5	441, 460	-	0.7	0.6	0.15, 0.11	[63]
SP-SL**43**a	ITO/PEDOT:PSS/**43**(130nm)/Ba/Al	5.3	442	2	2.07		0.15, 0.09	[64]
SP-SL**43**b	Device 1 **43**	3.5	442, 460	-	1.4	1.2	0.15, 0.12	[63]
SP-SL**43**c	ITO/PEDOT:PSS/**43**/LiF(3nm)/Ca(20nm) /Al(100nm)	4.0	-	-	2.0	1.7	0.15, 0.11	[63]

Table 9. Performance of SL-devices with OSC **36-43** as EML

	λ_{abs}^{sol}/ λ_{abs}^{film} [nm]	λ_{PL}^{sol}/ λ_{PL}^{film} [nm]	Φ^{sol}/ Φ^{film} [%]	HOMO [eV]	LUMO [eV]	Ref
36		425(DCM)/470	63(DCM)/-	-5.50[b]	-2.80[c]	[60]
37	383(THF)/379	440(THF)/436,455(sh)	87(THF)/76	-5.66[a]	-2.02[a]	[61]
38	366(THF)/367.5	407,431(sh)(THF)/414,436,464(sh)	81(THF)/72	-5.75[a]	-2.07[a]	[61]
39	350.5(THF)/350.5	430(THF)/434	52(THF)/45	-5.19[a]	-2.27[a]	[62]
40	371.5(THF)/368	446(THF)/444	75(THF)/68	-5.28[a]	-2.23[a]	[62-63]
41	374(THF)/373	443(THF)/442	80(THF)/76	-5.27[a]	-2.15[a]	[62]
42	360(THF)/363	440(THF)/439,456	85/73	-	-	[63-64]
43	366.5(THF)/373	440(THF)/437,455	88/75	-	-	[63-64]

[a]: from cyclic voltammetry, [b]: from ultraviolet photoelectron spectroscopy, [c]: from ΔE^{opt}-$HOMO^{el}$ -: not available

Table 10. Selected electronic properties of OSCs **36-43**

First, **39-41** only differ by the length of the oligofluorenyl units surrounding the central triazatruxene electron-rich core. The EL spectrum of SP-SL**39** exhibited a maximum at 454 nm (CIE: 0.17, 0.14, V_{on} of 4 V) and those of SP-SL**40**a and SP-SL**41**a are similar with a maximum at 444 nm (CIE: 0.16, 0.14 and 0.16, 0.15 *resp.*, V_{on} of 3.5/3.3 V) (same device architecture, ITO/PEDOT:PSS/EML(100nm)/Ba/Al)[62] (**Table 9**). The λ_{max} of the EL spectra seem hence to be only weakly dependent of the number of fluorenyl units. What is therefore the impact of the fluorene chains on the device characteristics?

SP-SL**39** reaches EQE_{max} of only 0.24 %, whereas that of SP-SL**40**a reaches 1.35 %, the best performance was obtained with SL**41**a with a high EQE_{max} of 2.16 %. The low V_{on} of the three device indicates an efficient charge injection likely due to the high-lying HOMO energy levels of the three azatruxene hybrids (-5.19, -5.28 and -5.27 eV for **39-41** *resp.*) (**Table 10**).

These HOMO levels match well the anode WF (-4.8 to -5.2 eV[48]) and thereby facilitate hole injection in the device. If the EL spectra remain roughly similar, both EQE and CE increase significantly with increasing the length of the oligofluorenyl arms. Moreover, the best device performance obtained with **41** may be linked to its larger molecular size and more bulky star-shaped architecture which give to this OSC better amorphous film forming ability and morphological stability.[62]

Changing the cathode, (using Ca/Al cathode[63] instead of Ba/Al cathode) in SP-SL**41**b has allowed to keep similar performance (1.7 Cd/A) but a bluest emission (0.15, 0.11) is reached. On the other hand, intercalation of a 3 nm thick interfacial LiF layer between the active material and the Ca cathode layer in SP-SL**41**c leads to a lowering of the performances with an increase of V_{on} from 3.5 to 4.0 V and a decrease of CE_{max} (1 cd A^{-1}) keeping nevertheless similar CIE (0.15, 0.10). All these results point the importance of the cathode choice and its influence on the SL-OLED performances.

SP-SL**37**, SP-SL**38** and SP-SL**41**c with the configuration ITO/PEDOT:PSS/EML(100nm)/-LiF/Ca/Al were also fabricated. The three OSCs only differ by their central donor core: a triphenylamine in **37**, a carbazole in **38** or a triazatruxene in **41**. SP-SL**37**-SP-SL**38** EL spectra are similar to their respective solid state PL spectra. The emission of SP-SL**38** is however red-shifted compared to that of SP-SL**37** and SP-SL**41**c with CIE of (0.18, 0.11), (0.16, 0.08) and (0.15, 0.10) *resp.* For the three devices, only luminance values are reported, 7390 cd m^{-2} for SP-SL**41c**, 830 cd m^{-2} for SP-SL**37** and 220 cd m^{-2} for SP-SL**38**. From these results, one may note that with three similar terfluorenyl antennas, the fluorophore with the central triazatruxene leads to higher OLED efficiency than those with the central triphenylamine or carbazole. This order of efficiency is in accordance with the HOMO energy levels of the three compounds -5.27 eV for **41**,[62] -5.66 eV for **37**[61] and -5.75 eV for **38**.[61]

Finally, **36**, a triphenylamine core decorated by two pyrenes and one fluorene (Figure 5)[60] was used in TE-SL**36** leading to a blue light emission (λ_{EL} at 476 nm and CIE:0.17, 0.29) at a low V_{on} of 2.7 V. The SL-OLED efficiency is however very low with CE_{max} reaching only 0.07 cd A^{-1}.

At the light of the results obtained with **40** and **41** with a central triazatruxene decorated with oligofluorenes, the same group has also synthesized triazatruxenes decorated by six difluorenyl groups in **42** or six terfluorenyl groups in **43**.[63] Different device configurations have been tested in SP-SL**42** and SP-SL**43**a-**43**c. All devices emit blue light with λ_{EL} around 442 nm (CIE: 0.15, 0.1). The blue emission is similar to that obtained with SP-SL**40** and SP-SL**41** and is driven by the oligofluorenyl antennas.

Due to the different device configurations, comparison between SP-SL**40**-SL**43** is not easy. At a first look, the best results are obtained with the six terfluorenyl decorated truxene **43**.

SP-SL**43**a[64] reaches a high EQE_{max} of 2.07 % comparable to the performance of SP-SL**41**a (2.16 %[62]). The only difference is V_{on}, which is higher for SP-SL**43**a (5.3 *vs* 3.3 V).

Changing the cathode from Ba/Al to Ca/Al in SP-SL**43**b leads to a V_{on} decrease from 5.3 to 3.5 V but also to a decrease of the performance especially CE which is lowered from 2.07 to 1.4 cd A^{-1}.[63] Such variation is not the same than that reported above with **41** as EML[62] (from 3.3 to 3.5 V for V_{on} and from 1.56 to 1.7 cd A^{-1} for CE from SP-SL**41**a to SP-SL**41**b).

The comparison of the devices performance with Ca/Al cathodes shows that the efficiency obtained with SP-SL**43**b (CE_{max}: 1.4 cd A^{-1}) is higher than that obtained with SP-SL**42** (CE_{max}: 0.7 cd A^{-1}) following the same trend than that observed for SP-SL**41** and SP-SL**40** (CE_{max}: 1.7 cd A^{-1} for SL**41**b *vs* 0.9 cd A^{-1} for SL**40**b). With this device architecture, SL-OLED performances increase as follows: **42** < **40** < **43** < **41**.

Finally, intercalation of a 3 nm thick interfacial LiF layer between the EML and the Ca cathode layer in SP-SL**43**c leads to an increase of the OLED performance from 1.4 cd A^{-1} in SP-SL**43**b to 2.0 cd A^{-1} in SP-SL**43**c. An increase of V_{on} from 3.5 to 4.0 V is nevertheless observed and similar emitted colour is observed. It should be noted that the presence of LiF between **41** and the Ca cathode was shown to induce a decrease of the performances (see above), a different result is obtained in the case of **43**.

In the present series, the best performances were obtained for SP-SL**43**a and SP-SL**43**c with either a Ba/Al or a LiF/Ca/Al cathode. As pointed above with **40** and **41**, the terfluorenyl units in **43** seem to improve the charge injection and transport in the EML compared to the bifluorenyl units in **42**. Increasing the number of terfluorenyl units decorating the central azatruxene core (from three in **41** to six in **43**) also leads to an increase of the performance except for SP-SL(**41**b-**43**b) with Ca/Al cathodes. With this configuration, the interface between Ca and **43** seems to be deleterious for the electron transfer and the devices SP-SL**43**b are slightly less efficient (1.4 cd A^{-1}) than SP-SL**41**b (1.7 cd A^{-1}).

All the results obtained from devices using azatruxene decorated OSCs (**39**-**43**) demonstrate the difficulty to precisely compare the efficiencies of the different devices as they depend not only on the fluorophore but also on the nature of the electrodes. Such a type of molecules display nevertheless interesting performances.

3.5. D-$(D)_2$, D-$(D)_3$ and D-$(D)_6$ design

Around the carbazole or the triazatruxene fragments, many different molecular designs have been developed. The chemical decoration is often done as exposed above by incorporation of electron-rich fragments. The number of pending units and the shape of the molecule are very important in the SL-OLED performance. This is the strategy exposed in this part. N-substituted carbazole (D-$(D)_2$ **44**[65], **45**[66] and **46**-**47**[67] or D-$(D)_3$ **48**-**49**[67]), triphenylamine

(D-(D)$_3$ **50**[68]) or triazatruxene (D-(D)$_6$ **51**[69]) are the central cores of all the molecules described in this part (**Figure 6**).

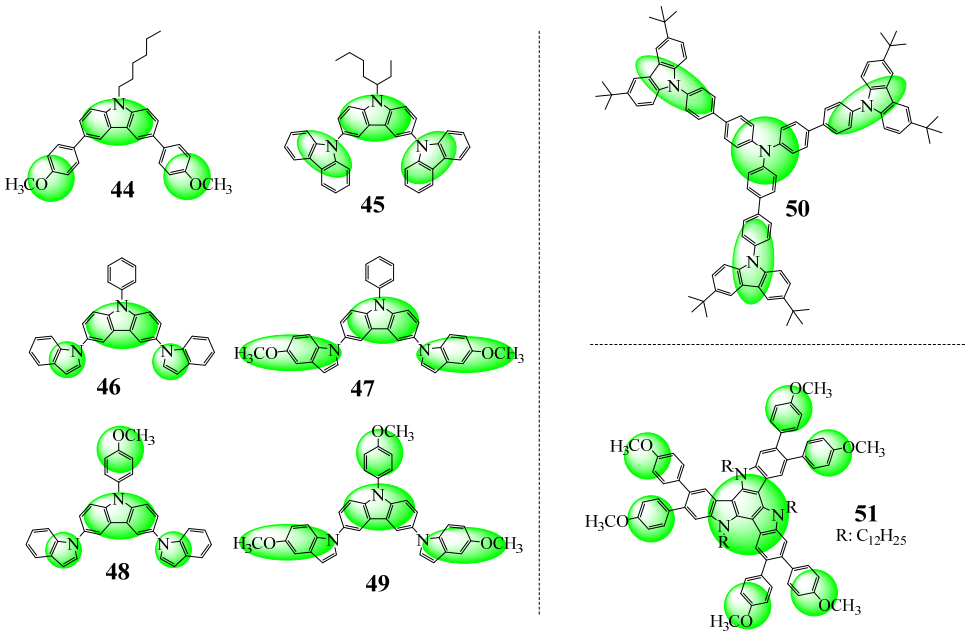


Figure 6. D-(D)$_2$, D-(D)$_3$ and D-(D)$_6$ design (OSCs **44**-**51**)

44 and **45** have identical energy gaps (3.17[65] eV and 3.19[70] eV, *resp.*) and their PL spectra are both centred in the blue emission range (**Table 11**). TE-SL**45** emits light since 4.5 V and reaches a high EQE of 1.72 % (CE_{max}: 11.5 cd A^{-1}) whereas SP-SL**44** emits light since 8.5 V and only reaches 0.062 cd A^{-1} (**Table 12**). The EL spectra of the two devices are similar to their solid-sate PL spectra. Comparison of the two devices performances must be treated with caution as in TE-SL**45**, a thin layer of CuI is used instead of PEDOT:PSS as the HIL. It has been shown that ITO/CuI possesses a slightly deeper HOMO (-5.2 eV) than ITO/PEDOT:PSS (-5.1 eV) improving the hole injection in the EML.[71] As CuI is deposited by thermal evaporation, this also leads to a better interface between the CuI amorphous film and the EML (a thickness of 12 nm for the CuI deposit has been demonstrated to be an optimal value).[71]

	λ_{abs}^{sol}/ λ_{abs}^{film} [nm]	λ_{PL}^{sol}/ λ_{PL}^{film} [nm]	Φ^{sol}/ Φ^{film} [%]	HOMO [eV]	LUMO [eV]	Ref
44	295,352,367(ACN)/-	407(ACN)/408	19(ACN)/-	-5.67[a]	-2.50[c]	[65]
45	344(Tol)/-	389(Tol)/394,410	-	-5.8[a]	-2.6[c]	[66, 70, 72]
46	251,270,296,349/312,375	387,404/396(sh),411	-	-5.68[b]	-2.56[c]	[67]
47	253,278,306,352/315,377	394,408/398,416	-	-5.52[b]	-2.38[c]	[67]
48	251,271,292(sh),352/312,376	391,406/397,415	-	-5.56[b]	-2.54[c]	[67]
49	251,278,308,353/312,367	396,409/404,418	-	-5.45[b]	-2.32[c]	[67]
50	240, 298, 353 (DCM)	404(Tol)/430	63(Tol)/-	-5.21[a]	-2.2[c]	[68]
51	391(DCM)/409	403,418(DCM)/426	-	-5.07[a]	-2.43[c]	[69]

ACN: acetonitrile, [a]: from cyclic voltammetry, [b]: from Electron Photoemission Spectroscopy, [c]: ΔE^{opt}-HOMO

Table 11. Selected electronic properties of OSCs **44-51**

Device numbering and structure		V_{on} [V]	λ_{EL} [nm]	EQE_{max} [%]	CE_{max} [cd A^{-1}]	CIE 1931 [x, y]	Ref
SP-SL**44**	ITO/**44**/Ca/Al	8.5	420	-	0.062	0.22, 0.21	[65]
TE-SL**45**	ITO/CuI/**45**(120nm)/Ca/Al(100nm)	4.5	388,406	1.72	11.5	-	[66]
TE-SL**46**	ITO/CuI/**46**(30nm)/Ca/Al	6.2	425	3.5	3.7	-	[67]
TE-SL**47**	ITO/CuI/**47**(30nm)/Ca/Al	4	400	4.8	4.0	-	[67]
TE-SL**48**	ITO/CuI/**48**(30nm)/Ca/Al	4	400	5.2	4.2	-	[67]
TE-SL**49**	ITO/CuI/**49**(30nm)/Ca/Al	3	425	2	3.6	-	[67]
SP-SL**50**	ITO/PEDOT:PSS(40nm)/**50**/LiF(1nm)/Al(100nm)	>8	-	-	<0.01	-	[68]
SP-SL**51**	ITO/**51**(80nm)/Ca-Al	2.8	408, 427, 439	-	-	0.16, 0.16	[69]

Table 12. Performance of SL-devices with OSC **44-51** as EML

46-**47** (D-$(D)_2$) and **48**-**49** (D-$(D)_3$) possess a central N-phenyl-carbazole (**46**-**47**) or N-(4-methoxyphenyl)-carbazole (**48**-**49**) substituted by indole or 5-methoxyindole units.[67] Solid-state PL spectra of **46**-**49** present two maxima around 400 nm without significant modulation induced by the methoxy groups. Nevertheless TE-SL(**46**-**49**) show different device performances. The EL spectra of TE-SL**47** and TE-SL**48** are identical to their respective solid state PL spectra. Oppositely, the EL spectra of TE-SL**46** and TE-SL**49** are broadened and red shifted compared to their PL spectra. The additional lower energy band is ascribed by the authors[67] to excimer emission.[43] The best device performances are obtained with TE-SL**48** with a low V_{on} of 4 V and a very high EQE_{max} of 5.2 %. As far as we know, this is the highest performance reported to date. Then, the device performances decrease from TE-SL**47** (V_{on}: 4 V and EQE_{max} 4.8 %), TE-SL**46** (V_{on}: 6.2 V and EQE_{max} 3.5 %) to TE-SL**49** (V_{on}: 3 V and EQE_{max} 2 %), all being nevertheless very high. The highest V_{on} is detected for TE-SL**46** (6.2 V) and the lowest for TE-SL**49** (3 V). This feature is in accordance with the corresponding HOMO levels: -5.68 eV for **46** and -5.45 eV for **49** indicating a more difficult charge injection in **46**

than in **49**. Thus, in **49**, the three methoxy groups borne by the molecules renders the charge injection easier. To sum up, all the devices (TE-SL**46-49**) display very high performances showing the efficiency of this molecular design.

It should be stressed that the performances of TE-SL**45-49** are higher than that of SP-SL**44** probably due to the intercalation of the thin CuI hole injecting layer between ITO and EML (and not from the OSC design).

On the other hand and despite a similar molecular design, SP-SL**50**[68] was almost not emissive (V_{on}: 8V and CE_{max} below 0.01 cd A^{-1}). This low performance is explained by the authors by an unbalanced hole and electron injection, the hole transport being strongly dominant. This shows the difficulty to properly design OSCs for SL-OLEDs.

Finally, the D-$(D)_6$ star-shaped **51** (Figure 6) with a central triazatruxene surrounded by six methoxyphenyl units, has been spin-coated as EML in SP-SL**51**. The device exhibited a deep blue emission (CIE: 0.16, 0.16) with λ_{EL} at 427 nm. The V_{on} (2.8 V) is very low suggesting a negligible barrier for hole injection due to a good alignment between PEDOT:PSS and the HOMO energy level of **51** (-5.07 eV). Unfortunately, no EQE or CE values were reported in this work. To conclude, it appears difficult to precisely evaluate the impact of the fluorophore due to the different device architectures and fabrication processes. Nevertheless, TE-SL**47** and TE-SL**48** reach the highest performance with very high EQE around 5 %.

It should be mentioned that other associations of donor fragments (phenoxy, carbazole or xanthene) with different π-conjugated systems (fluorene, pyrene, DHIF and pentaphenylene) have been developed with nevertheless low performances (**52-56**, in **Figure 7**).[30a, 60, 65, 68, 71, 73] The main physicochemical properties of these OSCs and the performances of their related devices (SL**52**-SL**56**) are gathered in **Table 13** and **Table 14** but will not be discussed herein.

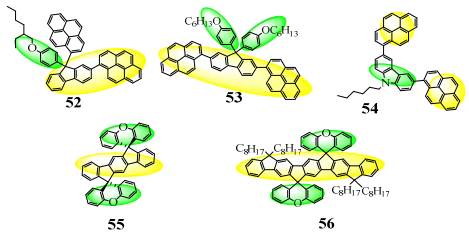


Figure 7. Bridged Oligophenylenes substituted with Donor groups (OSCs **52-56**)

	λ_{abs}^{sol}/ λ_{abs}^{film} [nm]	λ_{PL}^{sol}/ λ_{PL}^{film} [nm]	Φ^{sol}/ Φ^{film} [%]	HOMO [eV]	LUMO [eV]	Ref
52	351/355	405/467	75/-	-5.39[c]	-2.41[a]	[73a, 73b]
53	368(THF)/370	432(THF)/472	-/46	-5.08[b]	-1.63[b]	[73c]
54	279,345(ACN)/-	443(ACN)/458	56(ACN)/-	-5.74[c]	-2.80[a]	[65]
55	298,309,328,335,344(CyHx)/315,346	347,355,364(CyHx)/372,388,411(sh)	63(CyHx)/-	-5.79[c]	-2.15[c], -2.23[a]	[30a]
56	338,371,391(CyHx)/338,375,396	395,419,445,475(CyHx)/403,427,453,480	91(CyHx)/-	-5.45[c]	-2.20[c], -2.36[a]	[30a]

[a]: from ΔE^{opt}-HOMO, [b]: from theoretical calculation, [c]: from cyclic voltammetry

Table 13. Selected electronic properties of OSCs **52-56**

Device numbering and structure		V_{on} [V]	λ_{EL} [nm]	CE_{max} [cd A^{-1}]	CIE 1931 [x, y]	Ref
SP-SL**52**	ITO/PEDOT:PSS(40nm)/**52**(80nm)/CsF(2nm)/Al(120nm)	4.3	495	1.3	0.24, 0.37	[73a]
SP-SL**53**	ITO/PEDOT:PSS/**53**/Al	3.4		0.04	0.16, 0.14	[74]
SP-SL**54**	ITO/**54**/Ca-Al	9	460	0.112	0.18, 0.21	[65]
TE-SL**55**	ITO/PEDOT:PSS/**55**/Ca	12.7	413	0.018	0.18, 0.08	[30a]
TE-SL**56**	ITO/PEDOT:PSS/**56**/Ca	5.8	403+GEB	0.08	0.35, 0.38	[30a]

Table 14. Performance of SL-devices with OSCs **52-56** as EML

3.6. π-Acceptor design (π-A)

Although numerous OSCs have been investigated for applications in blue OLEDs, their vast majority present dominant p-type properties. Developing n-type OSCs incorporating electron-poor fragments is far less common and, to our knowledge, literature reports only nine examples of fluorophores with a formal π-A design, **57-65** (**Figure 8**), used as EML in blue SL-OLEDs (for clarity purpose, the acceptor groups are highlighted in pink in the following sections). Indeed, if many electron-poor OSCs have been designed for n-type organic field-effect transistors,[75] they are often not fluorescent and cannot be used as emitter in OLED.[36a, 76] Despite barely developed, this strategy appears nevertheless interesting as the electron injection/transport is often the weak link in a SL-OLED.

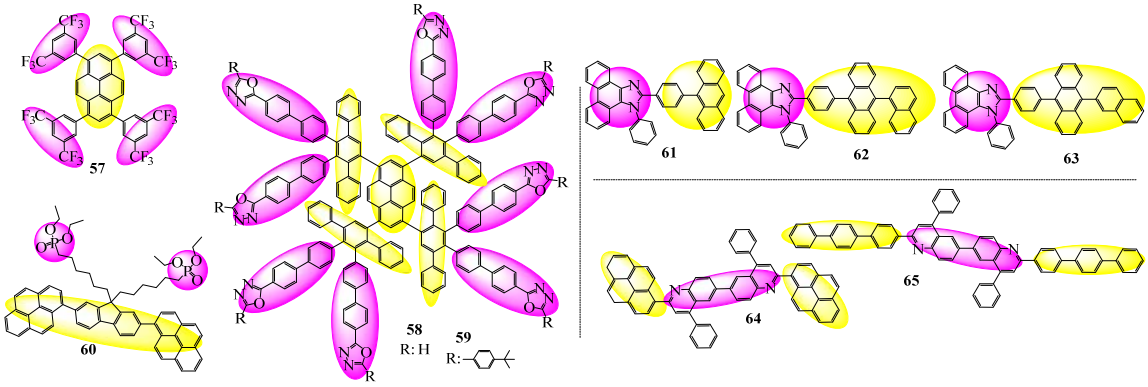


Figure 8. Different π-A designs (OSCs **57-65**)

	λ_{abs}^{sol}/ λ_{abs}^{film} [nm]	λ_{PL}^{sol}/ λ_{PL}^{film} [nm]	Φ^{sol}/ Φ^{film} [%]	HOMO [eV]	LUMO [eV]	Ref
57	382(CyHx) to 387(DMSO)/-	413(CyHx) to 427 (DMSO)/-	88($CHCl_3$)/91.1	-5.90[c]	-2.86[b]	[54]
58	308,392(THF)/309,395	429(THF)/455	39-70(THF)/-	-5.50[c]	-2.46[c],-2.54[b]	[55]
59	330.392(THF)/320,393	431(THF)/453	66-78(THF)/-	-5.50[c]	-2.52[c], 2.53[b]	[77]
60	361/370	427/423	-/27	-5.58[c]	-2.5[c]	[74]
61	349, 367, 387 (DCM)/-	427 (DCM)/456	87/-	-5.62[c], -5.30[a]	-2.54[b], -2.29[a]	[78]
62	358, 376, 393 (DCM)/-	431 (DCM)/455	71/-	-5.58[c], -5.25[a]	-2.56[b], -2.35[a]	[78]
63	359, 376, 396 (DCM)/-	437 (DCM)/457	64/-	-5.55[c], -5.24[a]	-2.55[b], -2.29[a]	[78]
64	286,344,380($CHCl_3$)/277,348,401	440($CHCl_3$)/491	91/50	-5.86[c]	-2.66[c]	[79]
65	307,373($CHCl_3$)/308,390	411($CHCl_3$)/460	86/54	-5.78[c]	-2.58[c]	[79]

[a]: from theoretical calculations, b: from ΔE^{opt}-$HOMO^{el}$, [c]: from cyclic voltammetry

Table 15. Selected electronic properties of OSCs **57-65**

Device numbering and structure		V_{on} [V]	λ_{EL} [nm]	EQE_{max} [%]	CE_{max} [cd A^{-1}]	PE_{max} [lm W^{-1}]	CIE 1931 [x, y]	Ref
TE-SL**57**	Device 1 **57**(80nm)	8.6	456	-	0.004	-	0.15, 0.12	[54]
SP-SL**58**	ITO/PEDOT:PSS/**58**(80nm)/Ca/Al	7	-	-	0.14	-	0.19, 0.28	[55]
SP-SL**59**	ITO/PEDOT:PSS/**59**(80nm)/Ca/Al	9.7	-	-	0.04	-	0.18, 0.18	[77]
SP-SL**60**a	ITO/PEDOT:PSS/**60**/Al	4.2	-	-	0.73	-	0.20, 0.24	[74]
SP-SL**60**b	ITO/PEDOT:PSS/**60**/LiF/Al	3.4	-	-	0.65	-	0.18, 0.21	[74]
SP-SL**60**c	ITO/PEDOT:PSS/Ink-Printed **60**/Al	3.8	-		1.12	-	0.18, 0.26	[74]
TE-SL**61**	ITO/MoO_3(10nm)/**61**(100nm)/cesium pivalate(2nm)/Al	3.05	456	1.16	1.59	1.36	0.17, 0.18	[78]
TE-SL**62**	ITO/MoO_3(10nm)/**62**(100nm)/cesium pivalate(2nm)/Al	2.96	468	0.69	0.93	0.78	0.16, 0.17	[78]
TE-SL**63**	ITO/MoO_3(10nm)/**63**(100nm)/cesium pivalate(2nm)/Al	2.9	468	1.03	1.72	1.40	0.19, 0.23	[78]
TE-SL**64**	ITO/ PEDOT:PSS/**64**/LiF-Ca/Al	3.0	479	0.004	0.006	-	-	[79]
TE-SL**65**	ITO/ PEDOT:PSS/**65**/LiF-Ca/Al	2.0	455	0.019	0.016	-	-	[79]

Table 16. Performance of SL-devices with OSC **57-65** as EML

Wang and co-workers have designed a series of **π-A** OSCs in which a phenanthroimidazole (PI) unit was linked to a *p*-phenyl-anthracene (**61**) or to a *p*-phenylanthracene-naphthalene (**62** and **63**) (Figure 8). [78] The introduction of the PI moieties increases the electron injection and transport ability and the LUMO is lying at low energy around -2.5 eV for the three OSCs (**Table 15**). TE-SL**61-63** (ITO/MoO_3/EML/cesium pivalate/Al) with MoO_3 as HIL and

cesium pivalate[80] as EIL were constructed. Interestingly, EQE of 1.16 %, 0.69 % and 1.03 % were reached with TE-SL**61**-**63** *resp* (**Table 16**). The three devices emit sky blue light (CIE: 0.17, 0.18 for TE-SL**61**, 0.16, 0.17 for TE-SL**62** and 0.19, 0.23 for TE-SL**63**). Thus, PI appears as a promising electron-withdrawing unit, which should be more investigated in the future.

Several pyrene-based dendrimers with different peripheral chromophores have also been incorporated in SL-OLEDs. For example, in **57**, the central pyrenyl core is linked to four 3,5-bis(trifluoromethyl)-phenyl units,[54] whereas it is linked to eight oxadiazole cores thanks to well suited oligophenyl links in **58**[55] and **59**[77] (Figure 8, Left).

The EL properties of these OSCs were investigated in either TE-SL**57**,[54] SP-SL**58**[55] or SP-SL**59**.[77] The device performances are low with CE_{max} only reaching 0.004 cd A^{-1} (TE-SL**57**), 0.04 cd A^{-1} (SP-SL**59**[77]) or 0.14 cd A^{-1} (SP-SL**58**[55]) despite low LUMO levels (-2.86 eV for **57**, -2.46 eV for **58** and -2.52 eV for **59**). The three devices emit light at high V_{on}: 9.7 V with **59**, 8.6 V with **57** and 7 V with **58**, translating a bad charge injection and showing that manipulation of the LUMO energy is not sufficient to reach high performance devices.

Similarly, Jenekhe and co-workers have reported oligoquinolines both possessing two end cappers, either pyrenyl in **64** or terphenyl in **65** (Figure 8, bottom right).[79] With HOMO/LUMO levels of -5.86/-2.66 eV for **64** and -5.78/-2.58 eV for **65**, both OSCs possess a similar energy gap of 3.2 eV. As for the above mentioned examples, the LUMO energy is particularly low due to the electron-poor quinoline fragment. The performances of both blue-emitting devices (479 nm for TE-SL**64** and 455 nm for TE-SL**65**) were nevertheless very low (EQE of 0.004 % for TE-SL**64** and 0.019 % for TE-SL**65**). Despite low V_{on} values (3 V for TE-SL**64** and 2 V for TE-SL**65**), the bad performances of the SL-OLEDs indicate inadequate

charge-carrier utilization with most of the holes and electrons passing through the device without recombination.

Exploring novel printable small-molecule materials with both efficient emitting and interfacial functionalities for optoelectronic applications, Huang and co-workers prepared **60** with phosphonate polar pendant groups linked to a highly emissive 2,7-dipyrenyl-fluorene core (Figure 8, bottom left).[73c, 74] Phosphonate groups endowed the OSC with good solubility in environmentally-friendly alcohol solvents. Moreover, these polar groups facilitated electron injection from high WF metal electrodes. This interesting combination of (i) fluorene as the main backbone structure, (ii) pyrene as the end-capper and (iii) phosphonate as the pendant group was expected to achieve multifunctional optoelectronic properties. SP-SL**60**a leads to much higher performances than the one reported for SP-SL**53** (Figure 7) indicating that the polar phosphonate groups play an important role in facilitating the electron injection from the cathode. The LUMO level is reported at -2.5 eV for **60** being more adapted to the Al WF than that of **53** (LUMO: -1.63 eV). With a V_{on} of 4.2 V, SP-SL**60a** reaches a CE_{max} of 0.73 cd A^{-1}. SP-SL**60**b device with LiF inserted as EIL, exhibits lower V_{on}: 3.4 V and CE_{max} of 0.65 cd A^{-1}. Finally, the "inkjet-printed" SP-SL**60**c with a similar configuration than that of SP-SL**60a** presents a blue emission (CIE: 0.18, 0.26) and higher performance (low V_{on} of 3.8 V and CE_{max} of 1.12 cd A^{-1}) doubling the performance of the "spin-coated" device SP-SL**60a** (V_{on} of 4.2 V and CE_{max} of 0.73 cd A^{-1}).

To sum up, only few examples of n-type OSCs have been investigated in blue SL-OLEDs. Depressing the LUMO level is a good strategy to favour electron injection but transport should also be carefully considered.

4. Donor/Acceptor (D/A) design

The need to develop highly efficient emitters for SL-OLEDs has resulted in the exploration of more sophisticated designs. Indeed, in the previous examples, the designs have been centred on the attachments of either electron-rich or electron-poor fragment on various π-conjugated systems, resulting most of the time to an unbalanced charge transport and hence low SL-OLED performances. The D/A combination capable of ambipolar charge transport (electron and hole) and high luminescence efficiency in the blue region has appeared as a promising alternative and has been particularly studied. This design strategy is based on the assembly of electron-rich (hole transporting) and electron-poor (electron transporting) units in a single molecule. Many different combinations have been explored leading to materials possessing drastically different electronic properties. Indeed, the strength of the electron-donating/-accepting fragments, their connection, and their capability to stack are key parameters, which drive the electronic properties of the resulting fluorophores and their efficiency when incorporated in SL-OLEDs. All these Donor/Acceptor designs are discussed below.

4.1. Donor/Acceptor/Donor (D/A/D), Acceptor/Donor/Acceptor (A/D/A) and Donor (Acceptor)$_3$ (D(A)$_3$) designs

Jenekhe and co-workers have reported the fluorophore **66** with a D/A/D design (**Figure 9**).[81] **66** is composed by a central diquinoline electron-acceptor core (as in **64** and **65**, Figure 8) linked to two triphenylamine electron-rich fragments. The HOMO of **66**[81] (-5.31 eV) is significantly higher than that of **64** and **65** (-5.86 and -5.78 eV *resp.*) but the LUMOs are almost identical (-2.66, -2.58 and -2.59 eV for **64**, **65** and **66** *resp.*) (Table 15 & **Table 17**). This indicates that the presence of two triphenylamines in **66** facilitates its oxidation and increases the HOMO level without significantly modifying its reduction ability. The gap of **66** (2.72 eV) is therefore contracted compared to that of **64**/**65** (3.2 eV). This is one of the

important point in the design of D/A/D materials and more generally all the D/A designs. Indeed, if the gap is too much contracted, the emission is not in the blue range. TE-SL**66** presents an EL spectrum with λ_{EL} at 470 nm (CIE: 0.18, 0.22) (**Table 18**) almost identical to the solid-state PL spectrum (480 nm). The similarity between PL and EL spectra means that the electrically generated intramolecular charge transfer (ICT) excited state responsible of EL is formed by recombination of the radical cation of the triphenylamine moiety with the radical anion of the diquinoline moiety. Despite a low V_{on} (2.7 V), the performance of TE-SL**66** was however very poor (EQE_{max} of 0.003 %). This indicates a good charge injection but an inadequate charge-carrier utilization in the devices with most of the holes and electrons passing through the device without recombination. This again shows the difficulty to design blue emitter for SL-OLEDs.

The decoration of a carbazole core with electro-deficient phenyl rings (*p*-acetophenyl in **67** and cyano-phenyl in **68**[65]) has also been reported (Figure 9). Due to the electron-with-drawing effect of the two substituted phenyl groups in **67** and **68**, their HOMO (-5.90 and -5.97 eV, *resp.*) and their LUMO (-3.0 and -2.93eV, *resp.*), were lower than in structurally re-lated **44** (-5.67/2.5 eV) (Table 17).[65] This shows the impact of the electron-deficient units on both HOMO and LUMO energy levels. SP-SL**67** and SP-SL**68** reach similar performances than those of SP-SL**44**, CE_{max} remaining very low (0.06 cd A^{-1} for SP-SL**67** and 0.09 cd A^{-1} for SP-SL**68**). λ_{EL} is reported at 450 and 460 nm (CIE: 0.20, 0.24 for SP-SL**67** and 0.17, 0.17 for SP-SL**68**), red shifted compared to SP-SL**44** (420 nm and CIE: 0.22, 0.21). The performance of SP-SL**68** despite low is improved compared to SP-SL**44** due to the bipolar character of **68**. There is notably a better charge injection in SP-SL**68** than in SP-SL**44**, (V_{on} of 5.0 V and 8.5 V *resp.*) showing some benefits of this molecular design strategy.

69 possesses a similar V-shaped architecture than **67** and **68**, with this time a central acceptor group (diphenylsulphone) linked to two donor units (9,10-dihydroacridine) (Figure 9).[82] Adachi's group has reported that **69** possesses TADF properties[82b] and used this compound as pure emitter in a SL-OLED.[82a] TE-SL**69** leads to a sky-blue emission (476-480 nm, CIE: 0.16, 0.27) with a V_{on} of 4.7 V and an EQE_{max} of 0.11 %.[82b] Despite the presence of two injection layers (MoO_3 as HIL and LiF as EIL) coated on the electrodes, the performance of the present device remains low. Using a blue TADF emitter in a SL-OLED nevertheless represents a future direction for research in the field.

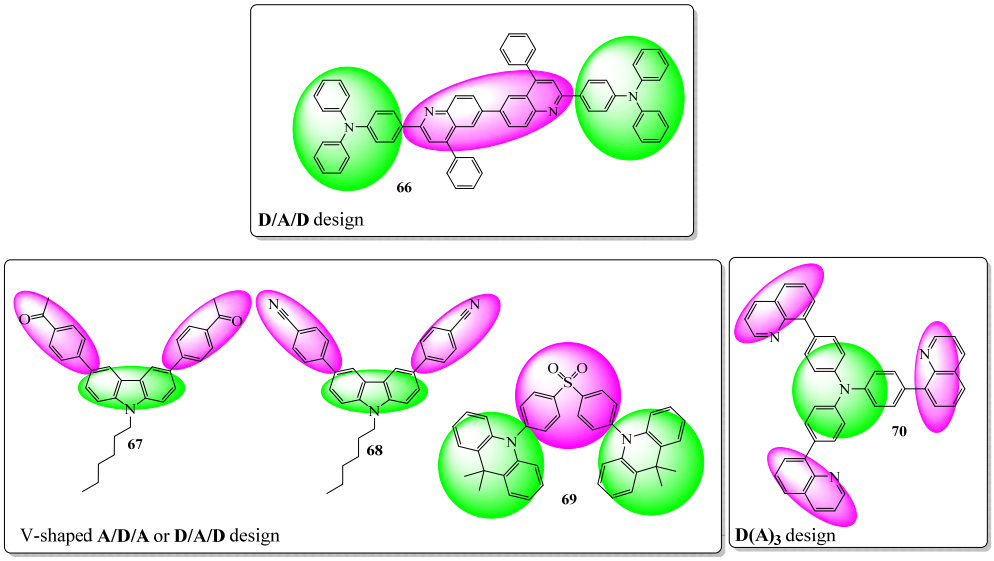


Figure 9. **D/A/D**, **A/D/A** and **D(A)$_3$** designs (OSCs **66-70**)

	λ_{abs}^{sol}/ λ_{abs}^{film} [nm]	λ_{PL}^{sol}/ λ_{PL}^{film} [nm]	Φ^{sol}/ Φ^{film} [%]	HOMO [eV]	LUMO [eV]	Ref
66	From 303,401(ACN) to 297,412(Tol)/276,306,421	From 441(Et_3N) to 524(ACN)/480	62(Tol)/-	-5.31[a]	-2.59[a]	[81]
67	310,350(ACN)/-	479(ACN)/459	21(ACN)/-	-5.90[a]	-3.00[c]	[65]
68	307,345(ACN)/-	421(ACN)/430(TE) or 455(SP)	96(ACN)/-	-5.97[a]	-2.93[c]	[65]
69	375(Tol)/-	460(Tol)/470	80(Tol)/88	-5.92[d]	-2.92[c]	[82a, 83]
70	290,370(Hex)/300,395	431(Hex)/476	-	-5.30[a]	-2.60	[84]

Hex: hexane, Et_3N: trimethylamine, [a]: from cyclic voltammetry, [b]: from theoretical calculation, [c]: from ΔE^{opt}-HOMO^{el}, [d]: from Photoelectron Spectroscopy

Table 17. Selected electronic properties of OSCs **66-70**

Device numbering and structure		V_{on} [V]	λ_{EL} [nm]	EQE_{max} [%]	CE_{max} [cd A^{-1}]	PE_{max} [lm W^{-1}]	CIE 1931 [x, y]	Ref
TE-SL**66**	ITO/**66**(80nm)/LiF(1nm)/Al	2.7	470	0.003	0.004	-	0.18, 0.22	[81]
SP-SL**67**	ITO/**67**/Ca-Al	6.5	450	-	0.06	-	0.20, 0.24	[65]
SP-SL**68**	ITO/**68**/Ca-Al	5.0	460	-	0.09	-	0.17, 0.17	[65]
TE-SL**69***	ITO/MoO_3(1nm)/**69**(120nm)/LiF(1nm)/Al(150nm)	4.7	476	0.11	-	0.08	0.16, 0.27	[82a]
TE-SL**70**	ITO/**70**(100nm)/LiF(0.5nm)Mg :Ag(200nm)	2.8	481	-	1.6	-	0.17, 0.32	[84]

Table 18. Performance of SL-devices with OSCs **66-70** as EML, **: this device used a non-doped TADF emitter in a SL-OLED configuration*

70 possess a $D(A)_3$ design with a central donor triphenyl amine core decorated by three quinoline units. The highest results are obtained with TE-SL**70** ($D(A)_3$ design, Figure 9).[84] The EL and the solid-state PL spectra were similar with sky-blue emission at λ_{max} 481 nm (CIE: 0.17, 0.32). The V_{on} of the device is only 2.8 V and the device reaches CE_{max} of 1.6 cd A^{-1}. It is interesting to note that HOMO/LUMO energy levels of **70** are identical to those of **66** but the device performance is significantly improved (CE_{max} increases by 400 from TE-SL**66** to TE-SL**70**). The C3 symmetry of **70** can be at the origin of this interesting feature.

4.2. Other Acceptor/Donor (A/D) designs

Many combinations of (i) electron-deficient units such as quinolines, oxadiazole, phenanthroimidazole,… (ii) electron-rich groups such as phenylamine, diphenylamine or carbazole and (iii) π-systems such as oligophenylenes, fluorene, spirobifluorene or thiophenes have been investigated with the aim to reach efficient blue SL-OLEDs. Different examples, **71-79**, are presented **Figure 10**. Due to the different combinations of donors, acceptors and π-systems, each compound presents specific electronic properties and a precise rationalization of the SL-OLED performances appears difficult to draw. However, some general design rules can be defined in the light of all the examples reported below.

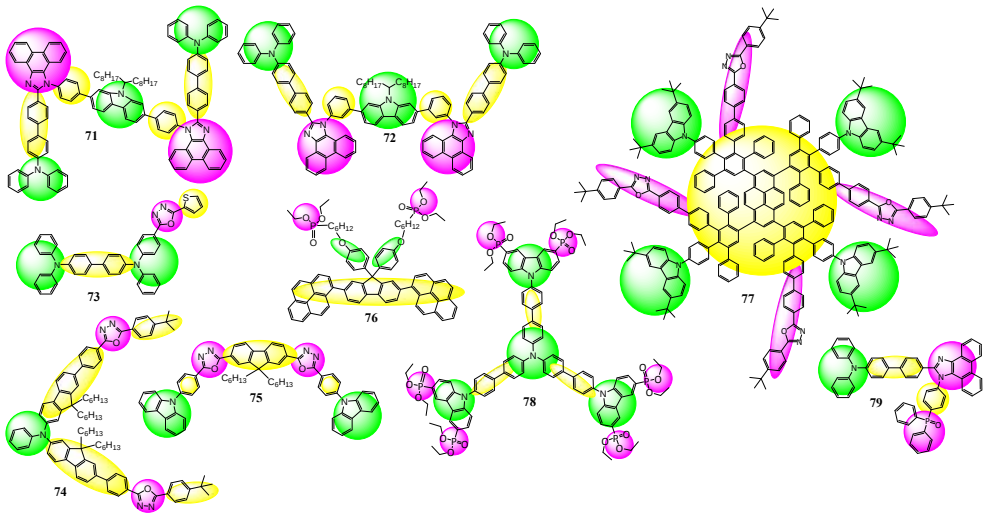


Figure 10. Other **A/D** designs (OSCs **71-79**)

71[85] is built on a central N-heptadecane carbazole linked at C2 and C7 (by a phenyl) to two electron-deficient phenanthroimidazole units themselves linked to two electron-rich diphenyl-biphenyl-amines. SP-SL**71** displays a V_{on} of 5.1 V, a high EQE_{max} of 2.88 % and its EL spectrum is centred at 461 nm (CIE: 0.16, 0.17) (**Table 19**). To the best of our knowledge, these performances are the highest recorded for solution processed SL-OLEDs reported to date.

Device numbering and structure		V_{on} [V]	λ_{EL} [nm]	EQE_{max} [%]	CE_{max} [cd A^{-1}]	PE_{max} [lm W^{-1}]	CIE 1931 [x, y]	Ref
SP-SL**71**	ITO/PEDOT:PSS(40nm)/**71**(50nm)/CsF(1nm)/Al(100nm)	5.1	461	2.88	3.71	2.32	0.16, 0.17	[85]
SP-SL**72**	ITO/PEDOT:PSS(40nm)/**72**(50nm)/CsF(1nm)/Al(100nm)	5.7	465	2.28	2.76	1.73	0.16, 0.16	[85]
TE-SL**73**a	ITO/**73**(50nm)/Ca(30nm)/Al(100nm)	6.8	482	-	0.4	-	0.2, 0.33	[86]
TE-SL**73**b	ITO/**73**(80nm)/Ca(30nm)/Al(100nm)	7.8	468	-	0.4	-	0.18, 0.27	[86]
TE-SL**73**c	ITO/**73**(120nm)/Ca(30nm)/Al(100nm)	9.0	476	-	0.9	-	0.16, 0.26	[86]
TE-SL**73**d	ITO/**73**(150nm)/Ca(30nm)/Al(100nm)	11	478	-	1.1	-	0.16, 0.27	[86]
TE-SL**73**e	ITO/CuPc(15nm)/**73**(85nm)/Ca(30nm)/Al(100nm)	1.8	470	-	0.6	-	0.16, 0.25	[86]
TE-SL**73**f	ITO/CuPc(15nm)/**73**(155nm)/Ca(30nm)/Al(100nm)	1.9	472	-	0.8	-	0.15, 0.24	[86]
TE-SL**74**	Device 1 **74**(110nm)	4.5	487	0.22	0.49	0.17	0.21, 0.36	[87]
SP-SL**75**	Device 1 **75**(110nm)	5.5	430	0.015	0.019	0.005	0.21, 0.16	[87]
SP-SL**76**	ITO/PEDOT:PSS/**76**/Al	4.2	-	-	0.27	-	0.19, 0.25	[74]
SP-SL**77**	ITO/PEDOT:PSS(40nm)/**77**/Ca/Al	4.0	-	-	0.048	-	0.16, 0.10	[77]
SP-SL**78**	ITO/PEDOT:PSS(40nm)/**78**/LiF(1nm)/Al(100nm)	4.0	450	-	0.76	-	0.15, 0.09	[68]
TE-SL**79**	ITO/MoO_3(3nm)/**79**(120nm)/LiF(1nm)/Al(120nm)	3.0	448	3.57	3.66	3.25	0.15, 0.12	[88]

Table 19. Performance of SL-devices with OSCs **71-79** as EML

72[85] is built on a similar design with the same donor and acceptor combination. However, the phenanthroimidazoles are connected in *meta* position of the phenyl ring instead of *para* position in **71**. This not only results in a different geometry but also to a different electronic coupling between the fragments (for a precise study of the influence of a linkage on the electronic

properties, please see references[27b, 44b, 89]). The PL spectrum of **72** is then blue shifted compared to that of **71** (439 *vs* 448 nm, **Table 20**). SP-SL**72**[85] also leads to blue emission (CIE: 0.16, 0.16) with slightly lower performances than those of SP-SL**71**: EQE_{max} of 2.28 % and V_{on} of 5.7 V, these performances remaining nevertheless high. The EL spectra remain roughly similar with λ_{EL} of 461 nm for SP-SL**71** and 465 nm for SP-SL**72**.

	λ_{abs}^{sol}/ λ_{abs}^{film} [nm]	λ_{PL}^{sol}/ λ_{PL}^{film} [nm]	Φ^{sol}/ Φ^{film} [%]	HOMO [eV]	LUMO [eV]	Ref
71	338(DCM)/374	448(DCM)/455	-/56	-5.71[a], -4.89[b]	-2.79[b], -2.65[b]	[85]
72	337.5(DCM)/374	439(DCM)/464	-/41	-5.76[a], -4.89[b]	-2.71[c], -2.57[b]	[85]
73	297,370(THF)/-	485(THF)/-	71(THF)/-	-5.21[a]	-2.20[c]	[86]
74	399(DCM)/-	483(DCM)/-	93(DCM)/-	-5.06[b]	-1.97[b]	[87]
75	361(DCM)/-	416(DCM)/-	87(DCM)/-	-5.67[b]	-2.43[b]	[87]
76	361/375	427/439	-/46	-5.64[a]	-2.50[a]	[74]
77	299,319,392(THF)/300,316,391	431(THF)/446	80(THF)	-5.52[a]	-2.45[a], -2.57[c]	[77]
78	250,270,288,356(DCM)/-	404(DCM)/438	58(Tol)/-	-5.29[a]	-2.13[a], -2.29[c]	[68]
79	367/-	443/457	86/88	-5.31[a]	-2.46[a], -2.29[c]	[88]

[a]: from cyclic voltammetry, [b]: from theoretical calculation, [c]: from ΔE^{opt}-$HOMO^{el}$

Table 20. Selected electronic properties of OSCs **71**-**79**

Thiophene-based bipolar OSCs **73** (Figure 10) with triphenylamine donor groups and oxadiazole acceptor fragment have also been investigated as EML in different SL-OLEDs.[86] In **73**, a central oxadiazole fragment is linked both to a tetraphenylbenzidine (TPB) donor group and to a thienyl π-system. The HOMO of **73** is reported at -5.21 eV and appears directed by the TPB group. This value is significantly higher than those of the precedent OSCs (**71** (-5.71 eV) and **72** (-5.76 eV)) theoretically indicating an easier hole injection from the anode in **73** than in **71** or **72**. On the other side, the LUMO is lying at -2.20 eV for **73**, strongly higher than the LUMO levels of **71** (-2.79 eV) and **72** (-2.71 eV), the electron-injection from the cathode being more difficult in **73** than in **72** or **71**.

Different SL-OLEDs architectures have been investigated: TE-SL**73**a-**73**f. In absence of HIL and with different EML thickness from 50 to 150 nm (TE-SL**73**a-**73**d), CE_{max} increases with the EML thickness from 0.4 to 1.1 cd A^{-1}. This increase indicates that the hole-electron recombination zone shifts from near the electrode toward the film centre when increasing the film thickness. Upon addition of CuPc as HIL (TE-SL**73**e-**73**f), V_{on} decreases from 7.8 V

(TE-SL**73**b) to less than 2 V (TE-SL**73**e-**73**f). In TE-SL**73**e and TE-SL**73**f, CE_{max} does not vary significantly with the film thickness (0.6/0.8 cd A^{-1} for a 85/155 nm film thickness). Moreover, CE_{max} of 1.1 cd A^{-1} (reached in TE-SL**73**d in absence of CuPc) is not reached with similar EML thickness in TE-SL**73**f in presence of CuPc. This suggests that either CuPc is absorptive or hole limiting. For all the devices, the EL spectra (from 468 to 482 nm) matched with the PL spectra (bluish green emission in THF, λ_{max}: 485 nm).

Lower performances were obtained with TE-SL**74**.[87] With a V_{on} of 4.5 V, TE-SL**74** reaches EQE_{max} of only 0.22 % and emits a clear blue light with λ_{EL} at 487 nm (CIE: 0.21, 0.36). Such a difference of performances between TE-SL**74** and SP-SL**71**/SP-SL**72** may be correlated to the HOMO/LUMO levels (-4.89/-2.65 eV, -4.89/-2.57eV and -5.06/-1.97 eV for **71**, **72**[85] and **74**[87], *resp.*). The energy gap is therefore 2.24 eV and 2.32 eV for **71** and **72**, and 3.09 eV for **74**, meaning a more difficult charge injection in the later than in the formers.

In **75** (Figure 10), a fluorenyl core is linked to two oxadiazole acceptors themselves linked to a N-phenyl-carbazole donor. This D/A/π/A/D arrangement leads to an efficient blue fluorophore in solution (λ_{max}: 416 nm and Φ^{sol}: 87 % in DCM). SP-SL**75** displays nevertheless very low EQE values of 0.015 % (λ_{EL} : 430 nm and CIE: 0.21, 0.16). The authors explain this low performance by a difficult hole injection and transport in **75**.[87]

Another design approach consists in introducing phosphonate groups at the periphery of a p-type blue emitting fluorophore possessing a central triphenylamine branched with three carbazole groups. This design has been already presented above (**60**, Figure 8) and presents several advantages.[68] Indeed, the presence of the phosphonate groups at the periphery of **78**[68] (Figure 10) endows the blue emitter with good solubility and high quality films can be formed by solution processes. Moreover, phosphonates improve the electron injection/transport properties. SP-SL**78** presents EL spectrum similar to the solid state PL spectrum and the

emission is stable whatever the current density (CIE: 0.15, 0.09). With a LUMO of -2.29 eV, electron injection is efficient in SP-SL**78** and excitons are effectively generated in the EML leading to CE of 0.76 cd A^{-1}.

Finally, following a similar strategy, Huang and co-workers have designed an OSC consisting of highly emissive fluorene and pyrene species functionalized with phosphonate polar pendant groups (**76**) linked to the fluorene C9 through a phenyl hexyloxy group.[73c, 74] SP-SL**76** shows higher performance than that of SP-SL**53** (Figure 7), CE_{max} increases from 0.04 cd/A for SP-SL**53** to 0.27 cd A^{-1} for SP-SL**76**, indicating that the polar phosphonate groups play an important role in facilitating the electron injection from the cathode by decreasing the LUMO levels (-2.5 eV for **76** and -1.63 eV for **53**). The LUMO level of **76** is more adapted to the Al WF. However, compare to **60** (Figure 8), in which the phosphonate units are linked to the fluorene thanks to alkyl chains, the presence of the donor phenoxy groups between the fluorene and the phosphonate units does not appear to increase the efficiency of the device. In fact, with similar configurations, SP-SL**60**a appears more efficient (0.73 cd A^{-1}) than SP-SL**76** (0.27 cd A^{-1}).

In conclusion, **60** and **76** have led to SL-OLEDs with higher performances than that of **53** showing the interest of the phosphonate polar pendant groups.

In 2018, Leung's group[88] has reported **79** (Figure 10), in which a triphenylphosphine-oxide (TPPO) unit is linked to the N1-position of a phenanthroimidazole (PI) core. This association forms a nearly orthogonal linkage between TPPO and PI and decreases the electronic coupling between the two units (**D/π/A/π/A** design).

The deep-blue emitted colour of **79** (λ_{PL}^{max} in solution: 443 nm), similar to that of **72** and **71** (λ_{PL}^{max} in solution: 439 or 448 nm *resp.*) is mainly controlled by the D/π/A core. Moreover, in the solid state, TPPO unit prevents close packing of the emitting centre and avoids emission

quenching. TPPO group also lowers the LUMO level (-2.46 eV), which is beneficial for electron injection. TE-SL**79** exhibits very high performance with an EQE_{max} of 3.57 %, a low V_{on} (3 V) and a blue colour index (0.15, 0.12).

In 2016, Müllen's group also designed dendrimers with a central pyrene core decorated alternatively by four donor and four acceptor units (**77**, Figure 10).[77] The acceptor unit is an oxadiazole and the donor unit is a carbazole. **77** possesses the same central core as that of **25-27**, dendrimers decorated by eight donor branches (Figure 3) and as that of **58**[55] and **59**[77] (Figure 8) with eight acceptor branches. The UV-vis absorption spectrum of **77** presents in THF three main bands at (i) 299 nm, characteristic of the carbazole absorption (also observed for **26**[55]), (ii) 319 nm, assigned to the absorption of the oxadiazole units (as observed for **58**[55] and **59**[77]) and finally (iii) a band centred at 392 nm, which originates from π-π* transitions of the central pyrene core (found in all the above mentioned dendrimers). The optical energy gap, ΔE^{opt}, of all the dendrimers is therefore similar, ca. 2.95 eV. The PL spectrum of **77** is also similar to that of all the dendrimers (λ_{max}: 431 nm in THF) revealing that the emission of the donor-acceptor dendrimer can be attributed to an efficient surface-to-core energy transfer. Φ^{sol} of **77** is rather high regardless if the excitation is done via the central core (80 %) or the surface moieties (93 %). The emission of **77** does not change with solvent polarity, indicating that no ICT occurs for **77**. The reason of the absence of ICT is due to the lack of electron donation from carbazole to the central core consistent with similar HOMO levels between carbazole (-5.52 eV) and the core (-5.50 eV).[77]

SP-SL**77** emits a pure blue light (CIE: 0.16, 0.10) with nevertheless a very low CE_{max} (0.048 cd/A) similar to that of SP-SL**26**[55] (CE_{max}: 0.06 cd/A, CIE: 0.16, 0.16). The comparison of SP-SL**77** with SP-SL**59** with its eight acceptor antennae (V_{on}: 9.7 V, 0.04 cd/A, CIE: 0.18, 0.18), leads to the same conclusion. Finally, compared to SP-SL**58**, with a similar donor

carbazole but different acceptor groups (non-substituted oxadiazole *vs* t-Bu-Ph-oxadiazole), the present device shows a lower CE_{max} (0.048 cd/A *vs* 0.14 cd/A) with nevertheless a decrease of V_{on} from 7 to 4V and a blue shift of the emission (CIE: 0.16, 0.10 *vs* 0.19, 0.28). These comparisons show the difficulty to rationalize the design rules of a blue fluorophore for SL-OLED.

4.3 Non-Conjugated branched carbazoles

As presented in section 3.2, carbazole units may be attached to different π-conjugated cores through non-conjugated links. This molecular design has led in some cases to an increase of the hole injection and an improvement of the quality of the films while retaining optical, thermal and electronic properties of the emitting cores. Incorporation of acceptor units in such a type of design has allowed to reach very efficient blue fluorophores described below. **Figure 11** presents different fluorophores (**80**-**83**), in which the non-conjugated carbazoles are linked through hexyl chains by their nitrogen atoms to the C9 of fluorenyl units. In **83**[58c] and **81**,[58d] the central acceptor core is linked to two fluorenyl units whereas in **80**[58d, 58e, 90] and **82**, [58d, 58e] the central core is linked to difluorenyl units. The electron-deficient core is a dibenzo[*b*,*d*]thiophene-5,5-dioxide unit in **80** and **81**, a 10-hexyl-10H-phenothiazine-5,5-dioxide unit in **82** and a dibenzo[*f*,*h*]quinoxaline in **83**. The four OSCs present solid state spectra in the blue region between 418 nm for **82** and 458 nm for **80** (**Table 21**).

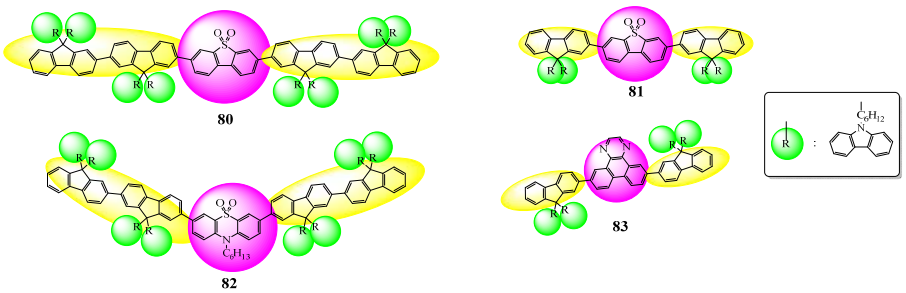


Figure 11. Bipolar OSCs with branched non-conjugated carbazoles (OSCs **80**-**83**)

	λ_{abs}^{sol}/ λ_{abs}^{film} [nm]	λ_{PL}^{sol}/ λ_{PL}^{film} [nm]	Φ^{sol}/ Φ^{film} [%]	HOMO[a] [eV]	LUMO[a] [eV]	Ref
80	382(THF)/391	444(THF)/458	84(THF)/53	-5.43	-2.84	[58d, 58e]
81	266, 298, 349, 392(THF)/	439(THF)/454	86(THF)/99	-5.46	-2.81	[58d]
82	369(THF)/374	406(THF)/418	74(THF)/28	-5.43	-2.34	[58e]
83	295,331,352(THF)/-	447(THF)/446	-/99	-5.40	**-2.74**	[58c]

[a]: from cyclic voltammetry

Table 21. Selected electronic properties of OSCs **80**-**83**

Device numbering and structure		V_{on} [V]	λ_{EL} [nm]	EQE_{max} [%]	CE_{max} [cd A^{-1}]	PE_{max} [lm W^{-1}]	CIE 1931 [x, y]	Ref
SP-SL**80**a	ITO/PEDOT:PSS(40nm)/**80**(80nm)/CsF(1.5nm) /Al(120nm)	3.8	454	2.6	2.8	-	0.17, 0.22	[58e]
SP-SL**80**b	ITO/PEDOT:PSS(40nm)/**80**(90nm)/CsF(1.5nm) /Al(120nm)	3.2	-	2.4	2.8	-	0.17, 0.22	[58d]
SP-SL**80**c	ITO/PEDOT:PSS(40nm)/**80**(90nm)/CsF(1.5nm) /Al(120nm)	4.0	-	-	2.8	1.9	0.18, 0.23	[90]
SP-SL**81**	ITO/PEDOT:PSS(40nm)/**81**(90nm)/CsF(1.5nm) /Al(120nm)	3.2	-	1.6	1.6	-	0.16, 0.16	[58d]
SP-SL**82**	ITO/PEDOT:PSS(40nm)/**82**(80nm)/CsF(1.5nm) /Al(120nm)	3.6	-	1.2	1.2	-	0.21, 0.19	[58e]
SP-SL**83**	ITO/PEDOT:PSS/**83**(105nm)/Ba/Al	4	448	-	0.7	-	0.15, 0.10	[58c]

Table 22. Performance of SL-devices with OSCs **80**-**83** as EML

Due to their high solubility, **80**-**83** have been spin-coated in a series of SL-OLEDs with configuration ITO/PEDOT:PSS/SP-EML/CsF/Al (**Table 22**). The best performances are reported for SP-SL**80**a (EQE_{max}: 2.6 %). Lower performances are reached with SP-SL**81** (1.86 %) and SP-SL**82** (1.2 %), which remain nevertheless high. This shows the efficiency of this design strategy.

In fact, **80** possesses HOMO/LUMO levels lying at -5.43/-2.84 eV almost identical to those of **81** (-5.46/-2.81 eV) with similar central dibenzothiophene dioxide core and only two fluorene units. However, the SP-SL**81** performances are lower indicating that the energy levels are far to be the only factors in determining the SL-OLED performance. The authors hypothesised that during the SP procedure, the eight alkyl chains in **80** forms stronger physical entanglement, which endow better film-forming ability to **80** compared to **81**.

82 with HOMO/LUMO levels of -5.43/-2.34 eV possess the largest energy gap (3.09 eV for **82**, 2.59 eV for **80**, 2.65 eV for **81**) and the injection of charges becomes therefore more difficult leading to the lowest SL-OLED performance of the series (EQE of 1.2, 1.6 and 2.6 % reported for SP-SL**82**, SP-SL**81** and SP-SL**80a** *resp.*).

Finally, SP-SL**83** reaches lower CE_{max} (0.7 cd A^{-1}). As **83** and **81** present similar HOMO/LUMO levels, the lowering of the performances from SP-SL**81** to SP-SL**83** may be assigned to the diode structure (Ba/Al instead of CsF/Al cathode) rather than to the OSC itself.[58c] To sum up, this linear design appears interesting and other acceptors should be inserted between the fluorene/carbazole π-systems in order to explore the full potential of this general design.

4.4. Conclusion

To conclude this part, among the 17 OSCs (**66**-**83**) which have been tested as EML in blue SL-OLEDs, five of them have led to high performances with EQE surpassing 3%. The best performances have been obtained with SP-SL**71**[85] and SP-SL**72**.[85] It is nevertheless difficult to say if this high performance originates from the general design of **72**-**71** or from the barely know phenanthroimidazole. We believe that this electron-poor fragment deserves to be more investigated in the future. A second interesting design strategy described in this part (Figure 11) consists in the introduction of non-conjugated pendant carbazoles. A high performance device (SP-SL**80**a) with EQE of 2.6 % has been obtained.[58e]

5. Donor-π-Acceptor (D-π-A) design

From the results presented above, one notes that the majority of SL-OLEDs using as EML polycyclic aromatic OSC (Part 1), π-donor or π-acceptor OSCs (Parts 2 or 3) or donor-acceptor OSCs (Part 4) present low efficiencies (75 % of the reported devices present EQE_{max} lower than 1%). This is due to many different factors: bad charge injection (mismatch between HOMO and LUMO levels of the OSC and the electrode WFs) and bad and/or unbalanced transporting capability of the OSCs leading to very few exciton formation, morphological instability or low quantum yield. An appealing strategy to obtain efficient blue SL-OLEDs involves the use of D-π-A conjugated fluorescent dyes with electron-donating and electron-accepting

groups directly linked to a central π-conjugated bridge.[91] This strategy allows to obtain, sometimes, ambipolar fluorophores with a good balance between the hole and electron mobilities, which is the most important property to reach when designing fluorophores for SL-OLEDs. Designing such D-π-A blue fluorescent molecules is nevertheless far from an easy task as extended conjugation length, which cause the emission to shift to higher wavelengths, must be avoided. The nature of the donor, the acceptor, the π-conjugated spacer and their connections is hence of key importance. In that field, numerous D-π-A OSCs have been designed and are presented in different sections below depending of their central π-conjugated bridge: phenyl and oligophenyl spacers (section 5.1), phenyl-oligofluorene spacers (section 5.2), or other aryl-spacers (section 5.3). Many of these D-π-A fluorophores have displayed high performance in SL-OLEDs (EQE>2%).

5.1. D-π-A design with phenyl/biphenyl/triphenyl/quaterphenyl as spacer

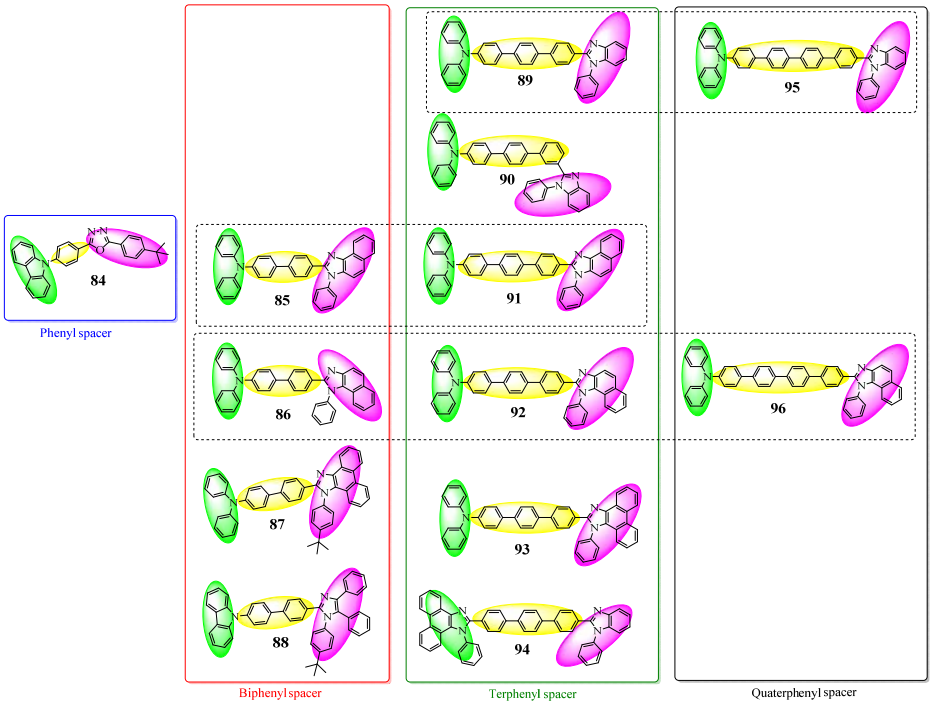


Figure 12. Oligophenyl spacer in D-π-A design (OSCs **84-96**)

The shortest π-system finds in this series is the phenyl unit (**Figure 12**). In **84**,[92] a N-carbazole unit is linked to an oxadiazole fragment through a *para*-substituted phenyl ring. In the so-

lid state, the emission of **84** is centred at 410 nm. TE-SL**84** emits light since 3.7 V and reaches a low EQE_{max} of 0.36 % with λ_{EL} at 428 nm (CIE: 0.16, 0.05) (**Table 24**).

A series of D-π-A OSCs possessing a central biphenyl π-system is presented Figure 12 (**85** to **88**). **85-87** possess (i) the same diphenylamine donor group (whereas in **88**, the donor group is a carbazole unit) and (ii) differently substituted imidazole acceptor groups. HOMO energy levels of **85**[93], **86**[93] and **87**[94] are all reported around -5.2 eV (driven by the diphenylamine core) whereas that of **88**[95] is reported at -5.52 eV (driven by the carbazole) (**Table 24**). This clearly shows the stronger electron-donating effect of the diphenylamine compare to that of carbazole. As diphenylamine and carbazole are the most studied electron-rich units in organic electronics, this is an important point when designing D-π-A materials in order to keep a blue emission and adequate HOMO energy levels.

The LUMO levels are reported close to -2.3 eV for **85-87** whatever their acceptor units (-2.32 eV for **85**[93], -2.30 eV for **86**[93] and -2.36 eV for **87**[94]) and -2.49 eV for **88**.[95] As the LUMO level is localized on the different acceptors, this may translate the stronger acceptor character of the diphenyl-imidazole of **88** compared to the other imidazole-like fragments found in **85-87**. Regarding the optical properties, **85**,[93] **86**,[93] **87**,[94] and **88**[95] are all efficient blue emitters both in solution (Φ^{sol} above 84%) and in the solid state with a PL spectrum centred at 445, 446, 436 and 412 nm (*resp.*).

First, with similar device configuration (ITO/HATCN (5 nm)/EML (80 nm)/LiF (1 nm)/Al), TE-SL**86** (EQE_{max} of 1.89 %) presents performance significantly higher than those of TE-SL**85** (EQE_{max} of 0.05 %). Despite these very different efficiencies, the two OLEDs present similar EL spectra (λ_{EL}: 444 nm - CIE: 0.15, 0.08 for TE-SL**85** and λ_{EL}: 442 nm - CIE: 0.15, 0.07 for TE-SL**86**). Studying the carrier injection and transport properties of the two materials,[93] the authors observed that electron injection is much easier in **86** than in **85** and

that hole-injection and hole-transport is largely predominant in **85**, explaining the very low performance of TE-SL**85**.

Device numbering and structure		V_{on} [V]	λ_{EL} [nm]	EQE_{max} [%]	CE_{max} [cd A^{-1}]	PE_{max} [lm W^{-1}]	CIE 1931 [x, y]	Ref
TE-SL**84**	Device 1 **84**(105nm)	3.7	428	0.36	0.124	0.075	0.16, 0.05	[92]
TE-SL**85**	ITO/HATCN(5nm)/**85** (80nm)/LiF(1nm)/Al	3.5	444	0.05	0.04	0.02	0.15, 0.08	[93]
TE-SL**86**	ITO/HATCN(5nm)/**86**(80nm)/LiF(1nm)/Al	2.8	442	1.89	1.38	1.44	0.15, 0.07	[93]
SL**87**	ITO/**87**(120nm)/LiF(0.5nm)/Mg:Ag(100nm)	3.5	452	0.51	0.49	0.17	0.15, 0.09	[94]
SP-SL**88**	ITO/PEDOT:PSS/**88**(80nm)/CsF(1.5nm)/ Al(100nm)	-	408	0.38	0.38	-	0.17, 0.08	[95]
TE-SL**89**a	ITO/**89**(80nm)/LiF(1nm)/Al(150nm)	3.0	456	2.4	1.9	1.5	0.14, 0.09	[91d]
TE-SL**89**b	ITO/HATCN(5nm)/**89**(80nm)/LiF(1nm)/Al	2.7	460	4.29	4.84	4.98	0.14, 0.13	[96]
TE-SL**90**	ITO/**90**(80nm)/LiF(1nm)/Al(150nm)	3.5	434	1.0	0.62	0.46	0.16, 0.07	[91d]
TE-SL**91**	ITO/HATCN(5nm)/**91**(80nm)/LiF(1nm)/Al	3.0	458	0.52	0.54	0.26	0.14, 0.11	[93]
TE-SL**92**	ITO/HATCN(5nm)/**92**(80nm)/LiF(1nm)/Al	2.7	452	4.37	4.28	4.32	0.15, 0.16	[93]
TE-SL**93**	ITO/HATCN(5nm)/**93**(80nm)/LiF(1nm)/Al	2.8	460	1.50	1.87	1.85	1.15, 0.14	[96]
TE-SL**94**a	ITO/**94** (70nm)/LiF (1nm)/Al(150nm)	3.1	452	2.98	3.77	3.4	0.15, 0.14	[97]
TE-SL**94**b	ITO/HATCN(5nm)/**94** (70nm)/LiF(1nm)/Al(150nm)	2.8	460	4.12	6.29	6.59	0.15, 0.17	[97]
TE-SL**95**	ITO/HATCN(5nm)/**95** (80nm)/LiF(1nm)/Al	2.6	451	4.40	4.22	4.34	0.15, 0.10	[98]
TE-SL**96**	ITO/HATCN(5nm)/**96** (80nm)/LiF(1nm)/Al	2.6	450.5	5.12	4.96	4.96	0.15, 0.11	[98]

Table 23. Performance of SL-devices with OSCs **84-96** as EML

	λ_{abs}^{sol}/ λ_{abs}^{film} [nm]	λ_{PL}^{sol}/ λ_{PL}^{film} [nm]	Φ^{sol}/ Φ^{film} [%]	HOMO [eV]	LUMO [eV]	Ref
84	349,339,285,284(CyHx) or 339,331,291,284(ACN)/-	358,377(CyHx) or 439(ACN)/410	95 (CyHx)/29	-5.4[a], -5.45[b]	-1.70[b]	[92]
85	298,362(DCM)/302,368	452(DCM)/445	92(DCM)/57	-5.21[a], -4.91[b]	-2.32[c], -1.28[b]	[93]
86	285,359(DCM)/289,363	448(DCM)/446	93(DCM)/61	-5.22[a], -4.90[b]	-2.30[c], -1.22[b]	[93]
87	256,361(DCM)/260,372	442(DCM)/436	100(DCM)/-	-5.26[d], -4.86[b]	-2.36[c], -1.20[b]	[94]
88	294,325(THF)/-	411(THF)/412	84(THF)/	-5.52[a]	-2.49[c]	[95]
89	306,355(Tol) or 306,354(DCM)/-	425(Tol) or 472(DCM)/457	86(Tol) or 64(DCM)/71	-5.28[a]	-2.18[c]	[91d]
90	296,346(Tol) or 296,348(DCM)/-	407(Tol) or 439(DCM)/433	77(Tol) or 82(DCM)/63	-5.28[a]	-2.08[c]	[91d]
91	302,359(DCM)/303,366	466(DCM)/448	92(DCM)/73	-5.22[a], -4.92[b]	-2.36[c], -1.39[b]	[93]
92	290,357(DCM)/294,363	462(DCM)/445	93(DCM)/70	-5.23[a], -4.92[b]	-2.34[c], -1.33[b]	[93]
93	354(Tol)/382	405(Hex)-483(ACN)/451	-/57	-5.20[a], -4.91[b]	-2.30[c], -2.33[b]	[99]
94	342(THF)/344	435(THF)/450	91.5/81.9	-5.46[a], -5.16[b]	-2.34[c], -1.53[b]	[97]
95	350/315, 354	467/453	100(DCM)/82	-5.17[a], -4.93[b]	-2.28[c], -1.43[b]	[98]
96	296, 355/300, 360	467/450	100(DCM)/81	-5.18[a], -4.92[b]	-2.35[c], -1.40[b]	[98]

[a]: from cyclic voltammetry, b: from theoretical calculation, [c]: from ΔE^{opt}-$HOMO^{el}$, [d]: from Ultraviolet Photoelectron Spectroscopy

Table 24. Selected electronic properties of OSCs **84-96**

It must be noted that the only difference between **85** and **86** is the position of the phenyl substituent of the naphto-imidazole group, which has no noticeable influence on the physicochemical properties of the two OSCs (Table 24). The reason why electrons are much easily injected in **86** than in **85** has been finely studied by the authors using ultraviolet photoelectron spectroscopy and X-ray photoelectron spectroscopy.[93] They demonstrated that a slight change in the chemical environment of **86** takes place along the gradual deposition of LiF layers, which is not observed for **85**. They suspected that a coordination effect between the exposed nitrogen atom of **86** and LiF may reduce the energy difference between the interface of **86** and

the cathode resulting in better injection and thus a reduced V_{on} in the device. From these studies the authors have shown that the acceptor group 1-phenyl-*1H*-naphtho[1,2-*d*]imidazol works better than its 1-phenyl-*3H*-naphtho[1,2-*d*]imidazol analogue highlighting the importance of positional isomerism in the organic devices performance. Positional isomerism is indeed nowadays an important concern in the field of organic electronics.[27b, 34, 36c, 37a, 38a, 76a, 89, 100]

The performances of SL**87** (EQE: 0.51 %)[94] or SP-SL**88** (EQE: 0.38 %)[95] are between those of TE-SL**86** (EQE_{max}: 1.89 %) and TE-SL**85** (EQE_{max}: 0.05 %). As in **87** and **88**, the non-substituted nitrogen atom of the acceptor group is in the same environment than in **85**, the improvement of SL**87** and SL**88** performances (compared to that of SL**85**), may therefore have different origins: the nature of the donor or the acceptor group, the anode or the cathode, or all these effects gathered. We note that EL spectrum of SL**87** is centred at 452 nm and that of SP-SL**88** at 408 nm in accordance with the shift between the solid-state PL spectra (436 nm and 412 nm *resp.*). The CIE coordinates for the SP-SL**88** (0.17, 0.08) appears slightly more purple than these of SL**87** (0.15, 0.09).

Two series of OSCs possessing a more extended central π-system, either terphenyl in **89-94** or quaterphenyl in **95-96** have also been studied (Figure 12). With the same diphenylamine donor unit, **89-93**, **95** and **96** all possess similar HOMO energy levels close to -5.2 eV, similar to that of the previous OSCs possessing a diphenylamine donor group (**85-86**) (Table 24). This shows that the length of the central π-spacer does not impact the HOMO energy levels and that the HOMO is mostly spread out on the diphenylamine unit.

The two sets of molecules **89-93** and **95-96** are only differenced by the structure of their benzimidazole (BI) unit [91d, 93, 96] and by the length of their central bridge leading to LUMO energies lying from -2.08 to -2.36 eV.

In contrast, **89** and **94**[97] possess the same BI acceptor unit but a different donor group (diphenylamine in **89** and phenanthroimidazole in **94**). Despite the PI group is also the acceptor in **93**, the authors[97] demonstrate that the HOMO of **94** is mainly centred on the PI unit (with partial contribution from the central terphenyl), whereas the LUMO is distributed on the terphenyl and the BI segment (with only a little contribution on the PI unit). PI has therefore a stronger electron-donating character over BI in **94**. Literature reports other examples of PI as donor group[101] showing that PI can both donate (as in **94**) or receive (as in **93**) electrons, see a recent review on phenanthroimidazole-based fluorophores.[102] Thus, **94** possesses a deeper HOMO (-5.46 eV) than **89** (-5.28 eV). The solid state PL spectra of **89**-**96** are centred between 433 and 457 nm, close to the values recorded for the parent compounds with a biphenyl central π-system (**85**-**88**). The shortest value is observed with **90** (433 nm), in which the acceptor group is linked in *meta*-position of the terphenyl, reducing the conjugation of the D-π-A core.

Finally, three sets of OSCs can be compared: **89**/**95**, **85**/**91** and **86**/**92**/**96**. The solid state PL spectra are centred at 457/453 nm for the first set, at 445/448 nm for the second set and at 446/445/450 nm for the third. Despite a slight difference of the PL spectra (λ_{max} varying of 3-5 nm), one may conclude that the central biphenyl, terphenyl or quaterphenyl cores only have a weak influence on the fluorescence properties of these OSCs, which are driven by the strength of D and A. These spacers play nevertheless an important role in the devices performance surely due to the different π-stacking abilities.

Thin films of **89**, **90** and **94** have been evaporated between an ITO anode and a LiF (1 nm)/Al (150 nm) cathode without any HIL. With such device configuration, the performance of TE-SL**94**a and TE-SL**89**a are remarkably very good (EQE_{max}: 2.98 % and 2.4 %, *resp.*) and higher than those of TE-SL**90** (EQE_{max}: 1 %). These are ones of the rare examples of high

performance SL-OLEDs, which do not use HIL. As observed in the solid state PL spectra, the maxima of the EL spectra are also shifted from 456 nm for TE-SL**89**a to 434 nm for TE-SL**90**. This shift is due to the *meta*-arrangement of the benzimidazole unit in **90**, which partially breaks the conjugation pathway compare to **89**. For both compounds, μ_e has been measured higher than μ_h (μ_e/μ_h: $19.3\times10^{-6}/7.32\times10^{-6}$ cm^2 V^{-1} s^{-1} for **89**[91d] and $144\times10^{-6}/17.6\times10^{-6}$ cm^2 V^{-1} $s^{-1}$for **90**[91d]). However, despite the higher μ_e measured for **90**, performances of TE-SL**90** remain more than twice lower than that of TE-SL**89**a which presents a more balanced charge mobility (μ_e/μ_h = 2.64 for **89** and μ_e/μ_h = 8.2 for **90**).

Significantly higher performances are obtained for TE-SL**94**b (EQE_{max}: 4.12 %), TE-SL**89**b (EQE_{max}: 4.29 %), TE-SL**92** (EQE_{max}: 4.37 %), TE-SL**95** (EQE_{max}: 4.4 %), and TE-SL**96** (EQE_{max}: 5.12 %), introducing a layer of HATCN as HIL between ITO and EML. These high performances are interestingly obtained with OSCs all possessing the imidazole fragment found in **86**, (Figure 12) for which the authors suspected a beneficial coordination effect with LiF (see above). This coordination effect leads to a better injection and therefore a reduced V_{on} and better SL-OLED performance (TE-SL**86**). From these results, one may definitively conclude that the acceptor groups 1-phenyl-1H-benzo[d]imidazol-2-yl (found in **89** and **94-95**) and 3-phenyl-3H-naphtho[1,2-d]imidazol-2-yl (found in **86**, **92** and **96**) are both more efficient than the other imidazole derivatives in which the nitrogen atom presents less tendency to the coordination effect with LiF.

The last question to address herein is: *what is the influence of the central π-system on the electronic properties and resulting devices?* It was found that in these systems, the π-spacer has a strong influence in the device performance. Thus, in TE-SL**86**, TE-SL**92** and TE-SL**96**, the increase of the π-system length (from biphenyl to quaterphenyl) leads to a slight contraction of the energy gap (from 2.92 to 2.83 eV) and induces a slight lowering of V_{on}

from 2.8 to 2.6 V and a strong increase of EQE from TE-SL**86** (1.89 %) to TE-SL**92** (4.37 %) and TE-SL**96** (5.12 %). This last effect may be correlated to higher μ_e than μ_h in **86**[93] and **88**[95] and a well balance between electron and hole in **96**.[98] Thus, the central π-system does not strongly influence the energy gap but modifies the intermolecular interactions in the solid state and the resulting charge transport. All these OSCs are among the best reported to date for blue SL-OLEDs.

5.2. D-π-A design with Phenyl-oligofluorene as spacer

The Bryce's group[87, 91c] has synthetized a series of D-π-A OSCs with a phenyl-fluorene as π-spacer (**Figure 13**, framed in blue). In this series, the π-spacer has been rigidified compare to the previous series (fluorene vs oligophenylene). *What are the consequences of this rigidification?* These are detailed below.

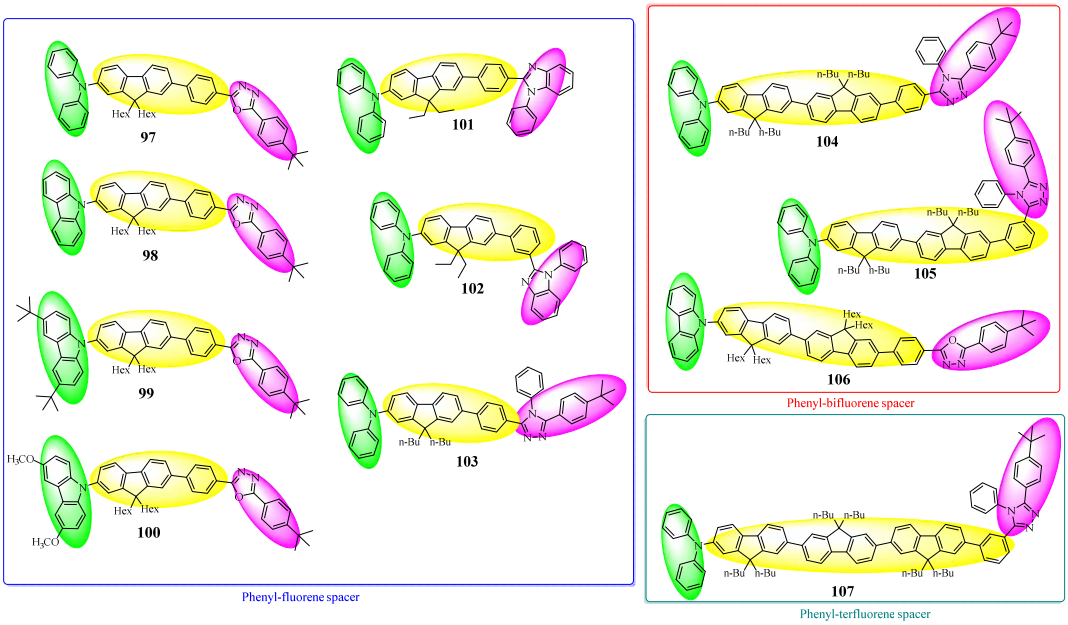


Figure 13. Phenyl-oligofluorene spacer in D-π-A design (OSCs **97**-**107**)

As presented Figure 13, the donor group is either a diphenylamine group (**97**, **101**-**103**) or different carbazole fragments (**98**-**100**) and the acceptor group is either an oxadiazole unit (**97**-**100**), a phenylbenzimidazole (**101**-**102**) or a triazole derivative (**103**). Systematic investiga-

tions of the effect of the donor, the acceptor on the electronic properties and the device performances can be herein performed.

Device numbering and structure		V_{on} [V]	λ_{EL} [nm]	EQE_{max} [%]	CE_{max} [cd A^{-1}]	PE_{max} [lm W^{-1}]	CIE 1931 [x, y]	Ref
TE-SL**97**a	Device 1 **97**(70nm)	4.30	484	0.63	0.93	0.30	0.16, 0.25	[91c]
SP-SL**97**b	Device 1 **97**(110nm)	3.53	487	0.26	-	-	0.19, 0.35	[91c]
SP-SL**97**c	Device 1 **97**(110nm)	3.60	487	0.26	0.6	0.29	0.19, 0.35	[87]
TE-SL**98**a	Device 1 **98**(105nm)	4.18	431	4.71	1.49	0.665	0.16, 0.08	[91c]
SP-SL**98**b	Device 1 **98**(70nm)	3.15	431	1.25	0.47	0.18	0.16, 0.07	[91c]
TE-SL**99**	Device 1 **99**(105nm)	3.03	453	1.89	1.96	0.960	0.15, 0.10	[92]
TE-SL**100**	Device 1 **100**(105nm)	2.80	455	1.48	0.15	0.125	0.15, 0.18	[92]
TE-SL**101**	ITO/**101**(80nm)/LiF(1nm)/Al(150nm)	2.9	452	2.50	2.5	2.0	0.15, 0.12	[91d, 103]
TE-SL**102**	ITO/**102**(80nm)/LiF(1nm)/Al(150nm)	3.5	436	0.85	0.56	0.43	0.15, 0.07	[91d]
TE-SL**103**a	ITO-CFx/**103**(70nm)/LiF(1nm)/Al(100nm)	3.4	440	2.00	1.54	0.95	0.15, 0.09	[104]
TE-SL**103**b	ITO-CFx/**103**(120nm)/LiF(1nm)/Al(100nm)	4.7	468	1.00	1.45	0.56	0.15, 0.18	[104]
TE-SL**104**	ITO-CFx/**104**(120nm)/LiF(1nm)/Al(100nm)	3.5	476	1.10	1.8	0.9	0.16, 0.24	[104]
TE-SL**105**	ITO/**110**(80nm)/LiF(1nm)/Al(150nm)	>4	436-464	-	0.83	-	0.16, 0.26	[105]
TE-SL**106**	Device 1 **106**(105nm)	3.22	452	0.54	0.153	0.084	0.16, 0.11	[92]
TE-SL**107**	ITO/**107**(80nm)/LiF(1nm)/Al(150nm)	>6	436-500	-	0.2	-	-	[105]

Table 25. Performance of SL-devices with OSC **97-107** as EML

In this series, the figure of merit is attributed to TE-SL**98**a with a very high EQE value of 4.71 %[91c] (**Table 25**). The carbazole/phenyl-fluorene/phenyloxadiazole combination appears hence as one of the best combination reported. Nevertheless, SP-SL**98**b only reaches an EQE of 1.25 % showing the influence of the deposition process on the performance of the device. However, whatever the deposition process, both devices emit blue light with CIE: 0.16, 0.08 for TE-SL**98**a and 0.16, 0.07 for SP-SL**98**b and λ_{EL}: 431 nm similar to the solid state PL spectrum (λ_{PL}: 430nm) (**Table 26**).

	λ_{abs}^{sol}/ λ_{abs}^{film} [nm]	λ_{PL}^{sol}/ λ_{PL}^{film} [nm]	Φ^{sol}/ Φ^{film} [%]	HOMO [eV]	LUMO [eV]	Ref
97	306,377/-	418,442,466/447 or 468	-/22 or 30	-4.89[a]	-1.67[a]	[91c]
98	344/-	387,409,431/427 or 439	-/38 or 50	-5.28[a]	-1.80[a]	[91c]
99	353,321(CyHx) or 350,321(ACN)/-	395,417(CyHx) or 498(ACN)/450	96(CyHx)/20	-5.15[c], -5.14[a]	-1.77[a]	[92]
100	363,312(CyHx) or 351,311(ACN)/-	402,424(CyHx) or 583(ACN)/470	80(CyHx)/17	-4.89[a]	-1.76[a]	[92]
101	310,376(Tol) or 309,372(DCM)/-	428(Tol) or 478(DCM)/466	89(Tol) or 65(DCM)/80	-5.19[c]	-2.2[b]	[91d, 103]
102	296,370(Tol) or 297,367(DCM)/-	405(Tol) or 435(DCM)/430	87(Tol) or 95(DCM)/63	-5.19[c]	-2.08[b]	[91d]
103	374(Tol)/376	419(Tol)/458	83(Tol)/47	-5.48[c]	-2.42[b]	[104]
104	375(Tol)/377	422(Tol)/458	89(Tol)/54	-5.48[c]	-2.46[b]	[104]
105	375($CHCl_3$)/-	435($CHCl_3$)/435	52($CHCl_3$)/-	-5.17[c]	-2.99[c]	[105]
106	357(CyHx) or 358(ACN)/-	400,420(CyHx) or 439(ACN)/450	99(CyHx)/21	-5.20[c], -5.22[a]	-	[92]
107	374($CHCl_3$)/-	435($CHCl_3$)/435	52($CHCl_3$)/-	-5.15[c]	-2.99[c]	[105]

[a]: from theoretical calculation, [b]: from ΔE^{opt}-$HOMO^{el}$, [c]: from cyclic voltammetry

Table 26. Selected electronic properties of OSCs **97-107**

A weak blue shift of the emission and a decrease of the performances are observed for TE-SL**99** and TE-SL**100**. In fact, increasing the donor strength of the carbazole group by t-Bu substitution in **99** or OCH_3 substitution in **100**, shifts the λ_{EL} to 453/455 nm and the CIE (0.15, 0.10 or 0.15, 0.18) and strongly decreases the EQE_{max} values from 4.71 % for TE-SL**98**a to 1.89 % for TE-SL**99** or 1.48 % for TE-SL**100**. This decrease may be linked to the decrease of Φ^{film} from 50 % for **98** to 20 or 17 % for **99** or **100** (Table 26). However, these EQE remain interesting showing the efficiency of such D-π-A design using a fluorenyl/phenyl core as central spacer.

To end with the phenyl-fluorene-oxadiazole series **97**-**100**, **97** possessing a diphenylamine as donor group displays the weakest performance with EQE equal or lower than 0.63% for TE-SL**97**a or SP-SL**97**b-c *resp.* The colour emitted by the **97**-based devices (λ_{EL} 484-487 nm) is red-shifted, compare that of the devices using **98** (λ_{EL} 431 nm), **99** (λ_{EL} 453 nm) or **100** (λ_{EL} 455 nm) as EML. This is caused by a stronger ICT in **97** due to the stronger electron donating effect of diphenylamine compared to carbazole (**98**-**100**).

In the **101**-**103** series, with similar D-π part, the acceptor is a phenyl-Benzimidazole in **101**-**102** or a triazole in **103**. For TE-SL**101**, EQE of 2.5 % is reached, similar to that of TE-SL**89**a (Figure 12, Table 23) with a central terphenyl core instead of a fluorene-phenyl one. The TE-SL**101** emission is centred at 452 nm (CIE: 0.15, 0.12) close to the emission of TE-SL**89**a (λ_{EL} 456 nm and CIE: 0.14, 0.09). Therefore, the rigidification of the central π-system from terphenyl in **89** to phenyl-fluorene in **101** only has a weak influence of the SL-OLED performances.

Oppositely, disruption of the conjugation by a *meta*-linkage in **102**, instead of the *para*-linkage in **101**, induces a strong decrease of the device performance with an EQE lower than 1 %

and a blue shifted emission centred at 436 nm (CIE: 0.15, 0.07) for TE-SL**102**. As for **89** and **90**, μ_e has been measured higher than μ_h (μ_e/μ_h: $65.7\times10^{-6}/20.5\times10^{-6}$ cm^2 V^{-1} s^{-1} for **101**[91d] and $90.1\times10^{-6}/11.2\times10^{-6}$ cm^2 V^{-1} $s^{-1}$for **102**[91d]). However, despite the higher μ_e measured for **102**, performance of TE-SL**102** remains three time lower than that of TE-SL**101**, which presents a better charge mobility balance (μ_e/μ_h = 3.2 for **101** and μ_e/μ_h = 8 for **102**).

With **103** as EML, increasing the TE-EML thickness from 70 nm (TE-SL**103**a) to 120 nm (TE-SL**103**b) leads to a decrease of EQE from 2% to 1 % (Table 25). This shows that the thickness of the EML is a very important parameter in single-layer devices. In addition, the EL spectra are also different as a function of the thickness (440 nm for TE-SL**103**a and 468 nm for TE-SL**103**b).

In the **104-107** series, the central π-system is either a difluorenyl-phenyl core in **104-106** or a terfluorenyl-phenyl core in **107**. In **105** and **107**, the acceptor triazole group is linked at the *meta*-position of the phenyl ring and is therefore decoupled from the oligofluorene π-system. Finally, in **106**, the donor is a carbazole and the acceptor is an oxadiazole group. Comparison of the devices performances will be done step by step.

First, one may directly compare the effect of the increase of conjugation length by the comparison of TE-SL**103**b and TE-SL**104**.[104] Both compounds possess similar HOMO and LUMO energy levels (-5.48/-2.42 eV for **103** and -5.48/-2.46 eV for **104**) as they are respectively driven by the donor and the acceptor units with no influence of the π-system. The optical properties are also similar for the 2 compounds: similar solid state λ_{PL} (458 nm) and Φ^{film} (0.47 for **103** and 0.54 for **104**). Performance of TE-SL**104** and TE-SL**103**b are roughly the same (EQE of 1.1 % for TE-SL**104** *vs* 1.0 % for TE-SL**103**b), the emission of the former (476 nm) being slightly red shifted (468 nm) compare to the latter due to the more extended π-conjugation pathway in **104** than in **103**. With a diphenylamine donor group and a triazole

acceptor group, the increase of the central π-system conjugation length from a phenyl-fluorene to a phenyl-bifluorene has no influence on the OLED performance. This is a different trend than that exposed above for **86**, **92** and **96** and highlights again the difficulty to draw precise design rules.

The influence of the central core may also be studied by the comparison of TE-SL**98**a and TE-SL**106**. **98** and **106** possess a donor carbazole and an acceptor aryl-oxadiazole unit with different spacers: a phenyl-fluorenyl in **98** or a phenyl-difluorenyl in **106**.

The physicochemical properties of **98**/**106** are similar with a HOMO spread out on the carbazole lying at -5.28/-5.22 eV, an emission maximum at 430/450 nm and Φ^{film} of 0.38/0.21 resp. (Table 26). A lowering of V_{on} is observed from 4.18 V for TE-SL**98**a to 3.22 V for TE-SL**106** signing an easier injection of the charge in the more conjugated **106**. However, despite this V_{on} lowering, the performance of TE-SL**106** is low with EQE of 0.54 % compared to 4.71 % for TE-SL**98**a. This is a very interesting feature surely due to the different mobility of the charge carriers. Finally, TE-SL**106** displays an EL spectrum centred at 452 nm (CIE: 0.16, 0.11) whereas that of TE-SL**98**a is centred at 431nm (CIE: 0.16, 0.08) due to the different π-conjugation pathway.

Comparison of the performance of TE-SL**105** and TE-SL**107** also shed light on the influence of the central core length (a bifluorene in **105** or a terfluorene in **107**).[105] With similar device configurations, one observes that TE-SL**105** exhibited higher performance than TE-SL**107** (CE_{max} reaching 0.83 or 0.20 cd A^{-1} *resp.*) (Table 25) showing again that increasing the central π-system does not always tend to higher performances.

To conclude on all these examples, it seems that terphenyl and phenyl-fluorene π-systems appear as the best central cores to bridge a donor and an acceptor unit. Increasing the length of the central core using phenyl-bifluorene or phenyl-terfluorene leads in most of the presented

examples to a lowering of the devices performance. From a more general point of view, the length of the π-spacer is directly linked to the emitted wavelength of the device (see for example TE-SL**98**a and TE-SL**106**, λ_{EL}: 431 and 452 nm *resp.* or TE-SL**103**b and TE-SL**104**, λ_{EL}: 468 and 476 nm *resp.*), but its impact on the performance is more difficult to predict.

5.3 D-π-A design with other aryl-spacers: spirobifluorene, thiophene, dihydroindenofluorene, anthracene or naphthalene.

In **Figure 14**, are gathered a series of D-π-A OSCs with aryl spacers derived either from spirobifluorene **108-109** framed in blue, DHIF **113** or aryl-fluorene **110-112** associated to donor (diphenylamine or carbazole derivatives) and acceptor units (benzimidazole or oxadiazole) framed in red. A last series of D-π-A derivatives (framed in green) possess a similar donor diphenylamine unit and differ (i) from their central aryl spacer which is a phenyl-binaphtalene in **114** and **115** or a bis(biphenyl)anthracene in **116** and (ii) from their acceptor unit which is a 1-phenyl-1H-benzo[d]imidazol-2-yl in **114** and **116** and a 2-phenyl-1H-benzo[d]imidazol-1-yl)phenyl in **115**.

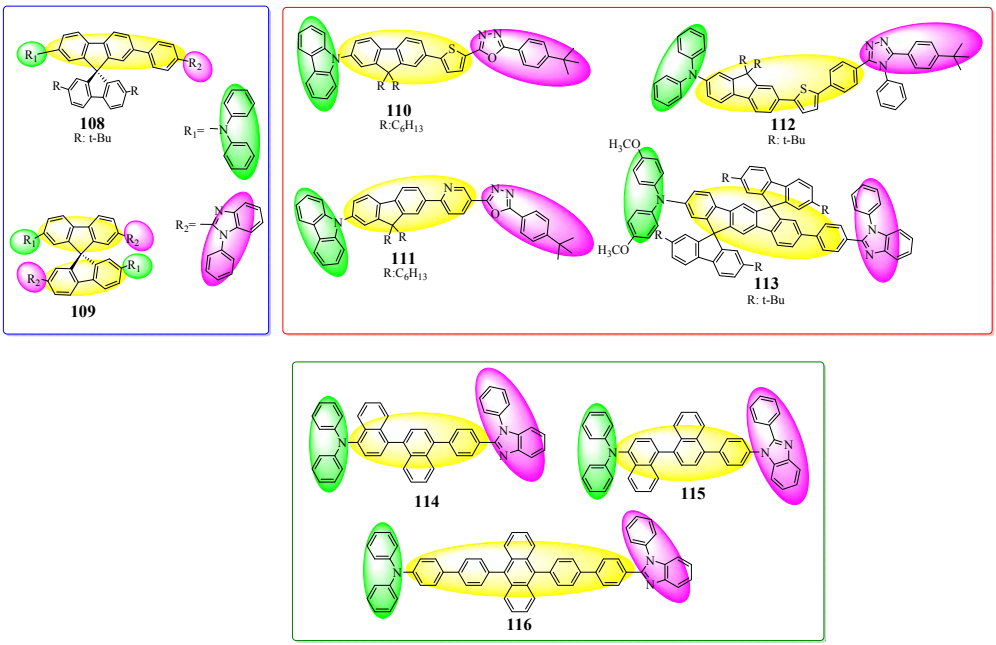


Figure 14. Other aryl-spacers in D-π-A design (OSCs **108-116**)

Device numbering and structure		V_{on} [V]	λ_{EL} [nm]	EQE_{max} [%]	CE_{max} [cd A^{-1}]	PE_{max} [lm W^{-1}]	CIE 1931 [x, y]	Ref
TE-SL**108**	ITO/**108**(80nm)/LiF(1nm)/Al(150nm)	2.9	458	1.40	1.8	1.1	0.15, 0.15	[91d, 103]
SL**109**	ITO/PEDOT:PSS(30nm)/**109**(100nm)/ LiF(0.5nm)/Al(100nm)	4	460	0.52	0.61	0.14	0.15, 0.14	[91e]
TE-SL**110**	Device 1 **110**(105nm)	3.04	484	0.38	0.703	0.41	0.18, 0.27	[92]
TE-SL**111**	Device 1 **111**(105nm)	3.87	453	0.2	0.034	0.014	0.16, 0.12	[92]
TE-SL**112**	ITO/CFx/**112**(70nm)/LiF(1nm)/Al(100nm)	2.9	488	1.18	2.85	2.1	0.20, 0.40	[104]
TE-SL**113**	ITO/PEDOT:PSS(40nm)/**113**(40nm)/ LiF(0.8nm)/Al(75nm)	5.3	470	-	0.12	-	0.17, 0.31	[35a]
TE-SL**114**	ITO/**114**(80nm)/LiF(1nm)/Al(100nm)	9.5	464	0.08	0.13	0.03	0.16, 0.21	[106]
TE-SL**115**	ITO/**115**(80nm)/LiF(1nm)/Al(100nm)	8.5	458	0.13	0.17	0.04	0.16, 0.17	[106]
TE-SL**116**	ITO/**116**(80nm)/LiF(1nm)/Al(100nm)	2.6	456	2.64	3.33	2.64	0.16, 0.16	[91f]

Table 27. Performance of SL-devices with OSCs **108-116** as EML

	λ_{abs}^{sol}/ λ_{abs}^{film} [nm]	λ_{PL}^{sol}/ λ_{PL}^{film} [nm]	Φ^{sol}/ Φ^{film} [%]	HOMO [eV]	LUMO [eV]	Ref
108	309,376(Tol) or 315,376(DCM)/-	428(Tol) or 475(DCM)/457	76(Tol) or 88(DCM)/72	-5.21[d]	-2.21[b]	[91d, 103]
109	307,386(CyHx)/310,381	412(CyHx) or 468(ACN)/460	84(DCM)/41	-5.46[d]	-2.6[d]	[91e]
110	370(CyHx) or 370(ACN)/-	412,435(CyHx) or 472(ACN)/467	86(CyHx)/17	-5.25[d], -5.28[a]	-2.04[a]	[92]
111	363(CyHx) or 353(ACN)/-	392,415(CyHx) or 505(ACN)/450	99(CyHx)/36	-5.29[d], -5.26 [a]	-1.97[a]	[92]
112	397(Tol)/403	452(Tol)/498	61(Tol)/23	-5.86[d]	-3.09[b]	[107]
113	410(CyHex)/-	435(CyHex)/-	85(CyHex)/-	-4.9[d]	-2.3[d], -2.07[b]	[35a]
114	304,364(DCM)/290	465(DCM)/449	33(Tol)/-	-5.84[c], -6.6[a]	-2.83[b], -0.10[a]	[106]
115	296,352(DCM)/290	457(DCM)/446	45(Tol)/-	-5.85[c], -6.88[a]	-2.80[b], -0.24[a]	[106]
116	320,357,377,397 (Tol) or 315,357,377,397 (DCM) or 315,357,377,397 (THF)/-	439 (Tol) or 498 (DCM) or 454 (THF)/444	82(Tol)/-	-5.28[d], -4.95[a]	-2.32[d], -1.62[b]	[91f]

[a]: from theoretical calculation, [b]: from ΔE^{opt}-$HOMO^{EPS}$ or $HOMO^{el}$, [c]: from Energy Photoelectron Spectrometry, [d]: from cyclic voltammetry

Table 28. Selected electronic properties of OSCs **108-116**

108 possesses a central spirobifluorene core, a diphenylamine (R_1) and benzimidazole (R_2) attached on the same phenyl-fluorene.[91d] TE-SL**108** with ITO/EML (80 nm)/LiF/Al configuration (**Table 27**) can be compared to TE-SL**89**a and TE-SL**101**.

89, **101** and **108** only differ by their spacer units (terphenyl in **89**, phenyl-fluorene in **101** or phenyl-SBF in **108**) and present similar HOMO/LUMO energy levels (-5.2 eV/-2.2 eV), similar λ_{PL}^{film} (ca 460 nm) and similar solid state Φ^{film} (ca 0.75) (**Tables** 24, 26 and **28**). This shows that in these examples the π-spacer only has a very weak influence on their electronic properties. The three devices emit similar blue-light centred at ca 455 nm (CIE: 0.14, 0.09 for TE-SL**89**a, 0.15, 0.12 for TE-SL**101** or 0.15, 0.15 for TE-SL**108**) with high EQE values: TE-SL**108** (1.4 %), TE-SL**101** (2.5 %) and TE-SL**89**a (2.4 %). Since the Φ^{film} of the three compounds are similar, the lowering of the performance found for TE-SL**108** may not come

from this difference of fluorescence efficiency. One explanation may come from the three dimensional architecture of **108** which modifies the interaction electrode/OSC and the packing in the solid state that may decrease the charge transport in the EML. Indeed, in the case of **89** and **101**, μ_e is higher than μ_h whereas in the case of **108**[91d], the opposite is observed (μ_e/μ_h: $11.7\times10^{-6}/23.8\times10^{-6}$ cm^2 V^{-1} s^{-1}).

Another spirobifluorene based OSC, **109**, possess two D-π-A chromophores bonded perpendicularly through a tetrahedral carbon atom, leading to an orthogonal configuration that impedes the π-orbital interactions between the individual D/A chromophore branches.[91e] The use of **109** as EML leads to a blue emission (λ_{EL}: 460 nm, CIE: 0.15, 0.14). The device performance is however lower than that reached by TE-SL**108** (EQE of 0.52 % *vs* 1.4 %) with a higher V_{on} as well (4 V *vs* 2.9 V). The lowering of the performances and the increase of the V_{on} may be explained by the difference of the HOMO energy level which is deeper for **109** (-5.46 eV) than for **108** (-5.21 eV). Charge-carrier mobility measurements of **109**[91e] using time-of-flight techniques provides μ_h of ca. 10^{-4} cm^2 V^{-1} s^{-1} and μ_e of ca. 3×10^{-6} cm^2 V^{-1} s^{-1} (μ_h / μ_e larger than 33).

Another series of D-π-A OSCs based on different arylene central cores, **110-113**, are also described in Figure 14. In this series, the central π-system is either a fluorenyl-thienyl group in **110**[92], a fluorenyl-pyridyl group in **111**[92], a fluorenyl-thienyl-phenyl group in **112** or a phenyl-dispirofluorene-indenofluorene derivative in **113**. In **110** and **111**, a carbazole/oxadiazole combination is used, in **112**, a diphenylamine/triazole combination and in **113** a diphenylamine/benzimidazole combination.

TE-SL**112** emits a green-blue light (λ_{EL}: 488 nm and CIE: 0.20, 0.40) whereas the devices using the other OSCs emit blue-light with EL spectra centred around 453 and 484 nm (CIE varying from 0.16, 0.12 with **111** and 0.18, 0.27 with **110**). As the four devices using **110-113**

have different architectures, the comparison is difficult. The higher EQE (1.18 %) is obtained for TE-SL**112** whereas the lowest one is obtained for TE-SL**113**. The comparison of the light emitted by **98**, **110**, **111** and **112** with only a modulation of the spacer between the fluorene and the oxadiazole acceptor core shows a shift of the emission from blue for TE-SL**98**a (CIE: 0.16, 0.08) with the phenyl spacer (Figure 13), to lighter blue for TE-SL**111** (CIE: 0.16, 0.12) with the pyridine link and TE-SL**110** (CIE: 0.18, 0.27) with the thienyl link, whereas extension to a phenyl-thienyl link in **112** shifts the light towards green of TE-SL**112** (CIE: 0.20, 0.40).

TE-SL**116** reaches high performance values with EQE_{max} of 2.64 % with a particularly low V_{on} of 2.6 V (especially since neat ITO is used) whereas those based on **114** and **115** only reach very weak performances (EQE_{max} of 0.13 % for TE-SL**115** and of 0.08 % for TE-SL**114**). Interestingly, in **116**, the acceptor group is the 1-phenyl-1H-benzo[d]imidazol-2-yl fragment also found in **86** and **93**, confirming the potential of this fragment. It should be noted that the anthracenyl core, which is a very efficient emitter, can also be involved in these high performances. The HOMO level of **116** is lying at -5.28 eV being the highest in this series. Higher performances should be obtained with ITO/PEDOT:PSS anode.

The weaker performance of TE-SL**114** (**114** also possesses the 1-phenyl-1H-benzo[d]imidazol-2-yl acceptor group) may be related both (i) to the lowest Φ^{sol} of **114** (33% in toluene) and (ii) to a weaker accessibility of the free nitrogen atom in **114** caused by the naphthalene group.

In conclusion, in the D-π-A series, the best performances (EQE_{max} around 4.5 %) have been reached with **98**, **92** and **89** as EML in devices of different architectures. In **98**, the donor is a carbazole unit and the acceptor an oxadiazole group. **89** and **92** with both a diphenylamine donor group and a phenylbenzimidazole derivative as acceptor group, used in a same device architecture (ITO/HATCN (5 nm)/EML (80 nm)/LiF (1 nm)/Al), also lead both to high

performances. One may also note that bridging the two phenyl units of **89** provides **101** and leads to a strong decrease of the EQE from 4.29 to 2.5 %. This shows that the best results obtained in **98** are not due to the phenyl-fluorenyl spacer but might also be due to the carbazole fragment and/or to the device configuration.

6. General Conclusions

Considering the 137 devices based on the 116 OSCs, one can note that only 21 devices (15 % of all the devices) reach an EQE_{max} equal or higher to 2%, then 15 % of the devices present an EQE between 2 and 1 % and the last 70 % devices present an EQE lower than 1 %, showing the high difficulty to obtain efficient blue SL-OLEDs. The following conclusions will be dedicated to the 15% most efficient devices which are gathered from the highest to the lowest performance (from 5.2 to 2 %) in **Table 29** and summarized in **figure 15**.

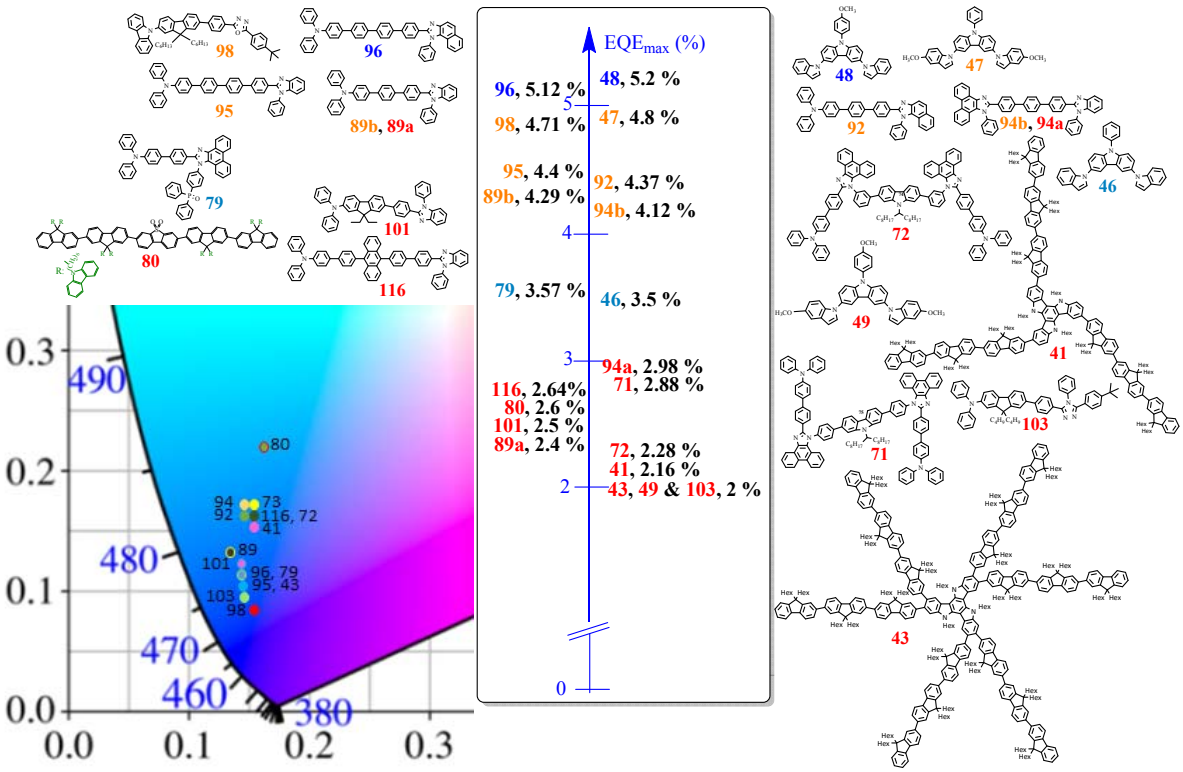


Figure 15. Summary of devices reaching EQE higher than 2% & their CIE coordinates.

First, except for **80** (CIE :0.17, 0.22) and for **46-49** for which only the emission wavelength around 400 nm is reported,[67] the CIE coordinates of almost all these devices are below (0.20, 0.20) indicating an emission in the blue region (Figure 15).

Device numbering and structure		V_{on} [V]	λ_{EL} [nm]	EQE_{max} [%]	CE_{max} [cd A^{-1}]	CIE 1931 [x, y]	Ref
TE-SL**48**	ITO/CuI/**48**(30nm)/Ca/Al	4.0	400	**5.20**	4.20	-	[67]
TE-SL**96**	ITO/HATCN(5nm)/**96** (80nm)/LiF(1nm)/Al	2.6	450	**5.12**	4.96	0.15, 0.11	[98]
TE-SL**47**	ITO/CuI/**47**(30nm)/Ca/Al	4.0	400	**4.80**	4.00	-	[67]
TE-SL**98**a	ITO/PEDOT:PSS/**98**(105nm)/Ca/Al	4.2	431	**4.71**	1.49 (@ 20 mA)	0.16, 0.08	[91c]
TE-SL**95**	ITO/HATCN(5nm)/**95** (80nm)/LiF(1nm)/Al	2.6	451	**4.40**	4.22	0.15, 0.10	[98]
TE-SL**92**	ITO/HATCN(5nm)/**92**(80nm)/LiF(1nm)/Al	2.7	452	**4.37**	4.28	0.15, 0.16	[93]
TE-SL**89**b	ITO/HATCN(5nm)/**89**(80nm)/LiF(1nm)/Al	2.7	460	**4.29**	4.84	0.14, 0.13	[96]
TE-SL**94**b	ITO/HATCN(5nm)/**94**(70nm)/LiF(1nm)/Al(150nm)	2.8	460	**4.12**	6.29	0.15, 0.17	[97]
TE-SL**79**	ITO/MoO_3(3nm)/**79**(120nm)/LiF(1nm)/Al(120nm)	3.0	448	**3.57**	3.66	0.15, 0.12	[88]
TE-SL**46**	ITO/CuI/**46**(30nm)/Ca/Al	6.2	425	**3.50**	3.7	-	[67]
TE-SL**94**a	ITO/**94** (70nm)/LiF (1nm)/Al(150nm)	3.1	452	**2.98**	3.77	0.15, 0.14	[97]
SP-SL**71**	ITO/PEDOT:PSS(40nm)/**71**(50nm)/CsF(1nm)/Al(100nm)	5.1	461	**2.88**	3.71	0.16, 0.17	[85]
TE-SL**116**	ITO/**116**(80nm)/LiF(1nm)/Al(100nm)	2.6	456	**2.64**	3.33	0.16, 0.16	[91f]
SP-SL**80**a	ITO/PEDOT:PSS(40nm)/**80**(80nm)/CsF(1.5nm)/Al(120nm)	3.8	454	**2.60**	2.8	0.17, 0.22	[58e]
TE-SL**101**	ITO/**101**(80nm)/LiF(1nm)/Al(150nm)	2.9	452	**2.50**	2.5	0.15, 0.12	[91d, 103]
TE-SL**89**a	ITO/**89**(80nm)/LiF(1nm)/Al(150nm)	3.0	456	**2.40**	1.90	0.14, 0.09	[91d]
SP-SL**72**	ITO/PEDOT:PSS(40nm)/**72**(50nm)/CsF(1nm)/Al(100nm)	5.7	465	**2.28**	2.76	0.16, 0.16	[85]
SP-SL**41**a	ITO/PEDOT:PSS/**41**(100nm)/Ba/Al	3.3	444, 465(sh)	**2.16**	1.56	0.16, 0.15	[62]
TE-SL**49**	ITO/CuI/**49**(30nm)/Ca/Al	3	425	**2.00**	3.60	-	[67]
SP-SL**43**a	ITO/PEDOT:PSS/**43**(130nm)/Ba/Al	5.3	442	**2.00**	2.07	0.15, 0.09	[64]
TE-SL**103**a	ITO-CFx/**103**(70nm)/LiF(1nm)/Al(100nm)	3.4	440	**2.00**	1.54	0.15, 0.09	[104]

Table 29. Summary of the performance of SL-devices with EQE higher than 2% (from **5.2** to **2** %).

The different performance of these SL-OLEDs may be discussed through three different standpoints: (i) the OSC design, (ii) the structure of the device and (iii) the EML deposition process.

- The nature of the OSCs.

Of course, we have shown in this review that the OSCs design in SL-OLEDs is very important to reach high performance. Despite very high performance have been reached with *all donor* designs ($D(\pi)_3$ for **41**, $D(\pi)_6$ for **43**, $D(D_2)$ for **46-47** or $D(D_3)$ for **48-49)**, it seems that the introduction of both electron-rich and electron-poor fragments on a π-conjugated fragment is the most efficient strategy to reach high efficiency devices ("D-π-A" design in **89**, **92**, **94-96**, **98**, **101**, **103** and **116**, different "A/D" designs in **71-72** and **79**, and "π-A-π" decorated by non-conjugated donor carbazole units for **80**). Thus, combining Donor and Acceptor fragments in a fluorophore allows to adjust both HOMO and LUMO energy levels

to favour the injection from the electrodes and to improve the charge carriers balance (note that however hole/electron mobilities are not very often reported in the works reviewed herein). Thus, and except three devices (TE-SL**103**a, TE-SL**101** and TE-SL**116** with EQE_{max} of respectively 2, 2.5 and 2.64 %), the eight others based on "D-π-A" designs have very good EQE_{max} higher than 4.37%, showing a kind of homogeneity in the performance obtained with such a design. However, not all the molecules constructed on this design are performant, which means that finding the good D/A combination is far from being an easy task. In addition, other parameters such as the ability to stack (which depends on each molecular structure) are also crucial in the devices performance and depends on the D/A combination. It is very difficult to select precisely the best electron-rich and electron-poor fragment used in SL-OLED as the combination is more important than the fragment itself. However, carbazole and imidazole are very often found in the best blue fluorophores reported herein, showing clearly the efficiency of these fragments. One can particularly note the efficiencies of the acceptor groups: 1-phenyl-1H-benzo[d]imidazol-2-yl (found in **89** and **94**-**95**) and 3-phenyl-3H-naphtho[1,2-d]imidazol-2-yl (found in **92** and **96**) for which the authors suspected a beneficial coordination effect with LiF.[93]

- The device structure

Despite the very simple architecture of SL-OLEDs, the device structure is also important. Considering the devices with EQE_{max} higher than 3.5 %, they all possess a (i) thin HIL (CuI, HATCN, or PEDOT-PSS) covering the ITO surface and (ii) similar cathodes (either Ca/Al or LiF/Al).

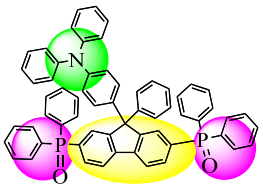
The influence of the presence of the HATCN layer is interestingly pointed (i) for devices TE-SL**89**b/TE-SL**89**a reaching EQE_{max} of 4.29/2.4% with/without the HATCN layer and (ii) for devices TE-SL**94**b/TE-SL**94**a reaching EQE_{max} of 4.12/2.98% with/without the HATCN layer.

Systematic studies of the impact of HIL should be done to clearly determine the best for blue SL-OLEDs. Thus, despite a wide range of hole injectors are used nowadays in multi-layer devices, only few of them have been tested in SL-OLEDs.

- The EML deposition process

Looking at the devices with EQE_{max} higher than 3.5 %, they are all constructed with the EML thermally evaporated on the HIL. This clearly indicates that this deposition process is better than the solution processing one. Using this deposition process may then increase the performance of the best SL-OLEDs reviewed herein (with **41**, **43**, **71**, **72** or **80** as EML). However, solution processed devices are highly appealing for the future.

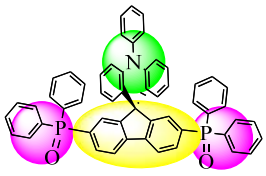
Nowadays, SL devices continue to hold the attention of research groups but are more focused on the second generations of OLEDs, namely phosphorescent-OLEDs,[44b, 108] which lead to higher device performances as they recover through Forster and Dexter energy transfers all the excitons (singlet and triplet). With EQE reaching more than 17 % with specific host materials doped with the blue phosphorescent dopant bis[2-(4,6-difluorophenyl)pyridinato-C2,*N*](picolinato)iridium(III) (**FIrpic**), blue SL-PhOLEDs already display very high performance, getting close to those of multi-layer PhOLEDs. As significant examples, devices with 2,7-bis(diphenylphosphoryl)-9-[4-(N,N-diphenylamino)phenyl]-9-phenylfluorene (**POAPF**)[109] or Spirophenylacridine-2,7-(diphenylphosphineoxide)-fluorene (**SPA-F(POPh$_2$)$_2$**)[110] (**Figure 16**) reach EQE_{max} of 20.3 and 17.6 % respectively.



POAPF

ITO/PEDOT :PSS/**POAPF**:**FIrpic** 8%/LiF/Al

EQE_{max}: 20.3 %



SPA-F(POPh$_2$)$_2$

ITO/PEDOT:PSS/**SPA-F(POPh$_2$)$_2$**:**FIrpic** 10%/LiF/Al

EQE_{max}: 17.6 %

Figure 16. Best host materials for Blue SL-PhOLEDs

To the best of our knowledge, efficient non-doped blue SL-OLEDs,[111] using the third generation of thermally activated delayed fluorescence OLED are not described in literature yet. This could be a very promising path to explore as the best blue TADF-OLEDs with multi-layer architecture display nowadays higher efficiency (EQE_{max} reaching 37 %[112]) than those of multi-layer blue PhOLEDs (33.2 %[113]).

Thus, thanks to their extreme simplicity, SL devices can reduce the energetic cost of an OLED and therefore reduce its environmental footprint. This is the reason why the '*single-layer technology*' undoubtedly needs nowadays fundamental researches.

Appendix-Abbreviations and Acronyms

-: not available
Underline the most intense band
ΔE^{opt}: optical energy gap
λ_{abs}^{film}: absorbance wavelength in solid state
λ_{abs}^{sol}: absorbance wavelength in solution
λ_{EL}: electroluminescence wavelength
λ_{PL}^{film}: photoluminescence wavelength in solid state
λ_{PL}^{sol}: photoluminescence wavelength in solution
μ_h: hole's mobility
μ_e: electron's mobility
Φ^{film}: fluorescent quantum yield solid state
Φ^{sol}: fluorescent quantum yield in solution

AcEt: ethylacetate
ACN: acetonitrile
Alq_3: 8-hydroxyquinoline aluminium
BI: benzimidazole
CE: current efficiency
CIE: Commission Internationale de l'Eclairage
CuPc: copper-phtalocyanin (CuPc)
CyHx: cyclohexane
DCM: CH_2Cl_2
Device 1: ITO/PEDOT:PSS/EML/Ca/Al
DHIF: dihydroindenofluorene
DMF: N,N-dimethylformamide
DMSO: dimethyl sulfoxide
EBL: electron blocking layer
EIL: electron injection layer
EL: Electroluminescence
EML: Emissive layer
EQE: external quantum efficiency
Et_3N: triethylamine
ETL: electron transporting layer
FIrpic: bis[2-(4,6-difluorophenyl)pyridinato-C2,*N*](picolinato)iridium(III)
GEB: green emission band
HATCN: Dipyrazino[2,3-f:2',3'-h]quinoxaline 2,3,6,7,10,11-hexacarbonitrile
HBL: hole blocking layer
Hex: hexane
HIL: hole injection layer
HOMO: highest occupied molecular orbital
HTL: hole transporting layer
LUMO: lowest unoccupied molecular orbital
ICT: intramolecular charge transfer
ITO: Indium Tin Oxide
OLED: Organic Light-Emitting Diode
OSC: organic semi-conductor
PE: power efficiency
PEDOT:PSS: poly(3,4-ethylenedioxythiophene):poly(4-styrenesulfonate)
PHC: pure hydrocarbon
PhOLED: phosphorescent OLED
PI: phenanthroimidazole
PL: photoluminescence
sh: shoulder
SL-OLED: Single-Layer OLED
SP-EML: solution processed EML
TE-EML: thermally evaporated EML
THF: tetrahydrofuran
Tol: toluene
TPB: tetraphenylbenzidine
V_{on}: threshold voltage

Acknowledgements

The authors would like to thank the CNRS, the University of Rennes 1, the ANR (11-BS07-020-01/14-CE05-0024), the ADEME and the Région Bretagne for their respective financial supports. Dr. J.F. Bergamini from ISCR (Rennes) is acknowledged for the design of the Scheme 2.

References

[1] a) A. Bernanose, M. Comte, P. Vouaux, *J. Chim. Phys.* **1953**, 50, 64; b) A. Bernanose, P. Vouaux, *J. Chim. Phys.* **1953**, 50, 261; c) A. Bernanose, G. Marquet, *J. Chim. Phys.* **1954**, 51, 255; d) A. Bernanose, F. Michon, *J. Chim. Phys.* **1954**, 51, 622; e) A. Bernanose, *J. Chim. Phys.* **1955**, 52, 396; f) A. Bernanose, *Brit. J. Applied Phys.* **1955**, 6, S54.

[2] M. Pope, H. P. Kallmann, P. Magnante, *J. Chem. Phys.* **1963**, 38, 2042.

[3] P. S. Vincett, W. A. Barlow, R. A. Hann, G. G. Roberts, *Thin Solid Films* **1982**, 94, 171.

[4] C. W. Tang, S. A. VanSlyke, *Appl. Phys. Lett.* **1987**, 51, 913.

[5] J. H. Burroughes, D. D. C. Bradley, A. R. Brown, R. N. Marks, K. Mackay, R. H. Friend, P. L. Burns, A. B. Holmes, *Nature* **1990**, 347, 539.

[6] R. Mertens, *The OLED Handbook- A guide to OLED technology, Industry & Market*, **2019**.

[7] a) L. S. Hung, C. H. Chen, *Mater. Sci. Eng., R* **2002**, 39, 143; b) S.-W. Wen, M.-T. Lee, C. H. Chen, *J. Disp. Technol.* **2005**, 1, 90; c) X. Yang, X. Xu, G. Zhou, *J. Mater. Chem. C* **2015**, 3, 913.

[8] C. Adachi, M. A. Baldo, M. E. Thompson, S. R. Forrest, *J. Appl. Phys.* **2001**, 90, 5048.

[9] a) Y. Im, S. Y. Byun, J. H. Kim, D. R. Lee, C. S. Oh, K. S. Yook, J. Y. Lee, *Adv. Funct. Mater.* **2017**, 27, 1603007; b) J.-H. Lee, C.-H. Chen, P.-H. Lee, H.-Y. Lin, M.-k. Leung, T.-L. Chiu, C.-F. Lin, *J. Mater. Chem. C* **2019**, 7, 5874.

[10] a) M. R. Maciejczyk, S. Zhang, G. J. Hedley, N. Robertson, I. D. W. Samuel, M. Pietraszkiewicz, *Adv. Funct. Mater.* **2019**, 29, 1807572; b) Y. Xu, X. Liang, X. Zhou, P. Yuan, J. Zhou, C. Wang, B. Li, D. Hu, X. Qiao, X. Jiang, L. Liu, S.-J. Su, D. Ma, Y. Ma, *Adv. Mater.* **2019**, 31, 1807388; c) S. Wang, M. Qiao, Z. Ye, D. Dou, M. Chen, Y. Peng, Y. Shi, X. Yang, L. Cui, J. Li, C. Li, B. Wei, W.-Y. Wong, *iScience* **2018**, 9, 532; d) W. Liu, S. Ying, R. Guo, X. Qiao, P. Leng, Q. Zhang, Y. Wang, D. Ma, L. Wang, *J. Mater. Chem. C* **2019**, 7, 1014.

[11] J. Lakowicz, R., *Principles of fluorescence spectroscopy*, Springer, New-York **2006**.

[12] L. Zhao, S. Wang, S. Shao, J. Ding, L. Wang, X. Jing, F. Wang, *J. Mater. Chem. C* **2015**, 3, 8895.

[13] C.-C. Wu, Y.-T. Lin, K.-T. Wong, R.-T. Chen, Y.-Y. Chien, *Adv. Mater.* **2004**, 16, 61.

[14] D. Xia, C. Duan, S. Liu, D. Ding, M. Baumgarten, M. Wagner, D. Schollmeyer, H. Xu, K. Müllen, *New J. Chem.* **2019**, 43, 3788.

[15] C. Poriel, J.-J. Liang, J. Rault-Berthelot, F. Barrière, N. Cocherel, A. M. Z. Slawin, D. Horhant, M. Virboul, G. Alcaraz, N. Audebrand, L. Vignau, N. Huby, G. Wantz, L. Hirsch, *Chem. Eur. J.* **2007**, 13, 10055.

[16] C. Poriel, J. Rault-Berthelot, D. Thirion, F. Barrière, L. Vignau, *Chem. Eur. J.* **2011**, 17, 14031.

[17] N. Cocherel, C. Poriel, J. Rault-Berthelot, F. Barrière, N. Audebrand, A. M. A. Slawin, L. Vignau, *Chem. Eur. J.* **2008**, 14, 11328.

[18] F. Liu, W.-Y. Lai, C. Tang, H.-B. Wu, Q.-Q. Chen, B. Peng, W. Wei, W. Huang, Y. C. Cao, *Macromol. Rapid Commun.* **2008**, 29, 659.
[19] B. Kaur, D. Moghe, A. Dey, D. Kabra, J. Jacob, *J. Lumin.* **2018**, 196, 511.
[20] Y. Zhou, L. Ding, L.-M. Xiang, J. Pei, *Aust. J. Chem.* **2011**, 64, 160.
[21] J. F. Tannaci, M. Noji, J. McBee, T. D. Tilley, *J. Org. Chem.* **2007**, 72, 5567.
[22] K.-T. Wong, Y.-Y. Chien, R.-T. Chen, C.-F. Wang, Y.-T. Lin, H.-H. Chiang, P.-Y. Hsieh, C.-C. Wu, C. H. Chou, Y. O. Su, G.-H. Lee, S.-M. Peng, *J. Am. Chem. Soc.* **2002**, 124, 11576.
[23] a) Y. Jiang, Y.-X. Lu, Y.-X. Cui, Q.-F. Zhou, Y. Ma, J. Pei, *Org. Lett.* **2007**, 9, 4539 ; b) Y. Jiang, L. Wang, Y. Zhou, Y.-X. Cui, J. Wang, Y. Cao, J. Pei, *Chem. Asian J.* **2009**, 4, 548.
[24] a) G. Klaerner, R. D. Miller, *Macromolecules* **1998**, 31, 2007; b) S. H. Lee, T. Tsutsui, *Thin Solid Films* **2000**, 363, 76.
[25] J. Rault-Berthelot, *Curr. Topics Electrochem.* **2004**, 10, 265.
[26] a) A. G. MacDiarmid, *Angew. Chem. Int. Ed.* **2001**, 40, 2581; b) A. C. Grimsdale, K. L. Chan, R. E. Martin, P. G. Jokisz, A. B. Holmes, *Chem. Rev.* **2009**, 109, 897.
[27] a) D. L. Horrocks, W. G. Brown, *Chem. Phys. Lett.* **1970**, 5, 117; b) L. Sicard, C. Quinton, J.-D. Peltier, D. Tondelier, B. Geffroy, U. Biapo, R. Métivier, O. Jeannin, J. Rault-Berthelot, C. Poriel, *Chem. Eur. J.* **2017**, 23, 7719.
[28] N. Fomina, S. E. Bradforth, T. E. Hogen-Esch, *Macromolecules* **2009**, 42, 6440.
[29] M. Belletête, M. Ranger, S. Beaupré, M. Leclerc, G. Durocher, *Chem. Phys. Lett.* **2000**, 316, 101.
[30] a) C. Poriel, N. Cocherel, J. Rault-Berthelot, L. Vignau, O. Jeannin, *Chem. Eur. J.* **2011**, 17, 12631; b) A. C. Grimsdale, *Curr. Org. Chem.* **2010**, 14, 2196; c) K. L. Chan, M. Sims, S. I. Pascu, M. Ariu, A. B. Holmes, D. D. C. Bradley, *Adv. Funct. Mater.* **2009**, 19, 2147; d) F. Montilla, R. Mallavia, *Adv. Funct. Mater.* **2007**, 17, 71.
[31] M. Y. Odoi, N. I. Hammer, H. P. Rathnayake, P. M. Lahti, M. D. Barnes, *ChemPhysChem* **2007**, 8, 1481.
[32] a) Y.-F. Bo, Y.-Y. Liu, H. Soleimaninejad, M.-N. Yu, L.-H. Xie, T. A. Smith, K. P. Ghiggino, W. Huang, *J. Phys. Chem. A* **2019**, 123, 2789; b) L. Sicard, O. Jeannin, J. Rault-Berthelot, C. Quinton, C. Poriel, *ChemPlusChem* **2018**, 83, 874.
[33] C.-C. Wu, T.-L. Liu, W.-Y. Hung, Y.-T. Lin, K.-T. Wong, R.-T. Chen, Y.-M. Chen, Y.-Y. Chien, *J. Am. Chem. Soc.* **2003**, 125, 3710.
[34] C. Poriel, J. Rault-Berthelot, *Acc. Chem. Res.* **2018**, 51, 1818.
[35] a) D. Thirion, J. Rault-Berthelot, L. Vignau, C. Poriel, *Org. Lett.* **2011**, 13, 4418; b) D. Thirion, M. Romain, J. Rault-Berthelot, C. Poriel, *J. Mater. Chem.* **2012**, 22, 7149.
[36] a) M. Romain, M. Chevrier, S. Bebiche, T. Mohammed-Brahim, J. Rault-Berthelot, E. Jacques, C. Poriel, *J. Mater. Chem. C* **2015**, 3, 5742; b) S. Bebiche, I. Bouhadda, T. Mohammed-Brahim, N. Coulon, J. F. Bergamini, C. Poriel, E. Jacques, *Solid State Electron.* **2017**, 130, 49; c) S. Bebiche, P. Cisneros-Perez, T. Mohammed-Brahim, M. Harnois, J. Rault-Berthelot, C. Poriel, E. Jacques, *Mater. Chem. Front.* **2018**, 2, 1631.
[37] a) M. Romain, S. Thiery, A. Shirinskaya, C. Declairieux, D. Tondelier, B. Geffroy, O. Jeannin, J. Rault-Berthelot, R. Métivier, C. Poriel, *Angew. Chem Int. Ed.* **2015**, 54, 1176; b) M. Romain, C. Quinton, D. Tondelier, B. Geffroy, O. Jeannin, J. Rault-Berthelot, C. Poriel, *J. Mater. Chem. C* **2016**, 4, 1692; c) M. Romain, D. Tondelier, B. Geffroy, O. Jeannin, E. Jacques, J. Rault-Berthelot, C. Poriel, *Chem. Eur. J.* **2015**, 21, 9426.

[38] a) M. Romain, D. Tondelier, J.-C. Vanel, B. Geffroy, O. Jeannin, J. Rault-Berthelot, R. Métivier, C. Poriel, *Angew. Chem Int. Ed.* **2013**, 52, 14147; b) R. P. Kaiser, D. Nečas, T. Cadart, R. Gyepes, I. Císařová, J. Mosinger, L. Pospíšil, M. Kotora, *Angew. Chem.* **2019**, 131, 17329; c) C. Poriel, J. Rault-Berthelot, D. Thirion, *J. Org. Chem.* **2013**, 78, 886.

[39] a) D. Thirion, C. Poriel, F. Barrière, R. Métivier, O. Jeannin, J. Rault-Berthelot, *Org. Lett.* **2009**, 11, 4794; b) J.-Y. Hu, Y.-J. Pu, Y. Yamashita, F. Satoh, S. Kawata, H. Katagiri, H. Sasabe, J. Kido, *J. Mater. Chem. C* **2013**, 1, 3871.

[40] a) S. Kappaun, H. Scheiber, R. Trattnig, E. Zojer, E. J. W. List, C. Slugovc, *Chem. Commun.* **2008**, 5170; b) X. Chen, H.-T. Tseng, J.-L. Liao, S.-A. Chen, *J. Phys. Chem. B* **2005**, 109, 17496.

[41] S. C. Tse, K. K. Tsung, S. K. So, *Appl. Phys. Lett.* **2007**, 90, 213502.

[42] F. Goubard, F. Dumur, *RSC Adv.* **2015**, 5, 3521.

[43] J.-Y. Hu, Y.-J. Pu, G. Nakata, S. Kawata, H. Sasabe, J. Kido, *Chem. Commun.* **2012**, 48, 8434.

[44] a) C. Poriel, J. Rault-Berthelot, *J. Mater. Chem. C* **2017**, 5, 3869; b) L. J. Sicard, H.-C. Li, Q. Wang, X.-Y. Liu, O. Jeannin, J. Rault-Berthelot, L.-S. Liao, Z.-Q. Jiang, C. Poriel, *Angew. Chem. Int. Ed.* **2019**, 58, 3848; c) Y. Tao, C. Yang, J. Qin, *Chem. Soc. Rev.* **2011**, 40, 2943; d) S. Thiery, D. Tondelier, C. Declairieux, G. Seo, B. Geffroy, O. Jeannin, J. Rault-Berthelot, R. Métivier, C. Poriel, *J. Mater. Chem. C* **2014**, 2, 4156; e) C. Fan, Y. Chen, P. Gan, C. Yang, C. Zhong, J. Qin, D. Ma, *Org. Lett.* **2010**, 12, 5648; f) M. Zhuo, W. Sun, G. Liu, J. Wang, L. Guo, C. Liu, B. Mi, J. Song, Z. Gao, *J. Mater. Chem. C* **2015**, 3, 9137; g) L.-S. Cui, Y.-M. Xie, Y.-K. Wang, C. Zhong, Y.-L. Deng, X.-Y. Liu, Z.-Q. Jiang, L.-S. Liao, *Adv. Mater.* **2015**, 27, 4213.

[45] Y. Park, V. Choong, Y. Gao, B. R. Hsieh, C. W. Tang, *Appl. Phys. Lett.* **1996**, 68, 2699.

[46] J.-H. Chang, S.-Y. Liu, I.-W. Wu, T.-C. Chen, C.-W. Liu, C.-I. Wu, *J. Appl. Phys.* **2014**, 115, 124510.

[47] T.-C. Li, R.-C. Chang, *Int. J. of Precis. Eng. and Manuf.-Green Tech.* **2014**, 1, 329.

[48] M. Ye, C. He, J. Iocozzia, X. Liu, X. Cui, X. Meng, M. Rager, X. Hong, X. Liu, Z. Lin, *J. Phys. D: Appl. Phys.* **2017** 50 373002.

[49] H. Kang, J.-H. Kim, J.-K. Kim, J. Seo, Y. Park, *J. Korean Phys. Soc.* **2011**, 59, 3060.

[50] S. M. Tadayyon, H. M. Grandin, K. Griffiths, P. R. Norton, H. Aziz, Z. D. Popovic, *Org. Electron.* **2004**, 5, 157.

[51] a) H. P. Rathnayake, A. Cirpan, P. M. Lahti, F. E. Karasz, *Chem. Mater.* **2006**, 18, 560; b) H. P. Rathnayake, A. Cirpan, Z. Delen, P. M. Lahti, F. E. Karasz, *Adv. Funct. Mater.* **2007**, 17, 115.

[52] a) J. N. Moorthy, P. Venkatakrishnan, D.-F. Huang, T. J. Chow, *Chem. Commun.* **2008**, 18, 2146; b) L. C. Palilis, A. J. Mäkinen, M. Uchida, Z. H. Kafafi, *Appl. Phys. Lett.* **2003**, 82, 1563838.

[53] C. Coya, A. de Andrés, C. Zaldo, A. L. Alvarez, B. Arredondo, R. Gomez, J. L. Segura, C. Seoane, *J. Appl. Phys.* **2009**, 105, 044510.

[54] T. H. El-Assaad, M. Auer, R. Castaneda, K. M. Hallal, F. M. Jradi, L. Mosca, R. S. Khnayzer, D. Patra, T. V. Timofeeva, J.-L. Bredas, E. J. W. List-Kratochvil, B. Wex, B. R. Kaafarani, *J. Mater. Chem. C* **2016**, 4, 3041.

[55] G. Zhang, M. Baumgarten, M. Auer, R. Trattnig, E. J. W. List-Kratochvil, K. Müllen, *Macromol. Rapid Commun.* **2014**, 35, 1931.

[56] L. Zhao, C. Li, Y. Zhang, X.-H. Zhu, J. Peng, Y. Cao, *Macromol. Rapid Commun.* **2006**, 27, 914.
[57] J. Kalinowski, G. Giro, M. Cocchi, V. Fattori, P. Di Marco, *Appl. Phys. Lett.* **2000**, 76, 2352.
[58] a) M. Li, S. Tang, F. Shen, M. Liu, W. Xie, H. Xia, L. Liu, L. Tian, Z. Xie, P. Lu, M. Hanif, D. Lu, G. Cheng, Y. Ma, *J. Phys. Chem. B* **2006**, 110, 17784; b) M. Li, S. Tang, S. Fangzhong, M. Liu, W. Xie, H. Xia, L. Liu, L. Tian, Z. Xie, P. Lu, M. Hanif, D. Lu, G. Cheng, Y. Ma, *Chem. Commun.* **2006**, 32, 3393; c) M. Zhang, S. Xue, W. Dong, Q. Wang, T. Fei, C. Gu, Y. Ma, *Chem. Commun.* **2010**, 46, 3923; d) L. Yao, S. Xue, Q. Wang, W. Dong, W. Yang, H. Wu, M. Zhang, B. Yang, Y. Ma, *Chem. Eur. J.* **2012**, 18, 2707; e) L. Yao, S. Sun, S. Xue, S. Zhang, X. Wu, H. Zhang, Y. Pan, C. Gu, F. Li, Y. Ma, *J. Phys. Chem. C* **2013**, 117, 14189.
[59] S. Tang, M. R. Liu, P. Lu, H. Xia, M. Li, Z. Q. Xie, F. Z. Shen, C. Gu, H. P. Wang, B. Yang, Y. G. Ma, *Adv. Funct. Mater.* **2007**, 17, 2869.
[60] S. Tao, Y. Jiang, S.-L. Lai, M.-K. Fung, Y. Zhou, X. Zhang, W. Zhao, C.-S. Lee, *Org. Electron.* **2011**, 12, 358.
[61] W.-Y. Lai, X.-R. Zhu, Q.-Y. He, W. Huang, *Chem. Lett.* **2009**, 38, 392.
[62] W.-Y. Lai, Q.-Y. He, R. Zhu, Q.-Q. Chen, W. Huang, *Adv. Funct. Mater.* **2008**, 18, 265.
[63] P. A. Levermore, R. Xia, W. Lai, X. H. Wang, W. Huang, D. D. C. Bradley, *J. Phys. D: Appl. Phys.* **2007**, 40, 1896.
[64] W.-Y. Lai, R. Zhu, Q.-L. Fan, L.-T. Hou, Y. Cao, W. Huang, *Macromol.* **2006**, 39, 3707.
[65] N. Agarwal, P. K. Nayak, F. Ali, M. P. Patankar, K. L. Narasimhan, N. Periasamy, *Synth. Met.* **2011**, 161, 466.
[66] V. V. Cherpak, P. Y. Stakhira, D. Y. Volynyuk, J. Simokaitiene, A. Tomkeviciene, J. V. Grazulevicius, A. Bucinskas, V. M. Yashchuk, A. V. Kukhta, I. N. Kukhta, V. V. Kosach, Z. Y. Hotra, *Synth. Met.* **2011**, 161, 1343.
[67] J. Keruckas, J. V. Grazulevicius, D. Volyniuk, V. Cherpak, P. Stakhira, *Dyes Pigm.* **2014**, 100, 66.
[68] B. Chen, J. Ding, L. Wang, X. Jing, F. Wang, *Chem. Commun.* **2012**, 48, 8970.
[69] C. Coya, C. Ruiz, Á. L. Álvarez, S. Álvarez-García, E. M. García-Frutos, B. Gómez-Lor, A. de Andrés, *Org. Electron.* **2012**, 13, 2138.
[70] M.-H. Tsai, Y.-H. Hong, C.-H. Chang, H.-C. Su, C.-C. Wu, A. Matoliukstyte, J. Simokaitiene, S. Grigalevicius, J. V. Grazulevicius, C.-P. Hsu, *Adv. Mater.* **2007**, 19, 862.
[71] Z. Hotra, P. Stakhira, V. Cherpak, D. Volyniuk, L. Voznyak, V. Gorbulyk, B. Tsizh, *Photonics Lett. Pol.* **2012**, 4, 35.
[72] N. Seidler, S. Reineke, K. Walzer, B. Lüssem, A. Tomkeviciene, J. V. Grazulevicius, K. Leo, *App. Phys. Lett.* **2010**, 96, 093304.
[73] a) F. Liu, C. Tang, Q.-Q. Chen, F.-F. Shi, H.-B. Wu, L.-H. Xie, B. Peng, W. Wei, Y. Cao, W. Huang, *J. Phys. Chem. C* **2009**, 113, 4641; b) C. Tang, F. Liu, Y.-J. Xia, L.-H. Xie, A. Wei, S.-B. Li, Q.-L. Fan, W. Huang, *J. Mater. Chem.* **2006**, 16, 4074; c) Y. Jiang, C. Cheng, J.-J. Huang, L.-W. Feng, X. Guo, C.-F. Liu, X.-W. Zhang, W.-Y. Lai, W. Huang, *J. Phys. Chem. C* **2015**, 119, 28117.
[74] M. Wang, L. Zhou, M. Yu, C. Liu, S. Chu, J. Pan, W.-Y. Lai, W. Huang, *J. Mater. Chem. C* **2017**, 5, 7075.

[75] a) Y. Zhao, Y. Guo, Y. Liu, *Adv. Mater.* **2013**, 25, 5372; b) X. Gao, Y. Hu, *J. Mater. Chem. C* **2014**, 2, 3099; c) X. Gao, Z. Zhao, *Sc. China Chem.* **2015**, 58, 947; d) W. Zhang, Y. Liu, G. Yu, *Adv. Mater.* **2014**, 26, 6898; e) Z. Liu, G. Zhang, Z. Cai, X. Chen, H. Luo, Y. Li, J. Wang, D. Zhang, *Adv. Mater.* **2014**, 26, 6965; f) C. Zhang, Y. Zang, E. Gann, C. R. McNeil, X. Zhu, C.-a. Di, D. Zhu, *J. Am. Chem. Soc.* **2014**, 136, 16176.

[76] a) J.-D. Peltier, B. Heinrich, B. Donnio, J. Rault-Berthelot, E. Jacques, C. Poriel, *ACS Appl. Mater. Interfaces* **2017**, 9, 8219; b) E. Jacques, M. Romain, A. Yassin, S. Bebiche, M. Harnois, T. Mohammed-Brahim, J. Rault-Berthelot, C. Poriel, *J. Mater. Chem. C* **2014**, 2, 3292.

[77] G. Zhang, M. Auer-Berger, D. W. Gehrig, P. W. M. Blom, M. Baumgarten, D. Schollmeyer, E. J. W. List-Kratochvil, K. Müllen, *Molecules* **2016**, 21, 1400.

[78] S. Zhuang, R. Shangguan, J. Jin, G. Tu, L. Wang, J. Chen, D. Ma, X. Zhu, *Org. Electron.* **2012**, 13, 3050.

[79] J. M. Hancock, A. P. Gifford, C. J. Tonzola, S. A. Jenekhe, *J. Phys. Chem. C* **2007**, 111, 6875

[80] R. Shangguan, G. Mu, X. Qiao, L. Wang, K.-W. Cheah, X. Zhu, C. H. Chen, *Org. Electron.* **2011**, 12, 1957.

[81] J. M. Hancock, A. P. Gifford, Y. Zhu, Y. Lou, S. A. Jenekhe, *Chem. Mater.* **2006**, 18, 4924.

[82] a) Q. Zhang, D. Tsang, H. Kuwabara, Y. Hatae, B. Li, T. Takahashi, S. Y. Lee, T. Yasuda, C. Adachi, *Adv. Mater.* **2015**, 27, 2096; b) Q. Zhang, B. Li, S. Huang, H. Nomura, H. Tanaka, C. Adachi, *Nat. Photonics* **2014**, 8, 326.

[83] Q. Zhang, B. Li, S. Huang, H. Nomura, H. Tanaka, C. Adachi, *Nat. Photon.* **2014**, 8, 326.

[84] S. Tao, L. Li, Y. Yu, Y. Zhou, C.-S. Lee, S.-T. Lee, X. Zhang, O. Kwon, *Chem. Mater.* **2009**, 21, 1284.

[85] Y. Bai, L. Hong, T. Lei, L. Zhang, X. Ouyang, Z. Liu, Y. Chen, W. Li, Z. Ge, *Dyes Pigm.* **2016**, 132, 94.

[86] T. H. Lee, K. L. Tong, S. K. So, L. M. Leung, *Synth. Met.* **2005**, 155, 116.

[87] K. T. Kamtekar, C. Wang, S. Bettington, A. S. Batsanov, I. F. Perepichka, M. R. Bryce, J. H. Ahn, M. Rabinal, M. C. Petty, *J. Mater. Chem.* **2006**, 16, 3823.

[88] Z.-L. Zhu, S.-F. Ni, W.-C. Chen, M. Chen, J.-J. Zhu, Y. Yuan, Q.-X. Tong, F.-L. Wong, C.-S. Lee, *J. Mater. Chem. C* **2018**, 6, 3584.

[89] C. Poriel, J. Rault-Berthelot, L. J. Sicard, *Chem. Commun.* **2019**, 55, 14238.

[90] S. Xue, X. Qiu, L. Yao, L. Wang, M. Yao, C. Gu, Y. Wang, Z. Xie, H. Wu, *Org. Electron.* **2015**, 27, 35.

[91] a) L. Duan, J. Qiao, Y. Sun, Y. Qiu, *Adv. Mater.* **2011**, 23, 1137; b) H. Jiang, *Macromol. Rapid Commun.* **2010**, 31, 2007; c) A. L. Fisher, K. E. Linton, K. T. Kamtekar, C. Pearson, M. R. Bryce, M. C. Petty, *Chem. Mater.* **2011**, 23, 1640; d) C.-H. Chen, W.-S. Huang, M.-Y. Lai, W.-C. Tsao, J. T. Lin, Y.-H. Wu, T.-H. Ke, L.-Y. Chen, C.-C. Wu, *Adv. Funct. Mater.* **2009**, 19, 2661; e) Y.-L. Liao, C.-Y. Lin, K.-T. Wong, T.-H. Hou, W.-Y. Hung, *Org. Lett.* **2007**, 9, 4511; f) J. Huang, J.-H. Su, X. Li, M.-K. Lam, K.-M. Fung, H.-H. Fan, K.-W. Cheah, C. H. Chen, H. Tian, *J. Mater. Chem.* **2011**, 21, 2957.

[92] K. E. Linton, A. L. Fisher, C. Pearson, M. A. Fox, L.-O. Pålsson, M. R. Bryce, M. C. Petty, *J. Mater. Chem.* **2012**, 22, 11816.

[93] M. Liu, X.-L. Li, D. C. Chen, Z. Xie, X. Cai, G. Xie, K. Liu, J. Tang, S.-J. Su, Y. Cao, *Adv. Funct. Mater.* **2015**, 25, 5190.
[94] Y. Zhang, S.-L. Lai, Q.-X. Tong, M.-F. Lo, T.-W. Ng, M.-Y. Chan, Z.-C. Wen, J. He, K.-S. Jeff, X.-L. Tang, W.-M. Liu, C.-C. Ko, P.-F. Wang, C.-S. Lee, *Chem. Mater.* **2012**, 24, 61.
[95] P. Wang, S. Fan, J. Liang, L. Ying, J. You, S. Wang, X. Li, *Dyes Pigm.* **2017**, 142, 175.
[96] X.-L. Li, X. Ouyang, D. Chen, X. Cai, M. Liu, Z. Ge, Y. Cao, S.-J. Su, *Nanotechnology* **2016**, 27, 124001.
[97] W.-C. Chen, Y. Yuan, S.-F. Ni, Z.-L. Zhu, J. Zhang, Z.-Q. Jiang, L.-S. Liao, F.-L. Wong, C.-S. Lee, *ACS Appl. Mater. Interfaces* **2017**, 9, 7331.
[98] X.-L. Li, M. Liu, Y. Li, X. Cai, D. Chen, K. Liu, Y. Cao, S.-J. Su, *Chem. Commun.* **2016**, 52, 14454.
[99] X. Ouyang, X.-L. Li, L. Ai, D. Mi, Z. Ge, S.-J. Su, *ACS Appl. Mater. Interfaces* **2015**, 7, 7869.
[100] a) J.-D. Peltier, B. Heinrich, B. Donnio, O. Jeannin, J. Rault-Berthelot, C. Poriel, *Chem. Eur. J.* **2017**, 23, 17290; b) M. Hempe, M. Reggelin, *RSC Adv.* **2017**, 7, 47183.
[101] a) X. Tang, Q. Bai, Q. Peng, Y. Gao, J. Li, Y. Liu, L. Yao, P. Lu, B. Yang, Y. Ma, *Chem. Mater.* **2015**, 27, 7050; b) Y. Yuan, J.-X. Chen, F. Lu, Q.-X. Tong, Q.-D. Yang, H.-W. Mo, T.-W. Ng, F.-L. Wong, Z.-Q. Guo, J. Ye, Z. Chen, X.-H. Zhang, C.-S. Lee, *Chem. Mater.* **2013**, 25, 4957.
[102] J. Tagare, S. Vaidyanathan, *J. Mater. Chem. C* **2018**, 6, 10138.
[103] M.-Y. Lai, C.-H. Chen, W.-S. Huang, J. T. Lin, T.-H. Ke, L.-Y. Chen, M.-H. Tsai, C.-C. Wu, *Angew. Chem. Int. Ed.* **2008**, 47, 581.
[104] X. J. Feng, S. F. Chen, Y. Ni, M. S. Wong, M. M. K. Lam, K.-W. Cheah, G. Q. Lai, *Org. Electron.* **2014**, 15, 57.
[105] Z. H. Li, M. S. Wong, H. Fukutani, Y. Tao, *Org. Lett.* **2006**, 28, 4271
[106] R. Muangpaisal, W.-I. Hung, J. T. Lin, S.-Y. Ting, L.-Y. Chen, *Tetrahedron* **2014**, 70, 2992.
[107] M. Zhu, T. Ye, C.-G. Li, X. Cao, C. Zhong, D. Ma, J. Qin, C. Yang, *J. Phys. Chem. C* **2011**, 115, 17965.
[108] M. A. Baldo, D. F. O'Brien, Y. You, A. Shoustikob, S. Sibley, M. E. Thompson, S. R. Forrest, *Nature* **1998**, 395, 151.
[109] F.-M. Hsu, L.-J. Chien, K.-T. Chen, Y.-Z. Li, S.-W. Liu, *Org. Electron.* **2014**, 15, 3327.
[110] F. Lucas, O. A. Ibraikulov, C. Quinton, L. Sicard, T. Heiser, D. Tondelier, B. Geffroy, N. Leclerc, J. Rault-Berthelot, C. Poriel, *Adv. Opt. Mater.* **2020**, 8, 1901225.
[111] M. Godumala, S. Choi, M. J. Cho, D. H. Choi, *J. Mater. Chem. C* **2019**, 7, 2172.
[112] T.-A. Lin, T. Chatterjee, W.-L. Tsai, W.-K. Lee, M.-J. Wu, M. Jiao, K.-C. Pan, C.-L. Yi, C.-L. Chung, K.-T. Wong, C.-C. Wu, *Adv. Mater.* **2016**, 28, 6976.
[113] K. Udagawa, H. Sasabe, C. Cai, J. Kido, *Adv. Mater.* **2014**, 26, 5062.